Fall 2014

Understanding preferred leg stiffness and layered control strategies for locomotion

Zhuohua H. Shen
Purdue University

Graduate School Form
(Revised /)

PURDUE UNIVERSITY
GRADUATE SCHOOL
Thesis/Dissertation Acceptance

This is to certify that the thesis/dissertation prepared

By Zhuohua Shen

Entitled
UNDERSTANDING PREFERRED LEG STIFFNESS AND LAYERED CONTROL STRATEGIES FOR LOCOMOTION

For the degree of Doctor of Philosophy

Is approved by the final examining committee:

Justin Seipel

Raymond Cipra

Bin Yao

Shirley Rietdyk

To the best of my knowledge and as understood by the student in the Thesis/Dissertation Agreement, Publication Delay, and Certification/Disclaimer (Graduate School Form 32), this thesis/dissertation adheres to the provisions of Purdue University's "Policy on Integrity in Research" and the use of copyrighted material.

Approved by Major Professor(s): Justin Seipel

Approved by: Ganesh Subbarayan 11/18/2014

Head of the Graduate Program Date

UNDERSTANDING PREFERRED LEG STIFFNESS AND LAYERED CONTROL STRATEGIES FOR LOCOMOTION

A Dissertation

Submitted to the Faculty

of

Purdue University

by

Zhuohua Shen

In Partial Fulfillment of the

Requirements for the Degree

of

Doctor of Philosophy

December 2014

Purdue University

West Lafayette, Indiana

I would like to dedicate my dissertation to my father, Shuifu Shen and my mother, Tiaozhen Yao. Without their support, I could never go this far.

ACKNOWLEDGMENTS

I would like to acknowledge the inspirational guidance of my major advisor Dr. Justin Seipel. I would also like to acknowledge the assistance and support from my committee members, Dr. Bin Yao, Dr. Raymond Cipra, Dr. Shirley Rietdyk, and my friends here at Purdue.

PREFACE

Legged robotics has been an exiting area during the past decades. The debut of robots such as Big Dog makes one wonder if the prime time for robots is eventually coming. However, just as with the intricacies of human locomotion, the fundamental dynamics behind walking and running are not entirely known and explored. This has prevented us from better understanding how we move and from developing principles of legged robot design. It is challenging to address this gap in locomotion dynamics through experiments alone as large variations exist among different human subjects and different species. In addition, many experiments are unethical to carry out. Modeling and simulation on the other hand offers us a wonderful approach to quickly advance our understanding and make testable predictions before certain experimental studies are pursued. Among all the questions to be answered, two important ones addressed in this thesis are how stability is formed and how energy efficiency is optimized in legged locomotion. Here we utilize dynamics modeling and control to offer key pieces towards a complete explanation to these questions.

TABLE OF CONTENTS

LIST OF TABLES

LIST OF FIGURES

Figure Page

ABSTRACT

Shen Zhuohua. PhD, Purdue University, December 2014. Understanding Preferred Leg Stiffness and Layered Control Strategies for Locomotion. Major Professor: Justin E. Seipel, School of Mechanical Engineering.

Despite advancement in the field of robotics, current legged robots still cannot achieve the kind of locomotion stability animals and humans have. In order to develop legged robots with greater stability, we need to better understand general locomotion dynamics and control principles. Here we demonstrate that a mathematical modeling approach could greatly enable the discovery and understanding of general locomotion principles.

It is found that animal leg stiffness when scaled by its weight and leg length falls in a narrow region between 7 and 27. Rarely in biology does such a universal preference exist. It is not known completely why this preference exists. Here, through simulation of the simple actuated-SLIP model, we show that the biological relative leg stiffness corresponds to the theoretical minimum of mechanical cost of transport. This strongly implies that animals choose leg stiffness in this region to reduce energetic cost. In addition, it is found that the stability of center-of-mass motion is also optimal when biological relative leg stiffness values are selected for actuated-SLIP. Therefore, motion stability could be another reason why animals choose this particular relative leg stiffness range.

We then extended actuated-SLIP by including realistic trunk pitching dynamics. At first, to form the Trunk Spring-Loaded Inverted Pendulum (Trunk-SLIP) model, the point mass of actuated-SLIP is replaced by a rigid body trunk while the leg remains massless and springy. It is found that exproprioceptive feedback during the flight phase is essential to the overall motion stability including trunk pitching. Either proprioceptive or exproprioceptive feedback during stance could generate stable

running motion provided that exproprioceptive feedback is used during flight. When both kinds of feedback are used during stance, the overall stability is improved. However, stability with respect to speed perturbations remains limited.

Built upon Trunk-SLIP, we develop a model called extended Trunk-SLIP with trunk and leg masses. We then develop a hierarchical control strategy where different layers of control are added and tuned. When each layer is added, the overall motion stability is improved. This layer by layer strategy is simple in nature and allows quick controller design and tuning as only a limited number of control parameters needs to be added and tuned at each step. In the end, we propose a future control layer where the commanded speed is controlled to achieve a higher level target such as might be needed during smooth walking to running transitions.

In summary, we show here that the simple actuated-SLIP model is able to predict animal center-of-mass translation stability and overall mechanical cost of transport. More advanced models are then developed based upon actuated-SLIP. With a simple layer by layer control strategy, robust running motion can be discovered. Overall, this knowledge could help better understand locomotion dynamics in general. In addition, the developed control strategy could, in principle be applied to future hip based legged robot design.

1. INTRODUCTION

During the past few decades, there has been significant advancement in the area of legged robots. Unlike wheeled robots, legged robots have the natural advantage of negotiating with rough terrain. In addition, there has been a dramatically growing need of robotic assitive devices such as exoskeletons and smart prostheses. The development of both legged robots and human assistive devices relies heavily on the understanding of how animals and humans walk and run.

However, the principles of locomotion dynamics are currently not well understood [1]. One approach to gain better understanding of locomotion dynamics has been physical experiments. Despite great insight and knowledge gained through experiments, this approach sometimes become limited due to large object variance and due to limitation arising from ethical considerations, especially for human experiments. In contrast, a modeling and analysis approach allows accurate manipulation and control during the study beyond what is possible for experiments. In addition, general behaviors across many animal species can be better explored using a modeling approach.

There still exists many general animal behaviors that remain to be understood and explained. Modeling and analysis could be a great approach to this kind of problem. For example, it is known that animals have an almost universal preference for particular values of relative leg stiffness, leg stiffness normalized by body weight and leg length. Legged animals from cockroaches to humans all prefer relative leg stiffness around ten. This kind of universal behavior is challenging to explore and understand through experimental studies. However, the core center-of-mass translation of legged animals can be described by simple models [1, 2]. Later in this dissertation, we show that this general preference of relative leg stiffness can be explained through the simulation of simple locomotion models.

In addition, legged locomotion control for stability remains an area in need of continued development. Recently, there has been development of several control strategies aiming at balancing the pitching rotation of the body while moving the body forward. However, most of the current strategies are not easy to employ. Here , as the second technical part of this dissertation, we show how simple yet effective control strategies can be derived and tested upon locomotion models. This in turn could allow a faster development of first principles from which legged robots can be designed upon.

1.1 Spring-Loaded Inverted Pendulum

At first, research on the dynamics of legged locomotion models has shed some light on how animals stabilize overall center-of-mass (CoM) locomotion [1,3]. Early passive walking and running models [4–6] first demonstrated that animal legged locomotion can be described by simple models and templates despite different morphologies [7]. Inspired by spring mass like running behaviors [8,9] found in the legged locomotion of various animals, a simple model called Spring-Loaded Inverted Pendulum (SLIP) [1, 2, 10, 11] is developed. As shown in Figure 1.1, it has a massless springy leg and a point mass as the body on top. Despite its simplicity, it mimics animal or robot CoM legged locomotion trajectories well [8, 12, 13].

As a general locomotion model, SLIP-like models of locomotion have been used to study human and other animal walking and running mechanics, such as leg stiffness, stride frequency, speed and etc [8,13–21]. Also, the stability of the point-mass motions of the SLIP model have been extensively studied to better understand how stable animal center-of-mass translation can be achieved [10, 22–24].

Initially it was suggested that legged locomotion could be controlled by embedding template models like SLIP [7]. Inspired by this concept, a number of locomotion controllers such as leg placement control and hip torque control [25–35] have been

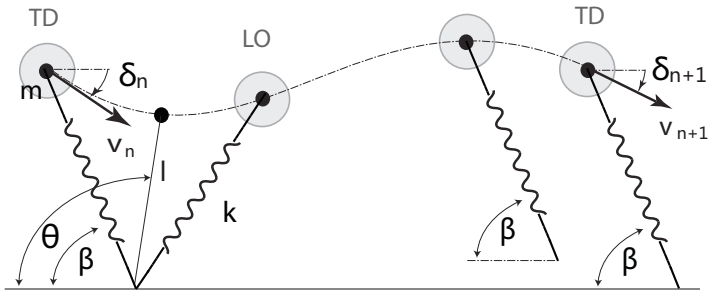

Figure 1.1. The Spring-Loaded Inverted Pendulum (SLIP) model. The parameters m, k and β stand for body mass, leg stiffness and landing angle respectively. The CoM position during stance is characterized by leg length l and leg angle θ. Here TD and LO stand for touchdown and liftoff, respectively.

developed. In addition, SLIP like running behaviors have been found in robot locomotion [12, 36–39].

In addition, SLIP has also been used in locomotion animation [40–44] as a governing physical model. Further, based upon the simple point-mass SLIP model, many advanced locomotion models have been developed [45–51] and many more new models are currently in development by the authors and others in the field. What is more, to enable easier use of SLIP for legged locomotion research, there has been development of SLIP analytical approximated solutions during the past decade [11, 52–57].

1.2 Actuated SLIP Models

The simple SLIP model is widely used for various applications. However, it lacks of realistic actuation and is energy conserving. Therefore, only partially asymptotic stability can be achieved [58]. Recently, there has been development of SLIP based locomotion models with actuation to improve overall model stability. The first category of locomotion model has been focusing on including actuation force along the leg [24, 34, 59]. One method is to improve locomotion stability by having a nonlinear leg stiffness [24, 59]. While another method produces extra leg thrust by adjusting

spring rest length during locomotion [34]. Both methods help improve overall center-of-mass motion stability.

Another category of actuation is hip joint torque and leg damping. Inspired by Hexapedal robot RHex [36, 60], a model called Clock-Torqued Spring-Loaded Inverted Pendulum (CT-SLIP) is developed with hip torque and leg damping. By using a clock based hip torque, center-of-mass motion with full asymptotic stability can be achieved [45, 46]. Similar to CT-SLIP, a model called Torque-Actuated Dissipative Spring Loaded Inverted Pendulum (TD-SLIP) with ramped hip torque and leg damping was presented [51] also with full asymptotic stability. It was demonstrated that TD-SLIP is capable to predict human ground reaction force directions. Then a general model called actuated Spring-Loaded Inverted Pendulum (actuated-SLIP), directly related to above knee amputees, was developed with a constant hip torque and leg damping during stance. It is found that hip torque and leg damping plays a fundamental role in stabilizing animal legged locomotion [48]. In a recent study, it is found that hip torque actuation in general produces more stable center-of-mass motion while solutions powered by radial forcing tend to be more energy efficient [61]. In addition, it showed that actuated-SLIP is capable of producing stable solutions with human related hip torque and mechanical cost of transport values. This implies that the simple actuated-SLIP could help explain the basic center-of-mass motion stability and energy efficiency.

1.3 Model Based Pitching Control and Robots

More recently, there has been development of trunk pitching control strategies on locomotion models with trunk pitching [35, 47, 62, 63]. These models are typically developed based upon SLIP and consist of a rigid body trunk and massless springy legs. A traditional method, known as the Raibert's approach [63] was to effectively utilizing three separate controllers to regulate robot hopping motion with a trunk body: (1) a proportional and derivative hip torque controller to maintain the trunk

upright; (2) a leg thrust controller to maintain a desired peak center-of-mass height during flight; (3) a leg angle controller during flight to modulate overall locomotion speed. Another strategy called virtual pivot point (VPP) [47, 64] is developed based on a bipedal Spring-Loaded Inverted Pendulum (SLIP) model by replacing the point mass with a realistic trunk as the body. It uses a controlled hip torque to redirect ground reaction forces so that overall pendulum like pitching behaviors can be realized and stabilized. Another approach uses the concept of hybrid zero dynamics and SLIP embedding [35, 49] to systematically design a feedback type controller for overall locomotion stabilization including trunk pitching.

Recently, it is demonstrated that above knee amputee like stable locomotion with only hip torque actuation and passive legs is possible for bipedal robots [62]. Based on the quadrupedal robot RHex [36, 60] which has damped springy legs, a bipedal version of RHex [62] is developed. It is capable of stable bipedal running, including body pitching. Its overall control strategy consists of a body pitching Proportional-Derivative (PD) controller, a forward speed proportional controller and a leg trajectory PD controller. For bipedal RHex, the hip motor actively tracks the time based desired leg trajectory without knowing the actual torque applied. In addition, the robot is unaware if it is in stance or flight as the leg touchdown and liftoff are not detected.

1.4 Dissertation Structure

This dissertation consists of 6 chapters. In chapter 2, we show how to explain the almost universal preference of relative stiffness through the simulation of a simple model called actuated-SLIP. It is found that locomotion mechanical cost of transport is minimized when biological relative stiffness values are selected. In chapter 3, we show that this preference of relative stiffness also relates to the optimization of center-of-mass motion stability. In chapter 4, we develop a simple model with trunk pitching dynamics and use it to study the effect of different sensory feedback. In chapter 5, we

demonstrate a complex locomotion model and a layered control strategy developed based on this model. For chapter 6, we provide a short summary of the most important points in this thesis.

Overall, this dissertation demonstrates a mathematical modeling and analysis approach to study general locomotion dynamics. We focus on three major aspects (shown as the three outer circles in Figure 1.2): (1) how to use a simple locomotion model to explain the general principle of relative stiffness; (2) how to develop models within trunk pitching to study the effects of different sensory feedback; (3) how to develop advanced locomotion models and control strategies of bipedal locomotion based upon simple models. Different models are used for these three aspects with growing complexity. The detail of these models will be explained in later chapters.

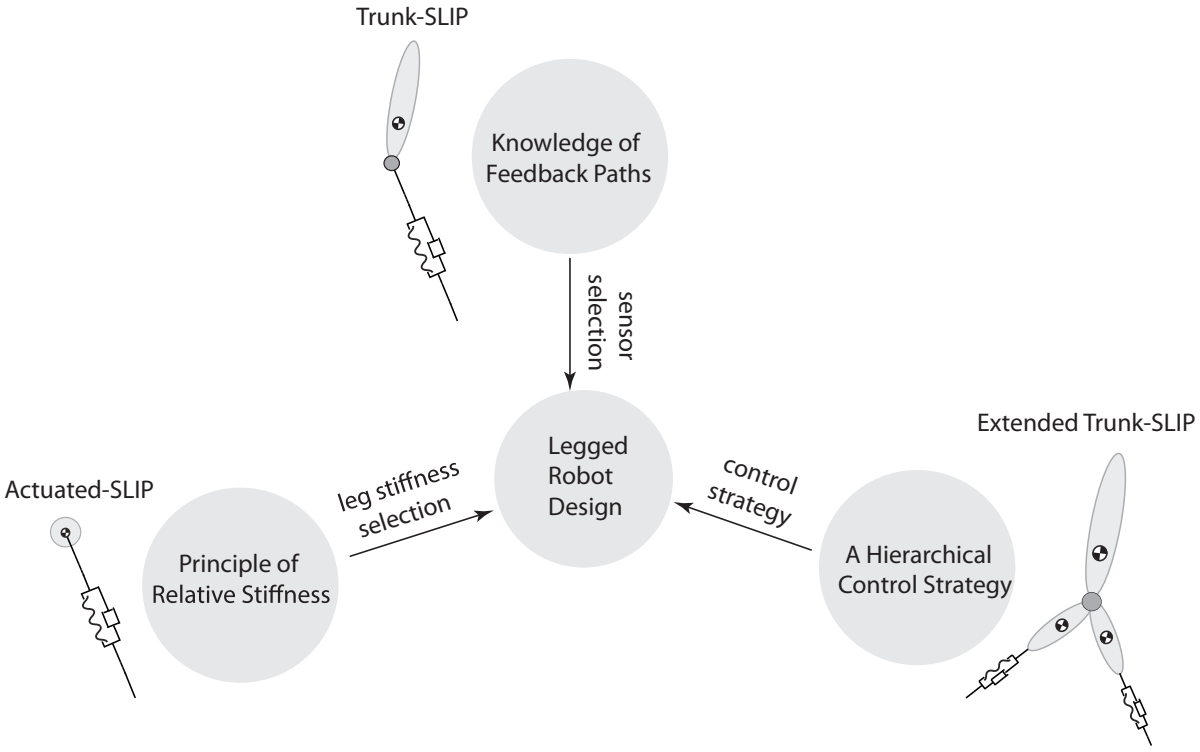

Figure 1.2. The fusion of different knowledge gained through mathematical models.

As shown in Figure 1.2, different pieces of knowledge gained through mathematical modeling of animal locomotion can be eventually applied to design better legged robots. The principles discovered about relative leg stiffness could help select appropriate leg stiffness for legged robots of different sizes. General knowledge about different feedback pathways helps to better select sensors for legged robots. In the end, the developed hierarchical control strategy could be employed to control bipedal robot locomotion.

2. UNIVERSAL ANIMAL RELATIVE STIFFNESS AND ENERGY EFFICIENCY

2.1 Background

Running is a fundamental behavior of legged animals arising from complex interactions of neurons, muscles, and the skeletal system [1, 65]. Despite the inherent neuromechanical complexity of running, some surprising and nearly universal patterns of behavior have been observed. Legged animals, across many species, exhibit whole-body center-of-mass motion during running that is similar to a pogo-stick (spring-mass) model where the leg is represented as an effective spring [7, 8]. In Figure 2.1(a)-(b), we show the animal spring mass running pattern and the classical SLIP model which describes animal like spring mass running pattern. In this model, the foot lifts off when the normal ground reaction force reaches zero and during flight resets to a landing angle β until the next touchdown, when the foot reaches ground. The effective leg spring stiffness k is empirically determined as the ratio of peak ground reaction force F to peak leg compression Δl [8], and expressed as $k := F/\Delta l$. To compare leg stiffness across species, the effective stiffness is nondimensionalized relative to body weight mg and resting leg length l_0, yielding the *relative leg stiffness*:

$$k_{rel} := \frac{F/mg}{\Delta l/l_0} = \frac{kl_0}{mg}\,. \tag{2.1}$$

The relative stiffness values of different animals are shown in Figure 2.1(c). Specifically, the shaded region stands for the *biologically preferred region* of relative leg stiffness. For multi-legged runners, the relative leg stiffness represents the collective effect of all legs sharing the same stance phase. Despite significant differences in size, morphology, and physiology, most animals prefer a relative leg stiffness between 7 and 27 [1, 8]. Why does this nearly universal pattern exist?

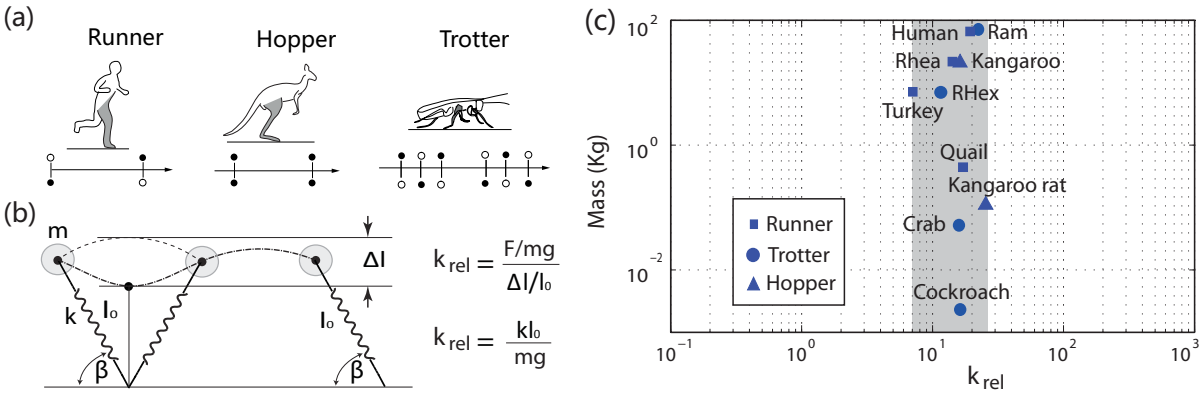

Figure 2.1. Spring mass running and animal relative stiffness. (a) Many animals produce similar whole body motion and ground reaction forces similar to a pogo-stick. (b) A pogo-stick or Spring-Loaded Inverted Pendulum (SLIP) model [2]. (c) The experimentally found relative leg stiffness of different animals.

In related studies, it was discovered that humans actively change the overall properties of the leg to accommodate for varying terrain stiffness [17,66], thus maintaining an effective leg stiffness (a combination of leg and terrain stiffness in these cases) near a constant level, with an effective dimensionless relative stiffness in the same range preferred by other legged animals. However, it is not known why maintaining an effective relative leg stiffness between 7 and 27 is beneficial.

Energetic cost of transport may be one reason for animals to exhibit preferred relative leg stiffness. It has been demonstrated that animals generally utilize energy efficiently when undergoing steady sustained locomotion [67]. For flying and swimming, animals prefer Strouhal numbers that have been associated with higher energy efficiency [68]. Humans and other animals also tend to choose a walking speed that can minimize energy expenditure [69–72]. Further, the adjustment of kinematic gait determinants such as step length, frequency and step width in humans and other animals is associated with reduced energetic cost [73–78].

Could the preferred relative leg stiffness exhibited and regulated by animals exist in order to reduce the energetic cost of legged locomotion? If so, this would

directly connect a high level goal such as energy efficiency with the regulation of a whole limb physiological property, leg stiffness. Given that the preferred leg stiffness is known to be actively regulated, we could then understand better how high level targets such as energy efficiency directly relate to the physiology and control of the neuro-musculo-skeletal system of animals. Knowledge of why and how leg stiffness is regulated during locomotion could also enable advancements for a range of applications including medical treatment of locomotion, orthoses, prostheses, legged robots, and wearable technology.

2.2 Methods

Our *objective* is to determine the relationship between relative leg stiffness and the energetic cost of motion. Our *overall approach* is to use a physics-based model of legged locomotion to calculate the minimum attainable mechanical cost of transport over a range of relative stiffness values from 1 to 100.

It is known that animals actively maintain overall effective leg stiffness [17, 66] during locomotion. Therefore, it is not trivial to independently vary effective leg stiffness in living animals, and this currently prohibits a study of this scope from being conducted experimentally. A physics-based mathematical model and simulation approach allows for direct and accurate control of the relative leg stiffness value during simulation.

We therefore construct a physics-based mathematical model of locomotion that depends on the relative leg stiffness and is capable of predicting a mechanical cost of transport, which can be directly compared with experimentally calculated values of the mechanical cost of transport. We developed a locomotion model based upon the canonical Spring-Loaded Inverted Pendulum (SLIP) model [2, 10, 11]. Previous research about SLIP has shown that there exists a certain relationship between relative stiffness and leg landing angle for periodic solutions [10]. However, SLIP is energy conserving and cannot predict net energetic cost of locomotion. We therefore

extended it to include a mathematically simple actuation and damping so that energetic cost predictions can be made. The governing equations of the model are derived and nondimensionalized to simplify analysis and comparison across many species of legged animals.

2.2.1 The Actuated Spring-Mass Model

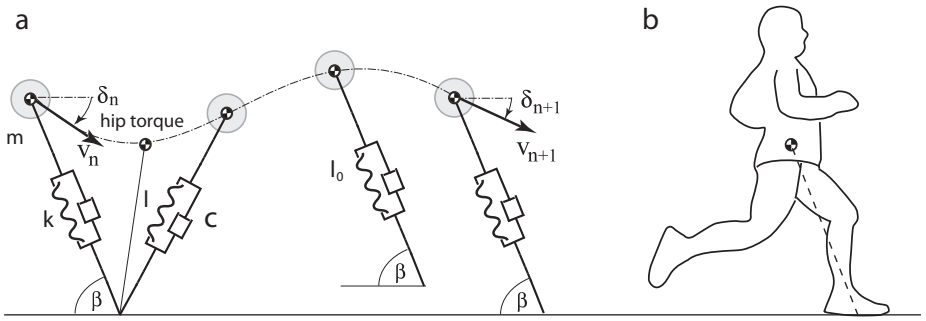

Figure 2.2. The illustration of actuated SLIP. a, the actuated SLIP model. Here m, k, c, l_0 β are body mass, leg stiffness, linear leg damping, leg original length and landing angle respectively. b, human running motion. The dashed line stands for the virtual spring leg.

As shown in Figure 2.2, an established physics-based model of locomotion is used for this study, based upon the canonical Spring-Loaded-Inverted-Pendulum model [48]. It includes actuation which is capable of representing the combined effects of both hip and ankle torque during locomotion, and the effective action of the knee is represented as a spring along the leg in order to agree with the established spring-mass modeling framework that has been used to analyze and compare experimental data collected from species across the animal kingdom. Note that, for actuated-SLIP, we focus on the center-of-mass translation and assume an infinite body rotating inertia. Thus, despite the existence of hip torque, the overall body is not allowed to rotate.

For actuated-SLIP, during stance, the leg swings forward under the actuation of hip torque and lifts off when the reaction force between the foot and the ground

becomes zero. Similar to SLIP, during flight, the leg is quickly reset to a constant landing angle β with an un-stretched leg.

The governing equations of the actuated SLIP model in terms of center-of-mass position x and y are described as:

$$m\ddot{x} = -F_l \cos\phi + F_\tau \sin\phi\,, \tag{2.2}$$

$$m\ddot{y} = F_l \sin\phi + F_\tau \cos\phi - mg\,. \tag{2.3}$$

Where F_l and F_τ denote the force acting on the center-of-mass along and perpendicular to the leg, while ϕ is the leg angle measured from the ground to the leg in a clockwise direction. The magnitude of F_l is given by $F_l = k(l_0 - l) - cl^{-1}[(x - x_f)\dot{x} + y\dot{y}]$. k, c, x_f, l and l_0 denote leg stiffness, leg damping, foot position, leg length and resting leg length respectively. Also, The magnitude of F_τ is calculated as $F_\tau = \tau/l$ with tau denoting the hip torque. The model was simulated using Matlab.

This extension of the SLIP model with active torque and damping is the simplest established model of legged locomotion known to the authors that is capable of predicting the mechanical cost of transport. This model is closely related to similar modeling frameworks that have been used to establish broad theories and testable hypotheses regarding animal physiology and mechanics [1, 45, 51]. Further, this model is directly related to at least one existing case of human locomotion, above-knee amputee running, in which actuation occurs at the hip and compliance and visco-elastic damping act along the leg [48]. This model is also representative of a class of legged robots with actuation only at the hip.

2.2.2 Nondimensionalization

To make the simulation more general across the animal kingdom, and to simplify analysis, we nondimensionalize the actuated SLIP model with respect to three base parameters: body mass m, the gravitational constant g, and the uncompressed leg length l_0. This allows for more general investigation of locomotion dynamics regard-

less of runner size and weight. To put this in other words, length in the model is rescaled by l_0, time is rescaled by $\sqrt{l_0/g}$, and mass is rescaled by m. The resulting dimensionless model parameters are then the leg landing angle β, the damping ratio $\zeta = c/(2\sqrt{km})$, the dimensionless hip torque $\tilde{\tau} = \tau/(mgl_0)$, and the relative leg stiffness $k_{rel} = kl_0/(mg)$.

2.2.3 Stable Solutions

The procedure for checking the stability of locomotion solutions of the actuated SLIP model is essentially to calculate whether small errors or perturbations of the system's state grow or decay in time. This is done by calculating the eigenvalues of a two-dimensional poincaré return map of the system states (speed $\tilde{v}$ and velocity direction angle δ) from the nth touchdown ($\tilde{v}_n$ and δ_n) to the $(n+1)th$ touchdown ($\tilde{v}_{n+1}$ and δ_{n+1}). When the model produces a periodic motion, we will have $\tilde{v}_{n+1} = \tilde{v}_n = \tilde{v}^*$ and $\delta_{n+1} = \delta_n = \delta^*$. To calculate the eigenvalues associated with a periodic locomotion solution, an iterative procedure is followed where successive small errors or perturbations are introduced and their effect after one step is measured. Each time, one variable in the mapping is perturbed from the periodic fixed value by a small amount: Δv or $\Delta\delta$. The resulting states at the next step due to both perturbations is recorded, ($\tilde{v}^{next}_{\Delta v}$ and $\delta^{next}_{\Delta v}$) and ($\tilde{v}^{next}_{\Delta\delta}$ and $\delta^{next}_{\Delta\delta}$). After the effects of all possible state errors or perturbations are accounted for, the corresponding Jacobian matrix is assembled:

$$\begin{bmatrix} (\tilde{v}^{next}_{\Delta v} - \tilde{v}^*)/\Delta v & (\tilde{v}^{next}_{\Delta\delta} - \tilde{v}^*)/\Delta\delta \\ (\delta^{next}_{\Delta v} - \delta^*)/\Delta v & (\delta^{next}_{\Delta\delta} - \delta^*)/\Delta\delta \end{bmatrix} \tag{2.4}$$

Then two eigenvalues λ_1 and λ_2 of this numerical Jacobian matrix are calculated. The periodic motion is stable if both eigenvalues have a magnitude less than one, unstable if either eigenvalue has a magnitude larger than one.

For the canonical SLIP model with zero actuation and leg damping, partially asymptotically stable solutions can be found and all solutions have zero energetic

cost of locomotion as the model is energy conserving and not intended for making predictions about the energetic cost of locomotion of animals. It has been shown that for the solutions to obtain full asymptotic stability, actuation in the actuated-SLIP model used here must exceed a non-zero threshold [48]. Therefore, a non-zero energetic cost is required to ensure locomotion stability.

2.2.4 Measuring the Mechanical Cost of Transport

An established method for quantifying the energetic efficiency of locomotion is by calculating the cost of transport . The cost of transport is the average energy required for an animal to travel a unit distance [3, 79]. Here we focus on the specific energy cost associated with animal mechanical movements, excluding the base metabolic cost, and define it as the *mechanical cost of transport*. This is the energy that was put into the mechanical motion divided by the distance traveled. The animal mechanical cost of transport data is obtained from Alexander [80], given in the units $\mathrm{J}/(\mathrm{m} \times \mathrm{kg})$. These values were then scaled by the gravitational constant g to yield a dimensionless mechanical cost of transport.

To obtain a dimensionless mechanical cost of transport prediction from the theoretical locomotion simulation, dimensionless mechanical energy expenditure of a single stride $\tilde{E}$ is first calculated as the product of the constant dimensionless hip torque $\tilde{\tau}$ and leg angle swept $\Delta\theta$ during stance. Also, the dimensionless stride length $\tilde{l}_{str}$ is recorded, and the dimensionless mechanical cost of transport is calculated as follows:

$$\text{Mechanical Cost of Transport} = \frac{\tilde{E}}{\tilde{l}_{str}}\,. \tag{2.5}$$

2.3 Results

2.3.1 Theoretical Minimum Mechanical CoT Versus Relative Leg Stiffness

First, we calculated the theoretical lowest attainable mechanical cost of transport as a function of relative leg stiffness, as shown in Figure 2.3. This calculation is for a fixed leg landing angle of 69° and a nondimensional speed of 1.1 (both typical for human locomotion [8,19]). For each value of relative leg stiffness, all stable locomotion solutions are found over a wide range of forcing and damping values. Among these solutions, the lowest attainable mechanical cost of transport is reported for each relative leg stiffness. This yields a curve of the lowest possible mechanical cost of transport versus the relative leg stiffness.

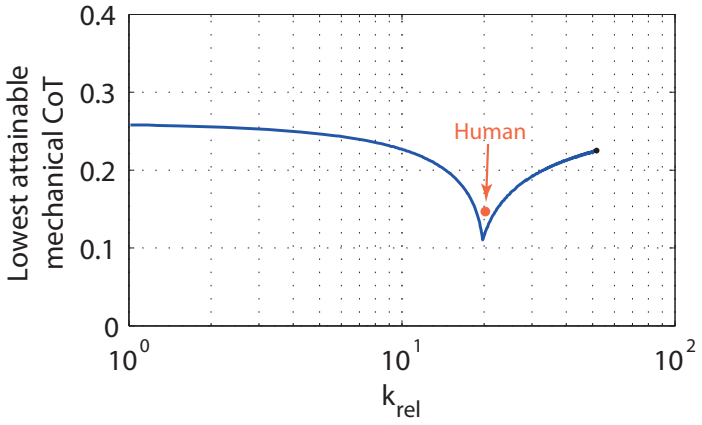

Figure 2.3. Simulated results using human related parameter values. (solid line) The lowest attainable mechanical cost of transport versus relative leg stiffness. The single dot represents the empirically determined preferred stiffness and associated mechanical cost of transport of human running [8, 80, 81].

We found that there is a particular relative stiffness for which an overall minimum mechanical cost of transport occurs, and we call this the *optimal relative stiffness*. Running is most efficient for this optimal relative stiffness value because a type of

nonlinear resonance occurs between the forward angular motion about the foot and the compressive motion along the leg, which leads to lower mechanical cost of transport. This type of nonlinear behavior is not easily explained in terms of linear system or continuous system dynamics due in part to the hybrid nature of leg liftoff and touchdown events, and so requires analysis of fully integrated locomotion solutions. When analyzing solutions that maintain a given running speed, we found that any deviation up or down from the optimal stiffness value moves the system away from the nonlinear resonance condition and requires additional actuation which increases the work done during the stride and thus increases the cost of transport.

The minimum cost of transport observed for the physics-based running model provides an explanation for why humans prefer to run with a particular relative leg stiffness. To compare the theoretical prediction directly with empirically collected data on human running, we superimpose the experimentally observed relative stiffness and mechanical cost of transport observed for humans [8, 80, 81] onto the plot of the theoretical cost of transport curve. Please see the relationship between the experimental data point representing preferred human running and the theoretical prediction from the running model in Figure 2.3.

Surprisingly, the experimentally observed relative stiffness that is preferred by humans, and the mechanical cost of transport observed for humans, coincide directly with the predicted theoretical minimum region. According to the predicted CoT-vs-stiffness curve shown in Figure 2.3, the cost of transport would sharply rise if humans ran with a different relative leg stiffness. This implies that the cost of transport is a significant factor in human selection and regulation of relative leg stiffness.

2.3.2 Effect of Changing Speed and Leg Landing Angle

We are interested in determining how these results might generalize across the animal kingdom. Since different animals have different preferred running speeds and leg

landing angles, we theoretically determine how the optimal relative stiffness depends on these parameters.

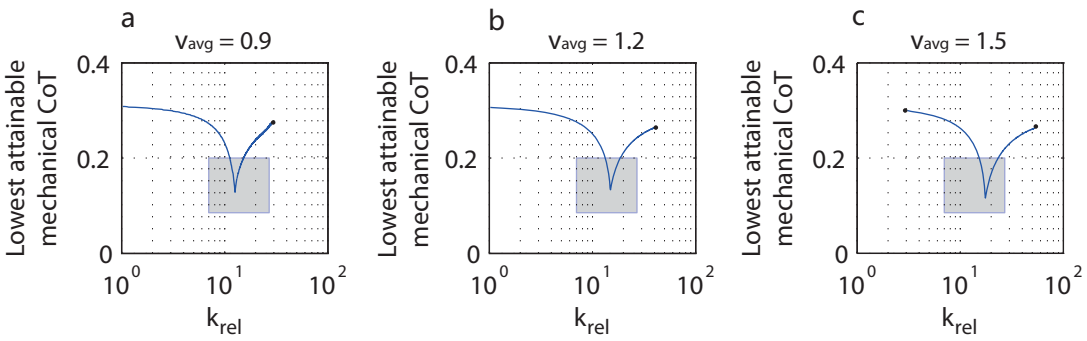

Figure 2.4. The lowest attainable mechanical cost of transport versus relative leg stiffness. The gray region stands for biologically preferred region with a relative leg stiffness from 7 to 27 and a mechanical cost of transport from 0.09 and 0.2.

The lowest attainable mechanical cost of transport is calculated as a function of relative stiffness for several different running speeds, as shown in Figure 2.4. Here, three panels are plotted for the nondimensional speeds 0.9, 1.2, and 1.5 (within the typical speed range of animals $(0.9, 1.7)$ [8]) while the leg landing angle is kept at 65°. The optimal relative stiffness value increases as the running speed is increased. The minimum mechanical cost of transport found first increases a small amount as the speed is increased from the first to second panel, but then decreases a small amount as the speed is increased further in the third panel.

If the leg landing angle is changed, the minimum mechanical cost of transport and corresponding optimal relative stiffness also change, as shown in Figure 2.5. Here, three panels are plotted for different leg landing angles 62°, 65°, and 68°, while the average forward speed is kept at 1.2. As the leg landing angle is increased, the minimum mechanical cost of transport decreases, and the associated optimal relative stiffness value increases.

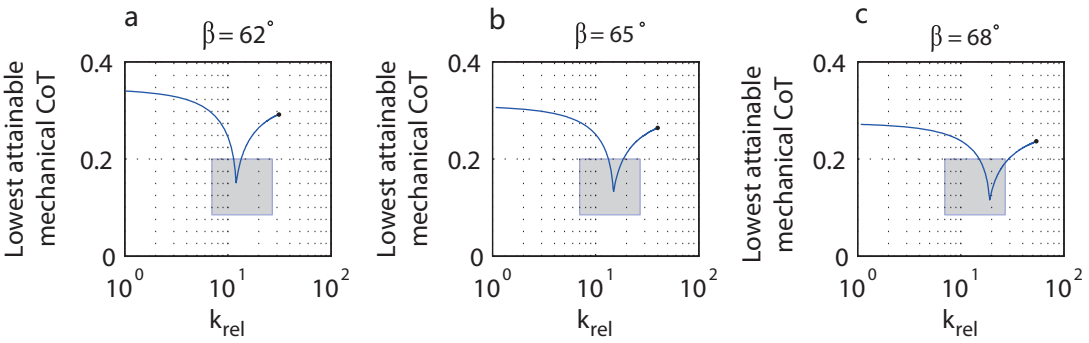

Figure 2.5. The lowest attainable mechanical cost of transport versus relative leg stiffness.

Overall the optimal relative leg stiffness generally falls within the biologically preferred region between 7 and 27. Additionally, the predicted minimum mechanical cost of transport is also within the biologically observed region between 0.09 and 0.2.

2.3.3 The Theoretical Minimum CoT for Multiple Animal Species

To represent multiple animals, we superimposed multiple theoretical mechanical cost of transport curves for multiple nondimensional speeds (from 0.9 to 1.7) and leg landing angles (from 60° to 70°) used by animals [8]. This yields a single, composite, theoretical minimum cost of transport curve as shown in Figure 2.6. On top of this plot, we superimposed the region of relative stiffness and cost of transport that are experimentally observed for both mammals and birds [8, 80].

A clear energy well of low mechanical cost of transport values centers over the biologically preferred stiffness values and correctly predicts the range of mechanical cost of transport observed experimentally, 0.09 to 0.20. The overall minimum mechanical cost of transport predicted lies below 0.09 and on either side of the biologically preferred stiffness range the theoretical cost of transport curve rises above 0.20. This result, along with the human prediction shown previously, implies that animals gen-

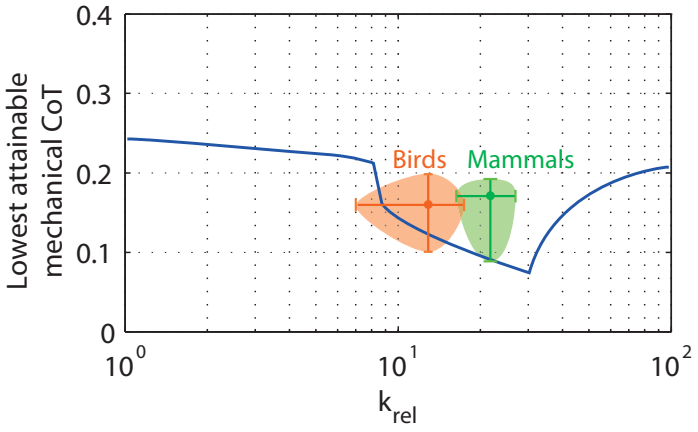

Figure 2.6. General results. (solid line) The lowest attainable mechanical cost of transport of stable periodic solutions found over a range of animal relevant parameter values.

erally prefer a particular range of relative leg stiffnesses because they can minimize the mechanical cost of transport.

2.4 Conclusion

Overall, the results presented here provide an explanation for why maintaining a preferred leg stiffness is valuable to a running animal. In short, we expect that selecting a relative leg stiffness in the range of 7 to 27 leads to a lower energetic cost of transport. We found that running is most efficient in this range because a type of nonlinear resonance occurs which leads to a lower mechanical cost of transport.

The results of this study may also help in determining an organizing principle for how animals control their underlying physiology to produce high level whole-body motion. Since the regulation of relative leg stiffness can be directly related to the properties of muscle, tendon, and other tissues of the leg, as well as the neural activation of the leg, the relationship between whole-body cost of transport and relative leg stiffness presented here provides a critical link across multiple scales of biological motion. Despite large variations in evolutionary history, morphology, and size, such

an organizing principle is expected to be general across animals and may be true of biologically-inspired systems as well. Therefore, the results of this work are expected to have general value across many fields such as biology, robotics, and human motion sciences and engineering.

3. UNIVERSAL ANIMAL RELATIVE STIFFNESS AND STABILITY

3.1 Background

As previously mentioned in Section 2.1, the "effective stiffness" of human and animal legs has been defined and empirically measured in many studies as the ratio of peak ground reaction force to peak leg compression [8, 82–85]. Despite significant differences in size, morphology, and physiology, most animals prefer a normalized leg stiffness (normalized by body weight and leg length) between 7 and 27 [8].

In the previous chapter, it is found that a simulation of locomotion predicted that preferred leg stiffness coincides with optimal energetic cost of locomotion. This finding agrees with related studies which show that animals, including humans, tend to minimize energy expenditure during locomotion by adjusting locomotion gait and speed [70, 71, 73–78]. Apart from the energetic cost, the authors are not aware of other explanations for the nearly universally observed preference for leg stiffness.

Here, we investigate whether the stability of motion could also be a primary factor influencing the preferred leg stiffness of animals. The dynamic stability of locomotion is of great importance to the success of animals since high speed locomotion would not exist without it. For example, it was previously found that *Blaberus discoidalis* is statically unstable when running at high speeds, thus it requires dynamic stability to maintain locomotion [86]. Subsequent simulation models predicted that insects move in a manner that ensures dynamic stability [1, 87–89]. Based upon these previous studies, we expect that stability may play an equally important role as energetic cost of locomotion in the universally observed preferred leg stiffness of animals.

3.2 Methods

The *objective* of our numerical simulation is to determine the relationship between the stability of locomotion and leg stiffness. Our *overall approach* is to simulate an established physics-based model of animal running and calculate the stability of locomotion over a range of relative leg stiffness values, ranging from from 1 to 100. It is currently prohibitively challenging to experimentally vary the leg stiffness of animals since animals actively regulate to maintain their leg stiffness regardless of treatments [17, 66]. A physics-based mathematical model and simulation approach allows for direct and accurate control of the relative leg stiffness value during simulation. Similar to the previous chapter, actuated-SLIP is used and nondimensionalized for simulation. The detailed model description, nondimensionalization and calculation of mechanical cost of transport can be found in previous section 2.2, thus omitted here for simplicity. In short, mechanical cost of transport is measured as the nondimensional mechanical energetic cost per stride divided by the nondimensional stride length.

3.2.1 Measuring Local Stability

The procedure for checking the stability of locomotion solutions of the actuated SLIP model is essentially to calculate whether small errors (perturbations of the system's state) grow or decay in time. Given that we have multiple directions in the system's state space, we use two methods to estimate the stability of locomotion which can account for both the direction of slowest recovery and the overall rate of recovery. One provides us with the perturbation decay constant associated with the slowest rate of perturbation recovery (the maximum magnitude eigenvalue of a Poincaré return map), and the other provides us with an overall contraction constant (based on the singular value decomposition of the Poincaré return map) associated with the average rate of perturbation recovery of all system states. In short, the perturbation decay constant and the contraction constant are meant to represent the worst case time

scale associated with perturbation recovery and the average perturbation rejection performance respectively.

Perturbation Decay Constant: Here we define the *perturbation decay constant* mathematically as the maximum eigenvalue of a Poincaré return map which describes how the dynamics of locomotion evolve from one stride to the next. We calculate the eigenvalues of the Poincaré return map of the system states (speed $\tilde{v}$ and velocity direction angle δ) from the nth touchdown ($\tilde{v}_n$ and δ_n) to the $(n+1)th$ touchdown ($\tilde{v}_{n+1}$ and δ_{n+1}). When the model produces a periodic motion, we have $\tilde{v}_{n+1} = \tilde{v}_n = \tilde{v}^*$ and $\delta_{n+1} = \delta_n = \delta^*$. To calculate the eigenvalues associated with a periodic locomotion solution, an procedure is followed where successive small errors or perturbations are introduced and their effect after one step is measured. Each time, one variable in the mapping is perturbed from the periodic fixed value by a small amount: Δv or $\Delta\delta$. The resulting states at the next step due to both perturbations is recorded, ($\tilde{v}^{next}_{\Delta v}$ and $\delta^{next}_{\Delta v}$) and ($\tilde{v}^{next}_{\Delta\delta}$ and $\delta^{next}_{\Delta\delta}$). After the effects of all possible state errors or perturbations are accounted for, the corresponding Jacobian matrix is assembled:

$$A = \begin{bmatrix} (\tilde{v}^{next}_{\Delta v} - \tilde{v}^*)/\Delta v & (\tilde{v}^{next}_{\Delta\delta} - \tilde{v}^*)/\Delta\delta \\ (\delta^{next}_{\Delta v} - \delta^*)/\Delta v & (\delta^{next}_{\Delta\delta} - \delta^*)/\Delta\delta \end{bmatrix} \tag{3.1}$$

The Poincaré return map can be approximated with respect to small perturbations, and the dynamics of perturbation can be described as:

$$\begin{bmatrix} \Delta v_{n+1} \\ \Delta\delta_{n+1} \end{bmatrix} = A \begin{bmatrix} \Delta v_n \\ \Delta\delta_n \end{bmatrix} \tag{3.2}$$

Where Δv_n and $\Delta\delta_n$ are the remaining system state error from the fixed point value v^* and δ^* after n mapping, starting from an initial perturbation Δv and $\Delta\delta$. Similarly, Δv_{n+1} and $\Delta\delta_{n+1}$ are the remaining system state error after $n+1$ mapping.

Then the two eigenvalues λ_1 and λ_2 of this numerical Jacobian matrix are calculated. The periodic motion is unstable if either eigenvalue has a magnitude larger

than one, stable if both eigenvalues have a magnitude less than one. When both eigenvalues are less than one, the maximum eigenvalue magnitude determines the slowest asymptotic decay of a small perturbation. This maximum eigenvalue magnitude, the *perturbation decay constant*, therefore provides us with a worst case decay rate. Please note that the decay constant here is inversely related to the rate of decay: For a discrete stride-to-stride map, a smaller perturbation decay constant will yield a faster rate of decay or recovery time form a small perturbation.

Perturbation Contraction Constant: We also use a second method to measure the stability of locomotion, as a complementary method to the use of eigenvalues. Besides the maximum eigenvalue magnitude which represents the recovering speed in the most vulnerable perturbation direction, we also seek to measure the overall contraction of perturbation. To quantify the perturbation contraction, we rely on the singular value decomposition of the Jacobian matrix A.

Figure 3.1 shows a graphical representation of the singular value decomposition. In the following, we show that any perturbation on the orange unit circle can be mapped to a point on the purple ellipse after a single mapping. Assuming there exists an initial perturbation on the unit circle expressed as $\cos\theta\nu_1 + \sin\theta\nu_2$, where θ can be any value from zero to 2π. After one liner mapping, it becomes $\sigma_1 \cos\theta u_1 + \sigma_2 \sin\theta u_2$. This corresponds to a certain point on the purple ellipse which can be described in local coordinate system as:

$$\frac{x^2}{{\sigma_1}^2} + \frac{y^2}{{\sigma_2}^2} = 1 \tag{3.3}$$

Where the direction of u_1 and u_2 are defined as positive x and y directions. Also, it is easy to prove that any perturbation within the orange circle can be mapped to a certain point within the purple ellipse. We therefore define the ratio of the purple ellipse area to the orange circle area as the *perturbation contraction constant* r as:

$$r = ({\sigma_1}^2 + {\sigma_2}^2)/2 \tag{3.4}$$

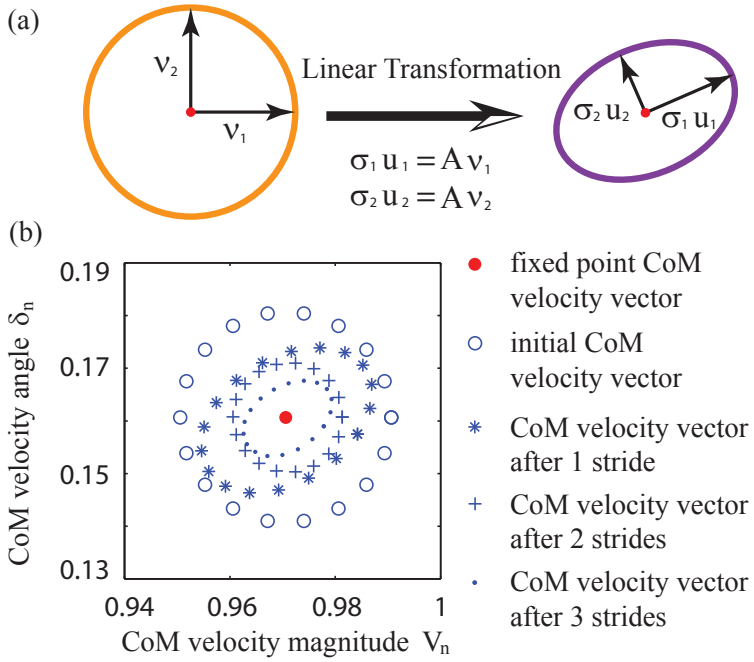

Figure 3.1. (a) A graphical illustration for singular value decomposition of the Jacobian matrix A. Here ν_1, ν_2, u_1 and u_2 are input and output unit vector pairs. σ_1 and σ_2 are two singular values. (b) Typical small perturbation response of the center-of-mass velocity vector at touchdown. The model parameters used are $k_{rel} = 11.224$, $\beta = 65°$, $\tilde{\tau} = 0.2236$, $\zeta = 0.5923$. When the nondimensional touchdown velocity magnitude and angle are 0.9706 and 0.1607, the model reaches stable periodic motion.

A smaller perturbation contraction constant yields a larger rate of perturbation contraction (a faster averaged recovery time of all system states).

To better explain the concept of perturbation contraction constant, a simulated small perturbation response of a typical periodic running solution is presented in panel (b) of Figure 3.1. When the touchdown velocity magnitude and angle is at the red dot, the center-of-mass motion becomes periodic from one touchdown to next touchdown. To cover all the possible perturbations, initial perturbations are equally added around the fixed point values. Different initially perturbed center-of-mass velocity vectors are shown as circles in panel (b). To test running solution stability, the subsequent

center-of-mass velocity vectors are recorded. It can be seen in Figure 3.1 panel (b), the perturbation shrinks as the center-of-mass velocity magnitude and angle gradually move towards fixed point values.

Together, the perturbation contraction constant r and the perturbation decay constant λ^* characterize two important properties of the local stability (response to small perturbations) of running solutions: the worst case recovery rate is described by the perturbation decay constant while the averaged recovery rate is described by the perturbation contraction constant.

3.3 Results

3.3.1 Local Stability Versus Relative Leg Stiffness

First, we calculated the perturbation decay rate of different running solutions versus relative leg stiffness. At first, to represent human locomotion, we fixed the leg landing angle, nondimensional average speed and mechanical cost of transport to be 69°, 1 and 0.13 respectively based on existing literature [8, 19, 80].

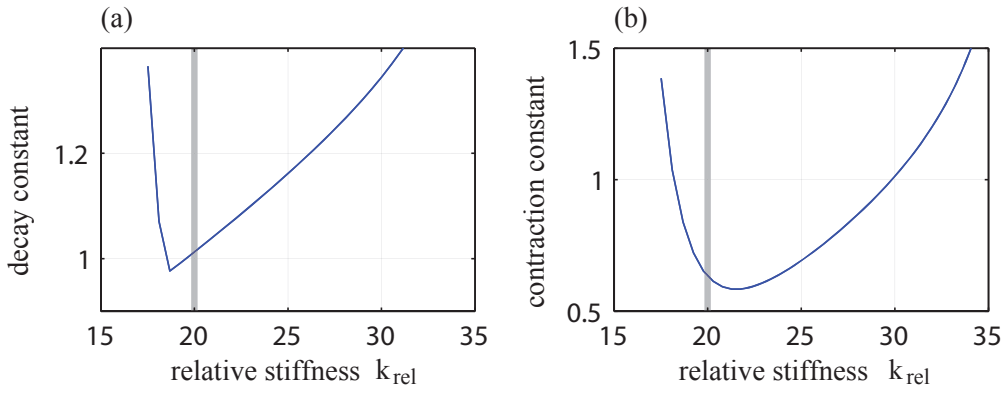

Figure 3.2. (a) The perturbation decay constant of periodic solutions versus relative leg stiffness. (b) The perturbation contraction constant r of periodic solutions versus relative leg stiffness. The light gray line in each panel stands for the human preferred leg stiffness value of 20 [8].

As shown in Figure 3.2 (a), the minimal perturbation decay constant occurs at values close to empirical human relative leg stiffness value 20, indicated as a gray line in panel (a). We define this value as the *optimal relative stiffness* for perturbation decay rate. Also, it is noticed that stable solutions with the perturbation decay constant less than one can only be found when the relative leg stiffness is near human empirical value. In addition, the perturbation contraction constant r, as a representative of the local stability, is calculated and plotted against relative stiffness in panel (b). Similarly, there exists a distinct relative stiffness where r is the smallest. We define this value as the *optimal relative stiffness* for perturbation contraction. The existence of both optimal relative stiffness values near the actual human value indicates that one possible reason humans adapt to this particular relative leg stiffness is to increase locomotion stability.

3.3.2 Effect of Changing Leg Landing Angle, Mechanical CoT and Speed

It is known that there exists certain variations among different people in terms of the preferred gait (leg landing angle), speed and the resulting mechanical cost of transport. As a next step, we simulate Hip-SLIP and calculate their perturbation decay constant and perturbation contraction constant while categorically varying each parameter and fixing the other two.

The perturbation decay constant (upper row) and perturbation contraction constant (lower row) are plotted against relative leg stiffness in Figure 3.3. The leg landing angle are varied around human preferred values: 68.5°, 69° and 69.5° from left to right columns. The average speed and mechanical cost of transport are fixed at 1 and 0.13. The optimal relative stiffness values for perturbation decay constant and perturbation contraction constant increase as leg landing angle increases. However, they still remain within the biologically observed relative leg stiffness range (from 7 and 27) and closely resides nearby the human empirical value 20.

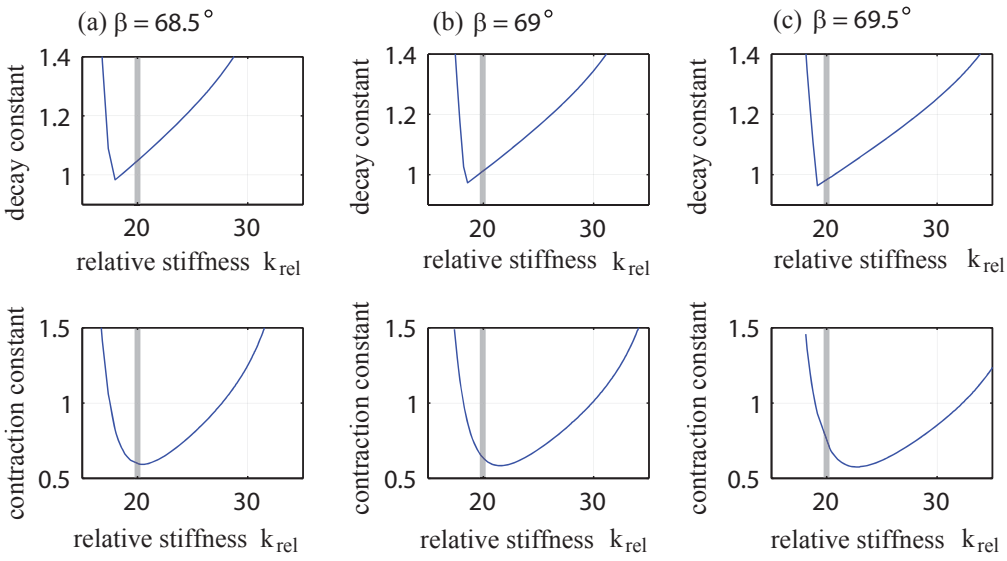

Figure 3.3. The perturbation decay constant and perturbation contraction constant versus relative leg stiffness. The gray line in each panel stands for the human perferred leg stiffness value of 20.

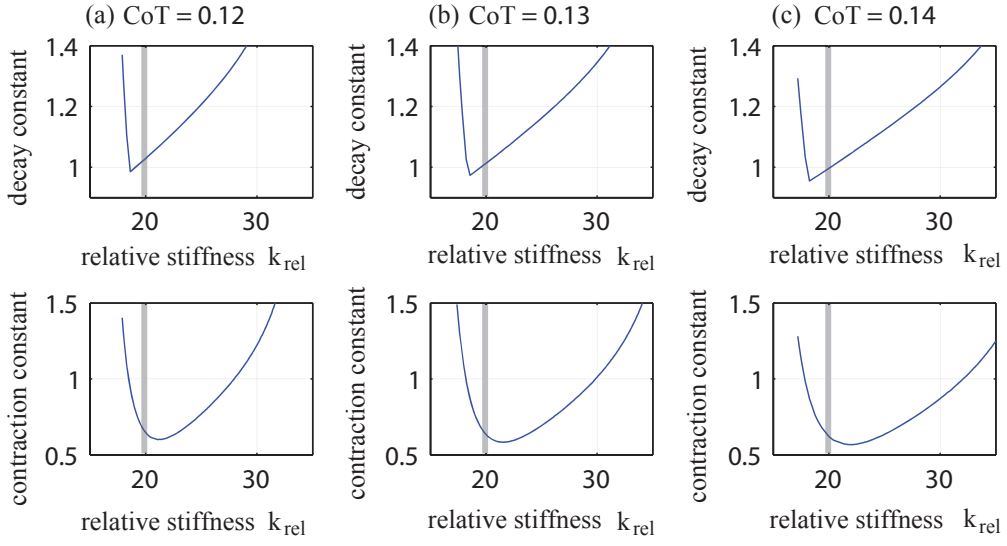

Figure 3.4. The perturbation decay constant and perturbation contraction constant versus relative leg stiffness. The gray line in each panel stands for the human perferred leg stiffness value of 20.

We then consider the variation of mechanical cost of transport. In Figure 3.4, we show the perturbation decay constant and perturbation contraction constant when the mechanical cost of transport is varied from 0.12 to 0.14 centered around experimental value of 0.13. The leg landing angle and speed are fixed at 69° and 1. Similarly, the optimal relative leg stiffness values mildly increases when humans run faster. But the optimal values are close to actual human value, and stable solutions are only found when relative leg stiffness is around 20.

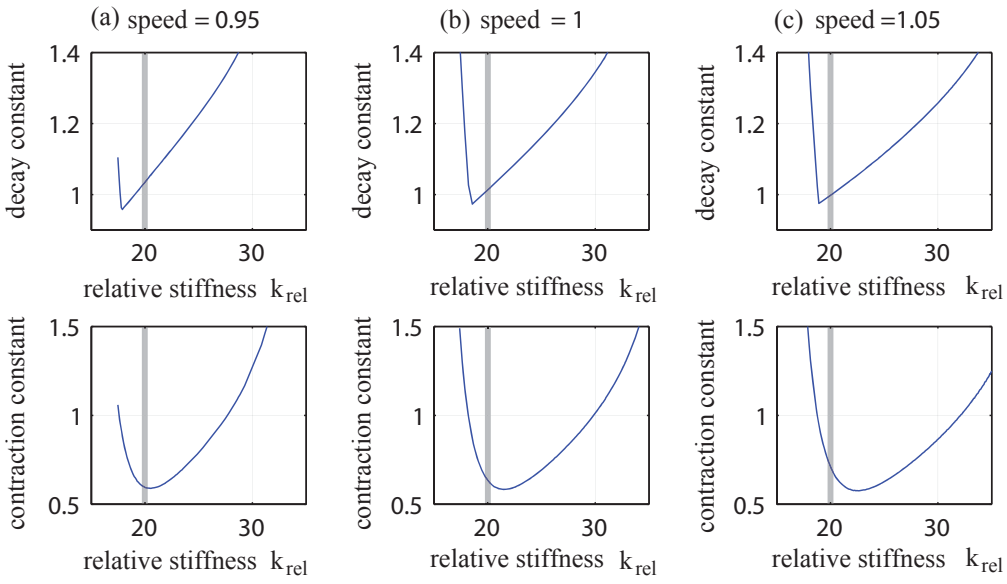

Figure 3.5. The perturbation decay constant and perturbation contraction constant versus relative leg stiffness. The gray line in each panel stands for the human preferred leg stiffness value of 20.

The last parameter varied is the average speed from 0.95 to 1.05 as shown in Figure 3.5. The leg landing angle and mechanical cost of transport are fixed at 69° and 0.13. Similar results can be observed with the optimal relative stiffness values near 20.

Combining the observations of Figures 3.3, 3.5 and 3.4, the optimal relative leg stiffness for perturbation decay constant is slightly less than the actual human value. In contrary, the optimal relative leg stiffness for perturbation contraction constant is

slightly larger than the human value. This could indicate that trade-off is made by choosing the relative stiffness between two optimal relative leg stiffness values.

3.3.3 Optimal Relative Leg Stiffness for Multiple Animal Species

We then seek to investigate the local stability of Hip-SLIP over a wider range of parameter space with a direct relevance to different legged animals. We vary the average speed over three levels: 0.9, 1.2 and 1.5 in order to represent animals preferred running speeds, typically within the range of 0.8 and 1.7 [8]. In addition, three representative running leg landing angles are selected to be 60°, 65° and 70°. This results in nine combinations of biologically representative average speeds and leg landing angles. With each combination, periodic solutions are calculated for three different mechanical cost of transport levels, 0.1, 0.15 and 0.2, to represent the biologically observed range of CoT between 0.09 and 0.2 [80]. In total, we then have 27 combinations of parameters to represent the biologically relevant range of this parameter space. For each combination of these parameters we compute a branch of locomotion solutions versus the relative leg stiffness. The perturbation decay constant and perturbation contraction constant is then calculated for each branch of locomotion solutions and plotted against the relative leg stiffness. Please see Figures 3.6 & 3.7.

In Figure 3.6, we show the perturbation decay constant versus relative leg stiffness for different combinations of leg landing angle and average speed. Each panel consists of three perturbation decay constant curves with a mechanical cost of transport of 0.1 (blue), 0.15 (green) and 0.2 (red). In general, within each panel, the majority of the stable solutions with the perturbation decay constant less than one are found within the biologically relevant relative stiffness region. In addition, there always exists an optimal relative leg stiffness. For most of the curves, perturbation decay constant increases when the relative stiffness is increased or decreased from the optimal value. For the bottom left panel, the perturbation decay constant is smallest at the left most end. No solutions can be found when the relative stiffness is increased above

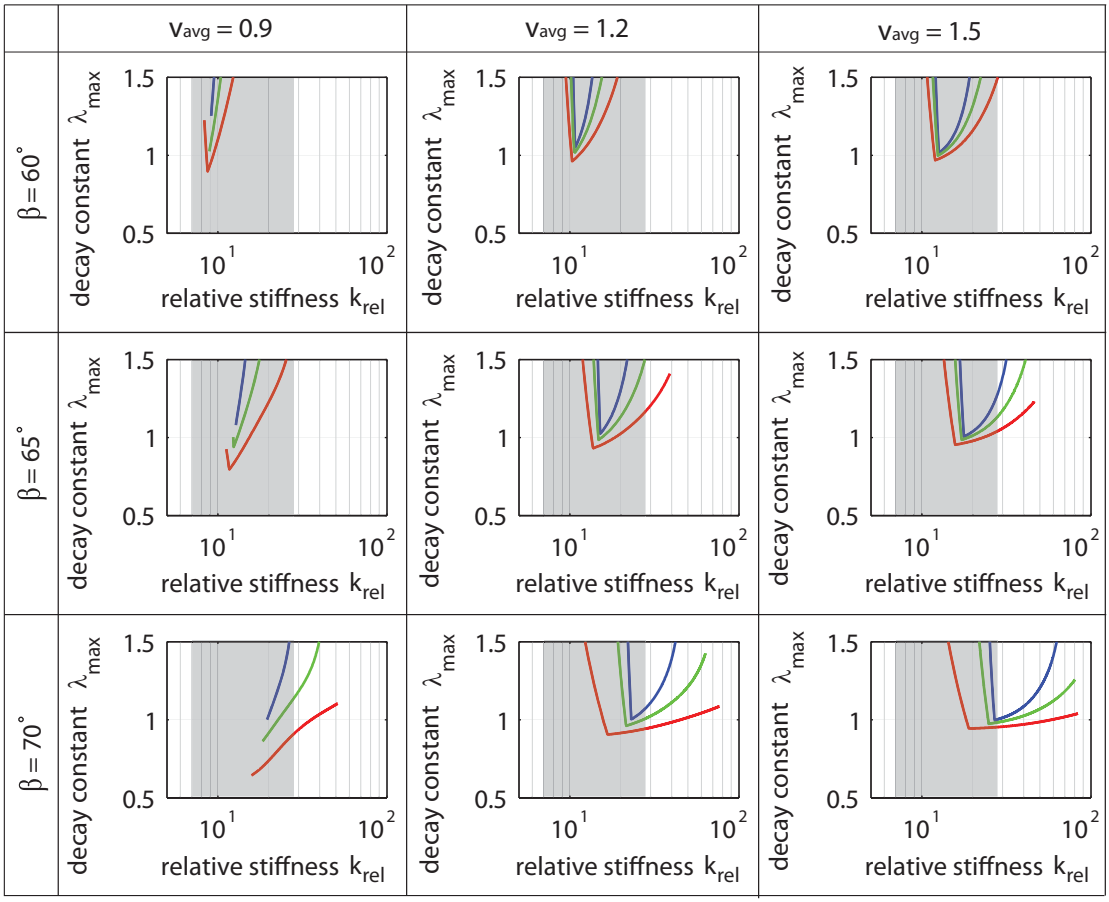

Figure 3.6. The perturbation decay constant versus relative leg stiffness. The blue, green and red lines stand for fixed points with a mechanical cost of 0.1, 0.15 and 0.2. Here the gray region stands for biologically relevant relative leg stiffness region from 7 to 27.

a critical value. Despite variations of leg landing angle, speed, and mechanical cost of transport, the optimal relative leg stiffness remains entirely within or nearby the biologically relevant relative stiffness region.

We next plot the perturbation contraction constant r versus the relative leg stiffness, as shown in Figure 3.7. Similarly, there always exists an optimal relative stiffness where the perturbation contraction constant r is the smallest. Any deviation from the optimal value will increase the resulting r value. The optimal relative leg stiffness

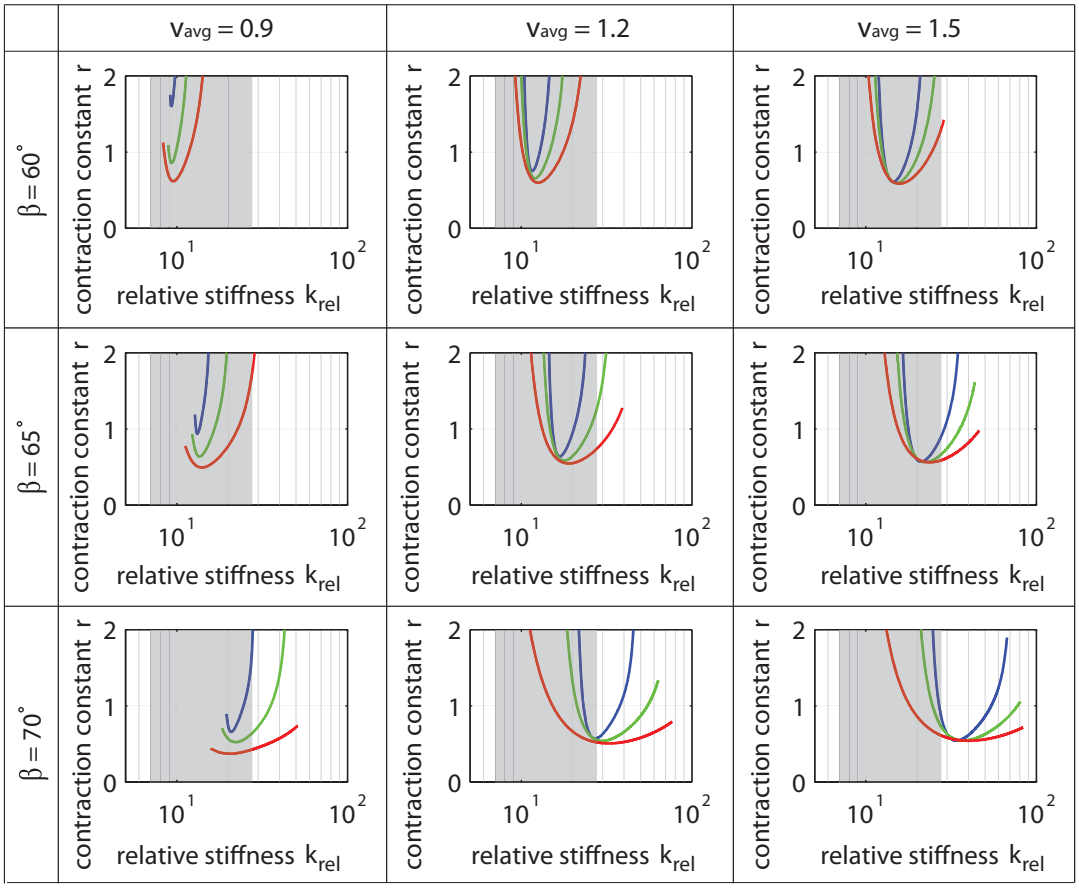

Figure 3.7. The minimum perturbation contraction constant r versus relative leg stiffness. The blue, green and red lines stand for fixed points with a mechanical cost of 0.1, 0.15 and 0.2. Here the gray region stands for biologically relevant relative leg stiffness region from 7 to 27.

generally increases with leg landing angle and average speed. However, the optimal value remains within the biologically relevant relative stiffness region.

We also found that locomotion solutions mostly exist within and near the biological relevant relative stiffness region, as shown in Figure 3.8 (a). This is also a significant and surprising result which indicates that animals may have to choose to run with these biologically relevant leg stiffnesses just to achieve locomotion. Within this range of biologically relevant leg stiffness, further refined selection of the relative

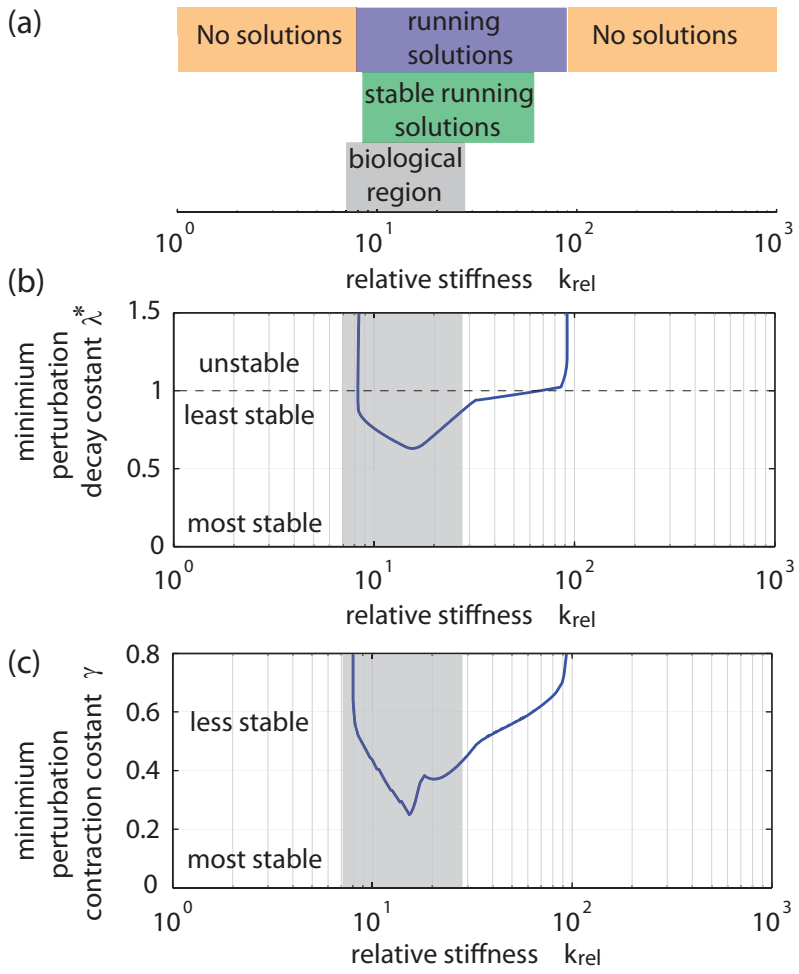

Figure 3.8. (a) The region of all periodic locomotion solutions (purple) and stable solutions (green), as well as the animal preferred stiffness range (gray). (b) The minimum perturbation contraction constant of stable solutions over a range of parameters. (c) The minimum perturbation decay constant of stable solutions over a range of parameters.

leg stiffness can result in optimization of the stability of locomotion, which was shown above to correctly predict the values selected by humans: please see again Figure 3.2.

Lastly, throughout the entire range of speeds (from 0.8 to 1.7 [8]), leg landing angles (from 60° to 70°), and Cost of Transport values (from 0.09 to 0.2 [80]) we considered above we now find and plot the minimal attainable perturbation decay constant and perturbation contraction constant versus relative stiffness: See Figure 3.8

(b) & (c). The leg landing angle, average speed and mechanical cost of transport are allowed to vary within the biologically relevant region for each value of relative leg stiffness tested. This approach ensures that we can determine how stability varies with respect to relative leg stiffness, even if there is variability in the other system parameters. This also provides a single aggregate curve that represents the optimal relative leg stiffness in a gross averaged sense, taking into account variations in the other parameters. Here we find that there exists a distinct optimal relative stiffness for both the perturbation decay constant and the perturbation contraction constant. Overall, both optimal relative stiffness values reside close to the middle of biological relevant relative stiffness region. This implies that animals prefer to choose a range of relative leg stiffness centered on the optimal relative leg stiffness value.

3.4 Conclusion

Legged animals, across many species, select relative leg stiffness in a nearly universal range between 7 and 27. It has been shown recently that one plausible reason for animals to prefer this range is in order to reduce the mechanical cost of transport.

However, the stability of behavior, locomotion in this case, is increasingly thought to be another important factor influencing animal preference and animal evolution. In this paper, we used a physics-based simulation of legged locomotion to determine whether the selection of relative leg stiffness correlates with the minimization of locomotion stability.

Overall, we showed that selecting a relative stiffness between 7 and 27 leads to optimal locomotion stability. This provides a novel explanation for why maintaining a preferred leg stiffness is valuable to a running animal. This work also provides support for the idea that motion stability could be a major factor influencing animals behavior and evolution in general, perhaps with similar significance as energetic efficiency.

4. FEEDBACK PATHWAYS IN RUNNING WITH TRUNK PITCHING

4.1 Background

Human and animal locomotion is easy to take for granted, and yet has proven difficult to understand and reproduce. Though it has long been known that the nervous system plays an essential role in providing feedforward activation and feedback control of animal locomotion [90–94], it is generally not known how this neural activation and control integrates with the underlying passive dynamics of locomotion, and there is currently no complete picture of the neural system architecture or function. The complexity and the high dimensionality of the neuromechanics of animal locomotion make it difficult to understand how neural (electrical) and mechanical contributions to stability integrate, and so a complete solution is difficult [95].

It is known that proprioceptive and exproprioceptive neural feedback, as two fundamental neural feedback pathways, are used in various human motion such as walking and dancing [96, 97]. Studies have showed that proprioceptive feedback is extensively used by human beings to detect and control postures [98–101]. In addition, the idea of proprioceptive feedback has been used to control robot locomotion [102]. On the other hand, exproprioceptive neural feedback is known to be employed in the control gait and postures [103, 104].

Here we focus on the effect of both feedback pathways on hip based locomotion, a special case of locomotion exhibited by above knee amputees and several robots with actuation only at the hip and passive compliant legs [36]. This represents a dramatic reduction of neuromechanical complexity of the leg when compared to a fully articulated and actuated human or robotic runner: See Figure 4.1. Specifically, we seek to understand what each feedback alone is capable of in human locomotion control. Is either alone could form basic locomotion stability? If so, in which phase of

motion are these critical or otherwise effective? What are the performance advantages of exproprioceptive feedback over proprioceptive feedback, if any?

The *objective* of this study is to determine how the the stability of pitching locomotion in the sagittal plane is affected by proprioceptive or exproprioceptive feedback control applied at the hip in the stance and flight phases of motion. In particular, we will determine and compare how stability depends on four different cases of feedback at the hip: a) proprioception of the leg angle with respect to the body during flight, and proprioception of the trunk angle w.r.t. the leg during stance; b) proprioception of the leg angle w.r.t. the body during flight, and exproprioception of the trunk angle (in the inertal frame) during stance; c) exproprioception of the leg angle (in the inertial frame) during flight, and proprioception of the trunk angle w.r.t. the leg during stance; and d) exproprioception of the leg angle during flight and exproprioception of the trunk angle during stance. These four cases are depicted in Figure 4.2. The knowledge gained from this work can provide principles regarding the underlying dynamics and control of hip-based locomotion, and is expected to provide foundational knowledge for the advancement of hip-based robots and amputee therapies and prostheses.

Initially, we *hypothesize* that exproprioceptive feedback throughout the entire stride will be needed in order to achieve stable locomotion. Without exproprioceptive feedback the controller would rely on information relative to a moving reference frame and this is expected to be unreliable and insufficient to yield stability, and so we expect that cases where proprioception is used instead of exproprioception will result in unstable locomotion. Further, we initially hypothesize that there will be a similar degree of instability for the two cases where a portion of the stride use proprioceptive feedback (either in flight or in stance), since we initially have no reason to expect that exproprioceptive feedback is more critical to one phase of motion than the other. We expect the case of proprioception in both stance and flight to be the least stable of the four cases considered.

The *overall approach* taken here is to utilize a theoretical study of hip-based locomotion dynamics in the sagittal plane. Currently, it is not feasible to analyze the feedback-based dynamics of human amputee subjects directly as it would require blocking of neural feedback pathways that is currently too difficult to achieve and unethical until more specific hypotheses are developed. Further, mathematical models provide analytical and theoretical insight not otherwise gained. Here, a simple model of sagittal plane legged locomotion with actuation only at the hip will be analyzed with multiple feedback rules applied at the hip. The stability of the model with different cases of feedback will be assessed using small perturbation studies (eigenvalues of a locomotion stride map) as well as large perturbation studies (basin of attraction).

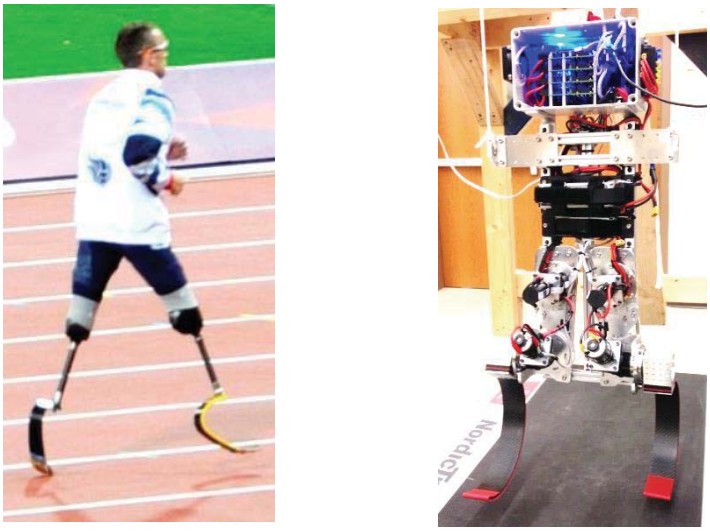

(a) Above Knee Athlete (b) Bipedal Robot

Figure 4.1. Examples of hip-based locomotion dynamics. (a) Dynamic running of an above-knee amputee on a passive compliant prosthesis (Richard Whitehead, Paralympic Gold Medalist) [105]. (b) An amputee-inspired bipedal robot currently in progress in the authors' lab [106].

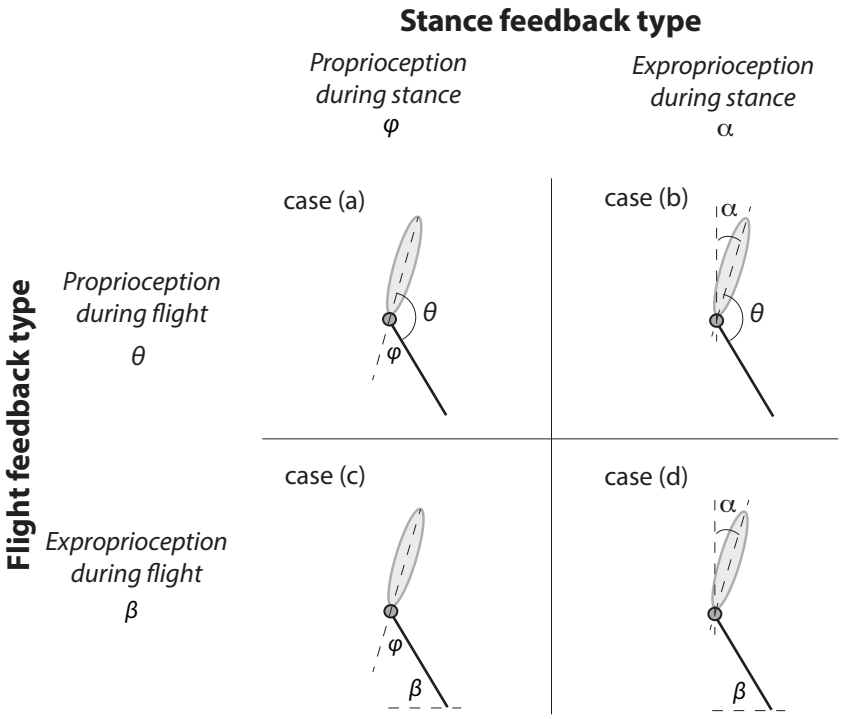

Figure 4.2. Four distinct cases of feedback are tested: a) proprioception of the leg angle with respect to the body during flight, and proprioception of the trunk angle w.r.t. the leg during stance; b) proprioception of the leg angle w.r.t. the body during flight, and exproprioception of the trunk angle (in the inertal frame) during stance; c) exproprioception of the leg angle (in the inertial frame) during flight, and proprioception of the trunk angle w.r.t. the leg during stance; and d) exproprioception of the leg angle during flight and exproprioception of the trunk angle during stance.

Note that in Figure 4.2, both ϕ and θ in essence represent the angle between trunk and leg. Here two angle notations instead of one are used here to denote feedbacks during stance and flight respectively. In addition, for case (b) in the figure, the exproprioceptive feedback α is only used during stance phase. Therefore, the absolute leg angle β cannot be obtained despite the fact that the relative angle θ is sensed during flight. Similarly, for case (c) the absolute leg angle feedback is only used during flight phase and the absolute trunk angle cannot be obtained during

stance. This is in order to allow only one type of sensory feedback during each phase of motion.

4.2 Approach

Here, we seek to model locomotion in the sagittal plane as a low dimensional system with a dynamic process similar to a pogo-stick or spring-loaded inverted pendulum (SLIP) [2]. In these models, the mass is assumed to be lumped in one body, a point-mass in many cases, and the leg is a massless spring.

In more recent models of hip-based locomotion, a torque was added at the hip and a damping element to the leg, such as in the Hip-actuated SLIP model [48], and this was found to yield significantly improved center-of-mass stability, especially with respect to large perturbations. Given the improvements in stability that the Hip-actuated SLIP model provided for center-of-mass dynamics, here we will extend this model to include a full pitching rigid-body trunk.

4.2.1 Trunk-SLIP Model

Inspired by previous knowledge of the Hip-actuated SLIP [48], which achieves a significant degree of robust stability with a damped springy leg and hip torque, we develop a new model called the Trunk-SLIP (as shown in Figure 4.3). To form the Trunk-SLIP model, we extend the point mass body of Hip-actuated SLIP into a trunk body with a specified mass and inertia.

Similar to Hip-actuated SLIP, the motion and dynamics of Trunk-SLIP consist of two stages: stance and flight. During stance, the body and leg starts with an initial position (α_n, β_n) and velocity $(v_n, \delta_n, \dot{\alpha}_n)$, as shown in Figure 4.3. Then the leg will swing forward about the ground contact point until the vertical component of the ground reaction force becomes zero. Upon liftoff, the model enters the flight mode, the hip torque is set to zero and the trunk keeps rotating at a constant angular speed.

The massless leg is set to the leg resting length and a fixed angle β with respect to the ground. It lands again when the foot reaches the ground.

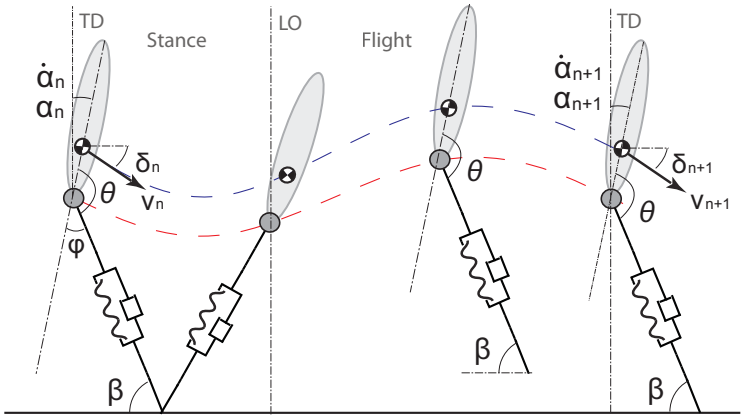

Figure 4.3. Configuration and motion of Trunk-SLIP. The blue and red lines are the body CoM and hip joint trajectories respectively. α and β are absolute pitching angle and leg landing angle respectively. ϕ stands for the angle between upper body and the leg. Here, LO stands for liftoff, TD stands for touchdown.

There exists multiple limitations to the this modeling framework. One limitation of Trunk-SLIP is that the effects of limb inertia and nonconservative ground impact/contact are not included in this model. However, this model is still adopted for its simplicity and less number of model parameters. Therefore, it allows a quicker and more complete analysis to provide insight for future analysis. Another limitation is that there exist higher levels of feedback, additional feedback pathways, and alternative feedback architectures that could potentially be used by above-knee amputees and possibly robots, but are outside the scope of this current analysis (this study is focused on producing knowledge of the effects of four basic feedback cases). Therefore, the predictions made from this model represent the basic influence of feedback control on the stability of pitching and center-of-mass motion.

4.3 Governing Equations

In this section, we first derive the equations of motion of Trunk-SLIP. Then we present the methods for calculating and comparing the stability of Trunk-SLIP locomotion solutions.

The parameters of the Trunk-SLIP model are: body mass m, body rotational inertia I, uncompressed leg length l_0, the distance between hip joint and mass center (CoM) r_0, leg stiffness k, leg damping c, and the leg landing angle β. As shown in Figure 4.4, the CoM and foot positions during stance are described by the vectors $[x, y]$ and $[x_f, 0]$ respectively. The leg length, leg angle, and body pitching angle during stance are l, θ and α respectively. Overall, Trunk-SLIP has three degrees of freedom x, y and α. Thus its dynamics can be described by three differential equations derived from Newton's Laws of motion.

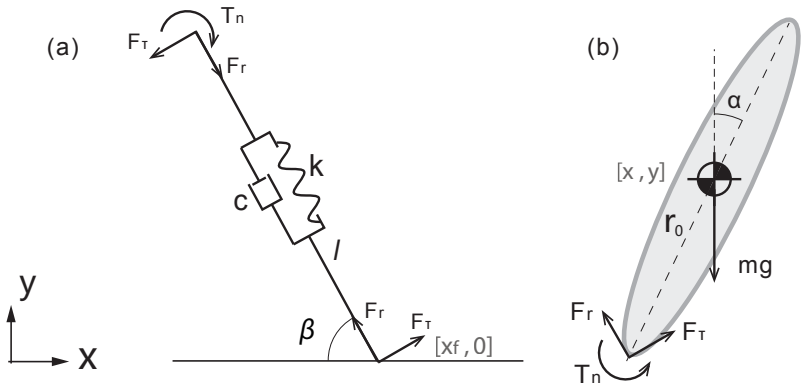

Figure 4.4. (a) Free body diagram of the springy leg during stance; (b) Free body diagram of the upper trunk during stance.

4.3.1 Stance and Flight Equations

When on the ground, the leg length and speed can be calculated as follows:

$$l = \sqrt{(x - r_0 \sin\alpha - x_f)^2 + (y - r_0 \cos\alpha)^2}\,,$$
$$\dot{l} = [(x - r_0 \sin\alpha - x_f)(\dot{x} - r_0\dot{\alpha}\cos\alpha) + (y - r_0\cos\alpha)(\dot{y} + r_0\dot{\alpha}\sin\alpha)]/l\,.$$

The forces along and perpendicular to the leg, denoted as F_r and F_τ, are then:

$$F_r = k(l_0 - l) - c\dot{l}\,, \tag{4.1}$$
$$F_\tau = \tau_n/l\,. \tag{4.2}$$

Where T_n is the hip torque applied between the leg segment and the body trunk. The forces both along and perpendicular to the leg (F_r and F_τ) can be transformed into the forces in the horizontal F_x and vertical F_y direction:

$$\begin{bmatrix} F_x \\ F_y \end{bmatrix} = \begin{bmatrix} -\cos\theta & \sin\theta \\ \sin\theta & \cos\theta \end{bmatrix} \begin{bmatrix} F_r \\ F_\tau \end{bmatrix}\,, \tag{4.3}$$
$$\theta = \cos^{-1}\left(\frac{x_f - x + r_0\sin\alpha}{l}\right)\,. \tag{4.4}$$

Applying Newton's second law, the equations governing the stance portion of motion are:

$$m\ddot{x} = F_x\,, \tag{4.5}$$
$$m\ddot{y} = F_y - mg\,, \tag{4.6}$$
$$I\ddot{\alpha} = -\tau_n + F_y r_0 \sin\alpha - F_x r_0 \cos\alpha\,. \tag{4.7}$$

During flight, as a consequence of having a leg with negligible mass, a negligible (approximately zero) torque is required to move the leg during flight. Thus, the trunk has negligible moments acting on it and is approximated to rotate with a constant

angular speed during the flight portion of motion, determined by the angular speed at liftoff. Note, however, that the model center-of-mass is affected by gravity during this phase of the motion:

$$\ddot{y} = -g\,. \tag{4.8}$$

4.3.2 Feedback During Flight

During the flight phase of motion, the main target of control is resetting the leg angle to a desired orientation. Therefore, actuation applied at the hip during the flight phase would be a function of either proprioceptive feedback of the leg angle measured with respect to the trunk θ (which can be directly related to the angle ϕ), or exproprioceptive feedback of the leg angle with respect to the inertial frame β.

Note that for the canonical SLIP models that the Trunk-SLIP model is based upon, the leg is reset to a specified angle during the flight phase of motion. This rule governing leg reset during flight implicitly requires that exproprioceptive feedback of leg angle be utilized during the flight phase of motion, along with at least a simple proportional-derivative control torque applied at the hip to stably bring the leg to the desired position. For the case of point-mass motion, where the trunk can be assumed to be constrained and not rotating, proprioceptive feedback could be used and yield the same result during swing. However, when the trunk is allowed to pitch, as is the case in the Trunk-SLIP model, there can be very different outcomes whether we use exteropceptive or proprioceptive feedback of leg position during the flight phase of running.

Proprioceptive Feedback of the Leg Angle With Respect to the Trunk:

When the proprioceptive feedback is used, the leg is reset to a constant angle ϕ_0 with respect to the trunk body. It touches down when:

$$\text{TD:} \quad y = r_0 \cos\alpha + l_0 \cos(\pi - \alpha + \theta_r)\,. \tag{4.9}$$

Upon touchdown, the foot position is updated as:

$$x_f = x - r_0 \sin\alpha + l_0 \sin(\pi - \alpha + \theta_r)\,. \tag{4.10}$$

exproprioceptive Feedback of the Leg Angle in the Inertial Frame:

If exproprioceptive feedback is used during the flight, the leg resets to a constant angle β with respect to the inertia frame. Therefore touchdown happens when:

$$\text{TD:} \quad y = r_0 \cos\alpha + l_0 \sin\beta_r\,. \tag{4.11}$$

The foot position can then be updated as:

$$x_f = x - r_0 \sin\alpha + l_0 \cos\beta_r\,. \tag{4.12}$$

4.3.3 Feedback During Stance

During the stance phase of motion, the main target of control is the trunk (body) pitch. Therefore, actuation applied at the hip is a function of either proprioceptive feedback of the trunk angle measured with respect to the leg ϕ, or exproprioceptive feedback of the trunk angle α measured with respect to the inertial frame.

Regardless the kind of the sensory feedback used, the model lifts off when the vertical force between the foot and ground becomes zero. Therefore the model enters the flight phase of motion when:

$$\text{LO:} \quad F_y = 0\,. \tag{4.13}$$

Proprioception of the Trunk Angle With Respect to the Leg:

Instead of directly measuring the trunk angle in order to control pitch, we assume in this case that the only measurement available is one with respect to the body, or in

this case with respect to a frame attached to the leg. Therefore, we measure the angle between the trunk and the leg. The hip torque of Trunk-SLIP is then governed by a proportional and derivative controller which uses the angle ϕ (as shown in Figure 4.3) between the body and the leg, with controller gains K_p, K_d and a trunk angle reference ϕ_r:

$$\tau_n = K_p(\phi - \phi_r) + K_d\dot{\phi}\,. \tag{4.14}$$

exproprioception of the Trunk Angle With Respect to the Inertial Frame:

We then consider a control strategy utilizing exproprioceptive feedback during stance. The hip torque is governed by a proportional and derivative control law using the absolute trunk pitching angle α as feedback (as shown in Figure 4.3). Different from the first approach, it requires ground truth to apply a corrective hip torque during stance. Its hip torque is thus governed by a proportional and derivative controller with controller gains K_p, K_d and the position reference α_r:

$$\tau_n = K_p(\alpha - \alpha_r) + K_d\dot{\alpha}\,. \tag{4.15}$$

4.3.4 Model Parameters

The resulting Trunk-SLIP model depends on several parameters, including those associated with SLIP, plus those for a trunk and leg damping, as well as controller gains for the various feedback controllers to be tested. In order to keep analysis as simple as possible, and relevant for human-scaled locomotion, we hold most of the system parameters constant, at values representative of human running [47]. This enables the study of parameter variations to be focused mostly on the control gains used in the various feedback approaches studied in this chapter. Overall, the model physical parameter values used in this simulation can be found in Figure 4.1

The remaining system parameters can be categorized into two groups: i) hip torque control parameters and ii) changeable physical system parameters such as leg

Table 4.1 Physical system parameter values.

Constant	Description	Value	Units (SI)
g	gravitational constant	9.81	ms^{-2}
m	body mass	80	kg
I	body moment of inertia	4.58	kgm^2
l_0	leg length and resting spring length	1	m
r_0	distance from hip to mass center	0.1	m
k	leg spring stiffness	20	kN/m
c	leg damping	50	Ns/m

damping and leg stiffness. The hip torque control parameters include proportional K_p and derivative K_d feedback gains for any feedback control present, and control references such as ϕ_r for stance proprioceptive feedback, α_r for stance exproprioceptive feedback, θ_r for flight proprioceptive feedback, and β_r for flight exproprioceptive feedback. ii) The changeable physical system parameters include the leg stiffness k and leg damping coefficient c. For an above-knee amputee, the control parameters could be adjusted by the nervous system, and the leg damping and stiffness could be designed as part of the prosthesis.

4.3.5 Stability Quantification

To quantify the model stability, we establish a four-dimensional return map: from the nth touchdown (v_n, δ_n, α_n and $\dot{\alpha}_n$) to $(n+1)$th touchdown ($v_{n+1}, \delta_{n+1}, \alpha_{n+1}$ and $\dot{\alpha}_{n+1}$). When the model reaches a fixed point (a periodic motion), we will have $v_{n+1} = v_n = v^*$, $\delta_{n+1} = \delta_n = \delta^*$, $\alpha_{n+1} = \alpha_n = \alpha^*$ and $\dot{\alpha}_{n+1} = \dot{\alpha}_n = \dot{\alpha}^*$. The stability of a fixed point is thus quantified with the corresponding four eigenvalues associated with this four dimensional mapping. To evaluate the eigenvalues of the mapping, the Jacobian matrix of the return map needs to be numerically approximated. Each time, one variable in the mapping vector is perturbed from the fixed point value by a small amount: Δv $\Delta\delta$, $\Delta\alpha$ or $\Delta\dot{\alpha}$. The next vector in the mapping is recorded in

the simulation, and so on until the effects of perturbations in all state directions are compiled. The corresponding Jacobian matrix is therefore approximated using the following equations:

$$\begin{bmatrix} (v_{\Delta v}^{next} - v^*)/\Delta v & (v_{\Delta \delta}^{next} - v^*)/\Delta \delta & (v_{\Delta \alpha}^{next} - v^*)/\Delta \alpha & (v_{\Delta \dot{\alpha}}^{next} - v^*)/\Delta \dot{\alpha} \\ (\delta_{\Delta v}^{next} - \delta^*)/\Delta v & (\delta_{\Delta \delta}^{next} - \delta^*)/\Delta \delta & (\delta_{\Delta \alpha}^{next} - \delta^*)/\Delta \alpha & (\delta_{\Delta \dot{\alpha}}^{next} - \delta^*)/\Delta \dot{\alpha} \\ (\alpha_{\Delta v}^{next} - \alpha^*)/\Delta v & (\alpha_{\Delta \delta}^{next} - \alpha^*)/\Delta \delta & (\alpha_{\Delta \alpha}^{next} - \alpha^*)/\Delta \alpha & (\alpha_{\Delta \dot{\alpha}}^{next} - \alpha^*)/\Delta \dot{\alpha} \\ (\dot{\alpha}_{\Delta v}^{next} - \dot{\alpha}^*)/\Delta v & (\dot{\alpha}_{\Delta \delta}^{next} - \dot{\alpha}^*)/\Delta \delta & (\dot{\alpha}_{\Delta \alpha}^{next} - \dot{\alpha}^*)/\Delta \alpha & (\dot{\alpha}_{\Delta \dot{\alpha}}^{next} - \dot{\alpha}^*)/\Delta \dot{\alpha} \end{bmatrix} \quad (4.16)$$

Here, $v_{\Delta v}^{next}$, $\delta_{\Delta v}^{next}$, $\alpha_{\Delta v}^{next}$ and $\dot{\alpha}_{\Delta v}^{next}$ are the components of the new mapping vector when the velocity magnitude is perturbed,$v_{\Delta \delta}^{next}$, $\delta_{\Delta \delta}^{next}$, $\alpha_{\Delta \delta}^{next}$ and $\dot{\alpha}_{\Delta \delta}^{next}$ are the new mapping vector components when the velocity angle is perturbed, $v_{\Delta \alpha}^{next}$, $\delta_{\Delta \alpha}^{next}$, $\alpha_{\Delta \alpha}^{next}$ and $\dot{\alpha}_{\Delta \alpha}^{next}$ are the new mapping vector components when the body pitching angle is perturbed, and finally, $v_{\Delta \dot{\alpha}}^{next}$, $\delta_{\Delta \dot{\alpha}}^{next}$, $\alpha_{\Delta \dot{\alpha}}^{next}$ and $\dot{\alpha}_{\Delta \dot{\alpha}}^{next}$ are the new mapping vector components when the body pitching angular velocity is perturbed.

Based on the approximated Jacobian matrix, four eigenvalues of a fixed point can be calculated. The maximum eigenvalue magnitude can thus be used to measure the stability of a fixed point. When all the eigenvalues have a magnitude less than one, the fixed point is stable.

4.4 Results

Before presenting a systematic analysis of locomotion stability as a function of the four proposed feedback cases, and their respective parameters, we first briefly present one stable locomotion solution for case (d), where exproprioception is used throughout the entire stride. We hypothesized that stable locomotion would be possible if exproprioceptive feedback is used throughout the entire stride, as in case(d). In Figure 4.5(a) the center-of-mass trajectory and trunk angle is shown at several instances

of time. In Figure 4.5(b) we show a plot of the center-of-mass and trunk angle as they respond to a perturbation, demonstrating the stability of this locomotion solution.

We also hypothesized that stable locomotion might only be possible if exproprioceptive feedback is used throughout the entire stride, and that the stability of the cases where there is partial exproprioceptive feedback would be similar in quality. Next, we investigate whether the other cases of feedback (a)-(c) can also achieve stable locomotion like case (d) exproprioception throughout stance, and we systematically vary multiple parameters for each case to determine how each parameter influences stability of locomotion.

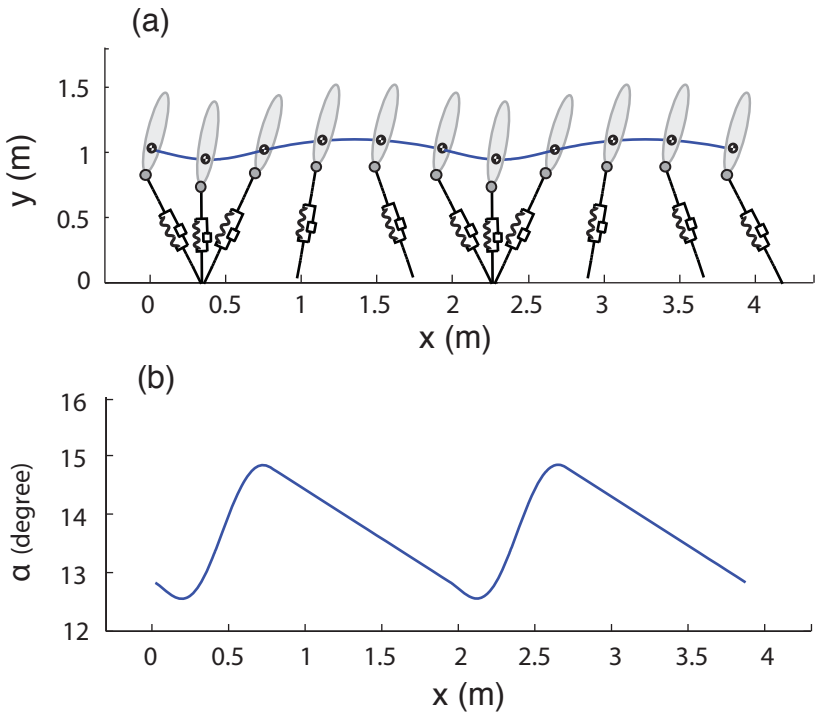

Figure 4.5. (a) The Motion of the Trunk-SLIP model with exproprioceptive feedback used throughout the entire stride (case (d)). (b) The trunk angle α versus the horizontal position x. Human-representative parameters as shown in Table 4.1 are used. The feedback control parameters are listed in Table 4.2. The periodic states at touchdown (fixed point values) are $(v^*, \delta^*, \alpha^*, \dot{\alpha}^*) = (4.78$ m/s, $15.30°$, $12.83°$, $-7.72°/\text{s})$.

4.4.1 Stability with Respect to Small Perturbations

Cases (a) and (b): Proprioception during Flight: We seek to determine if stable periodic solutions are possible when proprioceptive rather than exproprioceptive feedback of the leg angle is used during the flight phase of motion. In most SLIP-based models of locomotion, like the Virtual Pivot Point model [47], it is assumed that the leg is reset to an angle fixed in the inertial frame. This implies that exproprioceptive feedback is used. What if this is not the case?

In Figure 4.6 columns (a) and (b), we show the eigenvalue of Trunk-SLIP with proprioceptive feedback during flight. To test all combinations of feedback, we varied the feedback during stance such that the hip torque is controlled either by (a) proprioceptive or (b) exproprioceptive feedback. As observed in Figure 4.6(a)-(b), the eigenvalue magnitude remains above one despite varying system parameters. No stable solutions were found with proprioceptive feedback during flight regardless the type of feedback used during stance.

Case (c) exproprioception during Flight, Proprioception in Stance: The trunk-SLIP with exproprioceptive feedback used during the flight phase and proprioceptive feedback during the stance phase was then studied. Stable solutions were found. In Figure 4.6 column (c), the lowest attainable max eigenvalue is shown to approach a magnitude of 0.9, a value below 1. The locomotion model can be best stabilized when the leg landing angle β_r is around 67°, which is a representative value for human running [19].

It is surprising that stable motion is possible in this case given the results for the unstable case (b), with exproprioception in stance and proprioception in flight. Given that stable locomotion can be achieved with proprioception in stance, but not when proprioception is used in flight, suggests that the feedback that occurs during the flight phase of motion is either more sensitive or more critical (or both).

Case (d) exproprioception during Flight, exproprioception in Stance: The trunk-SLIP with exproprioceptive feedback throughout the whole stride (feedback used during the flight phase and stance phase of motion) was then studied. Stable solutions were found. In Figure 4.6 column (d), the best attainable eigenvalue is shown to approach a magnitude of 0.9, a value below 1. The locomotion model can be best stabilized when the leg landing angle β_r is around 67°, which is a representative value for human running [19].

Interestingly, the small perturbation stability, measured by the eigenvalue, is similar for both case (d) and (c). Since case (c) has no exproprioceptive feedback, we hypothesized that its stability would not be as good as case (c), and that it may not achieve stable locomotion at all. The optimal eigenvalues for both control strategies are similar in magnitude, mostly around 0.9 when different parameters are varied. The Trunk-SLIP model with exproprioceptive feedback controlled hip torque can be stabilized over a wider parameter range but otherwise does not appear to confer other substantial benefits or value over proprioceptive feedback during stance. This is a surprising result.

This result for case (d), along with the result for case (c) implies that feedback during the flight phase of motion is more critical to the overall stability of locomotion. This could potentially be because there are fewer means for passive dynamic correction that can occur during the flight phase of motion relative to the stance phase of motion, and so exproprioception is more critical during that phase.

Stability Versus Feedback Control Type and Physical Leg Parameters:

Other parameters that are likely to be varied during locomotion are the effective leg damping and stiffness. In Figure 4.7 we show the maximum eigenvalue for all four cases of feedback considered, versus these two physical leg parameters: damping c and stiffness k. We find that for the cases of exproprioceptive feedback in flight (c)-(d), the system can achieve stable locomotion if the damping and stiffness are

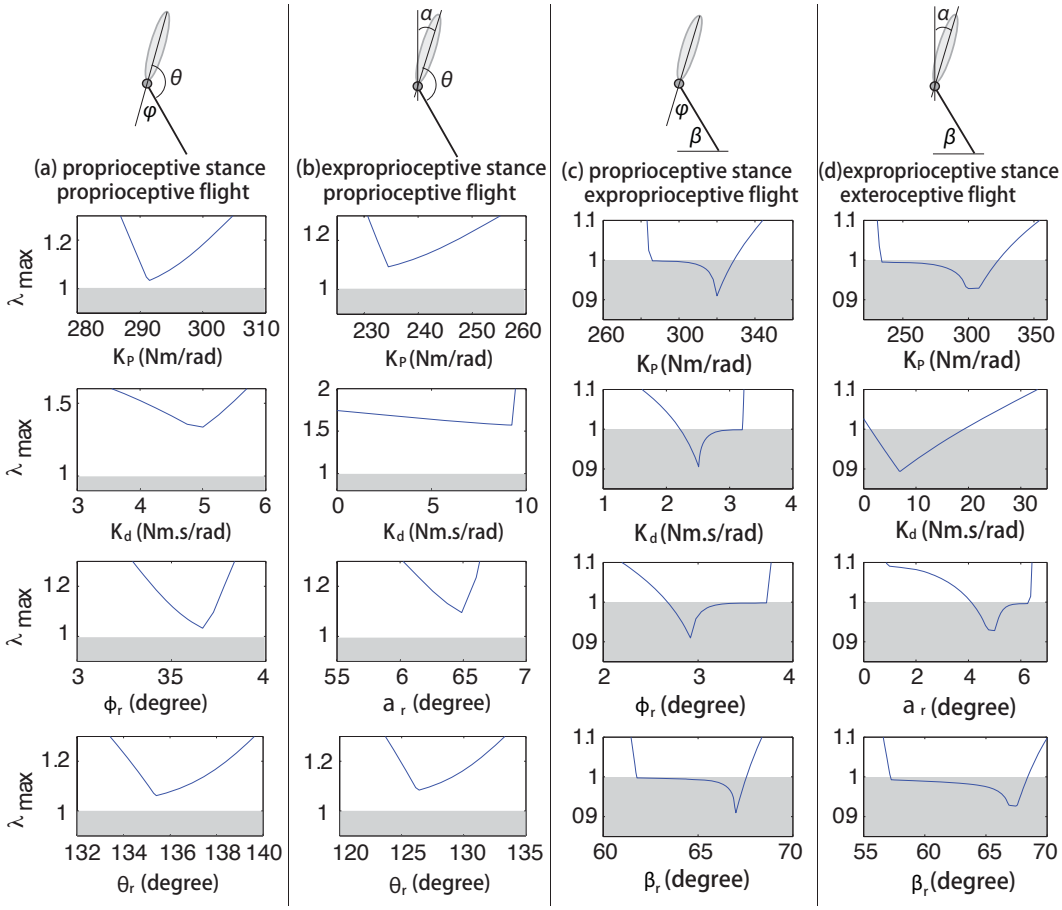

Figure 4.6. The maximum eigenvalue of the fixed points of Trunk-SLIP versus feedback control gains and reference values, where each column shows results for four different cases of feedback. The shaded region stands for the stable region. Human-representative parameters as shown in Table 4.1 are used. For each parameter variation, we began with a nominal fixed point and system parameters, and then varied the control parameters one-by-one (keeping the other parameters the same as the nominal case). The nominal periodic solutions and the control parameters used are listed in Table 4.2.

selected from an intermediate range of values. These values are physically reasonable when compared to estimated effective leg stiffness values for humans [47]. It is also apparent that in the case (d) of exproprioception throughout the entire stride, the

Table 4.2 Nominal feedback control parameters and periodic solutions.

		Nominal Values for Cases:				
Parameter	Description	(a)	(b)	(c)	(d)	Units
K_p	proportional gain	320	300	320	300	Nm/rad
K_d	derivative gain	2.5	5	2.5	5	Nms/rad
ϕ_r	proprioceptive trunk reference	2.92	–	2.92	–	deg
α_r	exproprioceptive trunk reference	–	5	–	5	deg
θ_r	proprioceptive leg reference	143	143	–	–	deg
β_r	exproprioceptive leg reference	–	–	67	67	deg
v^*	solution speed	4.74	4.78	4.74	4.78	m/s
δ^*	solution velocity angle	16.1	15.3	16.1	15.3	deg
α^*	solution trunk angle	13.8	12.8	13.8	12.8	deg
$\dot{\alpha}^*$	solution trunk angular speed	14.0	−7.7	14.0	14.0	deg/s

range of stiffness and damping values for which stable solutions exist is wider than the case of (c) proprioception used for stance.

4.4.2 Stability with Respect to Large Perturbations: Basins of Attraction

In this section we investigate further the stable cases of feedback, (c) and (d), by determining how these to cases respond to large perturbations. To measure the large perturbation response and stability of locomotion, basins of attraction are calculated. For the cases (a) and (b), with proprioception during flight, we found no stable locomotion solutions, and so these cases have no basin of attraction.

In Figure 4.8, we show the basin of attraction in terms of the pitching variables α and $\dot{\alpha}$. Note: as the full stride map representing the dynamics of locomotion solutions has four variables (v,δ,α,$\dot{\alpha}$), we plot slices of two variables at a time in order to provide some insight into the four-dimensional basin of attraction. Therefore, in this figure we test the response to large perturbations in the pitching variables α and $\dot{\alpha}$, but the CoM velocity magnitude and angle (v_0,δ) are not perturbed from their fixed point values.

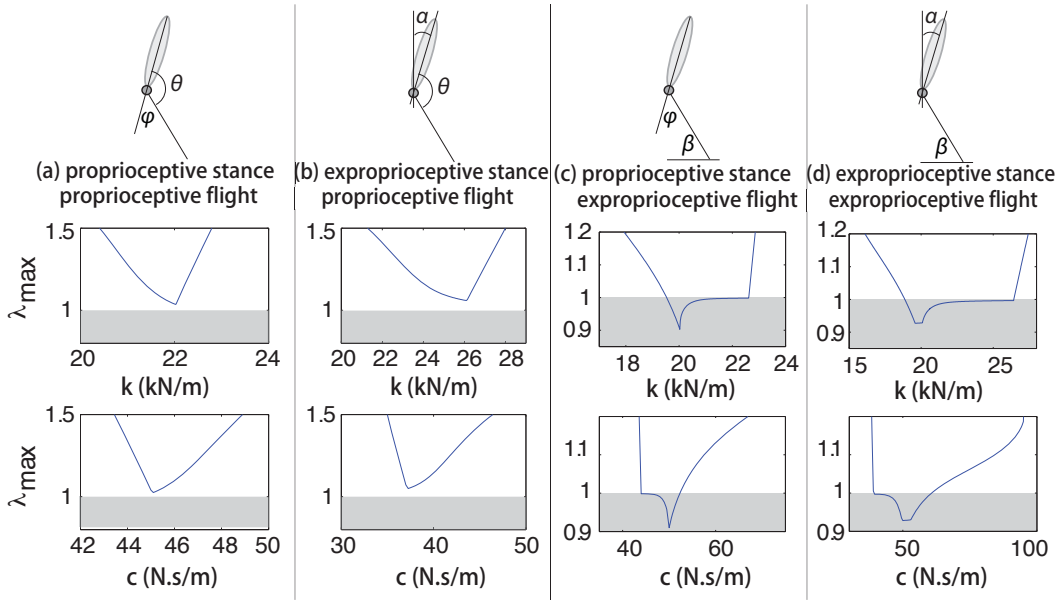

Figure 4.7. The maximum eigenvalue of the fixed points of Trunk-SLIP versus leg stiffness and leg damping, where each column shows results for four different cases of feedback. In each row, one model parameter is varied while the rest of model parameters are kept the same as those listed in Table 4.2.

The blue region in each panel stands for the basin of attraction for the fixed point solutions of each feedback case that were found to have the most stable eigenvalues in the previous section. Here the basin of attraction is defined as the region of initial conditions from which Trunk-SLIP returns to within a small neighborhood of the fixed point within 300 steps. The small neighborhood was defined to be when the difference between the current speed v_0 and fixed point speed v^* is less than 0.05 m/s, the difference between current touchdown velocity angle δ and fixed point velocity angle δ^* is less than 0.035 rad, the difference between the current trunk angle α and fixed point trunk angle α^* is less than 0.018 rad, and the difference between the current trunk angular speed $\dot{\alpha}$ and fixed point trunk angular speed $\dot{\alpha}^*$ is less than 0.018 rad/s. When the model initial condition is set to any point within the region, it will eventually return back to the original periodic motion (or fixed point in this view).

The possible absolute trunk position that is allowed is constrained between $-90°$ and $90°$ to be realistic. Similarly, the trunk angular speed is constrained between $-90°/s$ and $90°/s$.

In a rows of Figure 4.8, we show the basins of attraction of Trunk-SLIP in terms of pitching variables (α,$\dot{\alpha}$), and in another row the CoM translation variables (v,δ). Given that the mapping from touchdown to next touchdown involves four states defining pitching and center-of-mass motion, we cannot display the full four-dimensional basin of attraction on one plot. Therefore, we show two-dimensional slices in this larger four-dimensional space.

In Figure 4.8, it is shown that the case with exproprioception during stance has a larger basin of attraction than the case with proprioception during stance. Further, the stability for the proprioceptive feedback case is not robust in terms of CoM translation. As shown in Figure 4.8(a), the fixed point labeled as the red dot is close to the boundary of the basin of attraction. A moderate decrease in touchdown velocity magnitude v_0 could lead to the system crashing. Despite some of these differences, overall, the basins of attraction of the (c) stance proprioception and (d) stance exproprioception cases are similar.

4.4.3 Combined Feedback During Stance

Here, we add an extra final case to determine the effects of combining both proprioceptive and exproprioceptive feedback during stance. The combination or integration of these two feedback pathways could take on complex forms. Here, to gain an initial understanding and keep the overall analysis simple, we use a straightforward linear superposition of the proprioceptive and exproprioceptive feedback pathways previously studied in order to create a combined feedback scenario. Could this lead to a significant improvement in stability or make it worse?

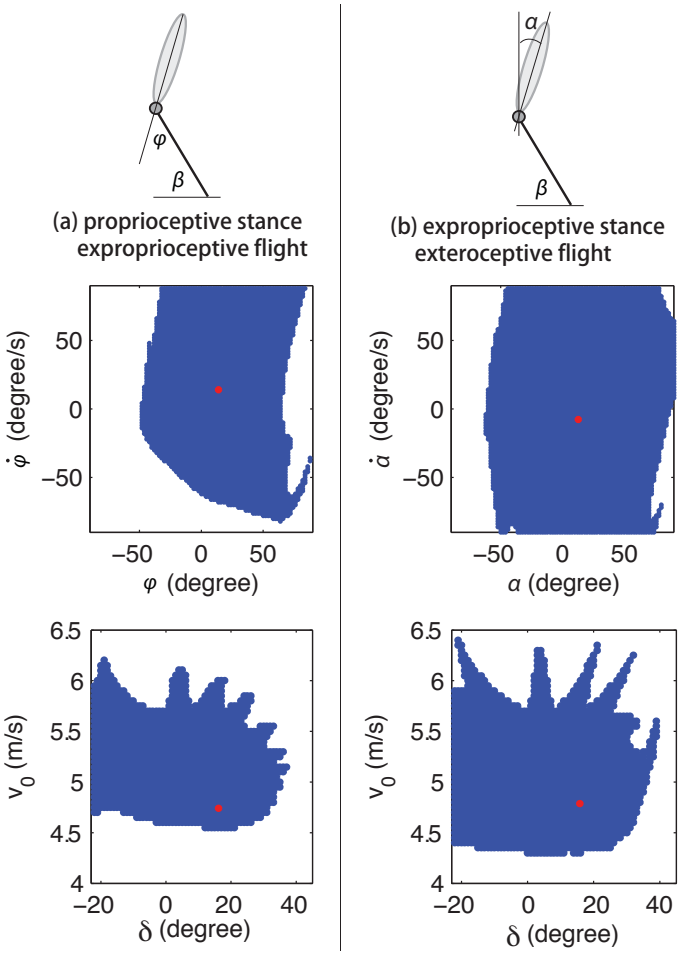

Figure 4.8. Columns (a) and (b) show the basin of attraction of Trunk-SLIP with proprioceptive feedback and exproprioceptive feedback respectively. The red dot in each panel stands for the corresponding fixed point. The model parameters and fixed point values for (a) and (b) are the same as those in Figure 4.6.

For this case of the Trunk-SLIP model with both sensory feedback pathways during stance, its hip torque can be determined as:

$$\tau_n = K_p^{ext}(\alpha - \alpha_r) + K_d^{ext}\dot{\alpha} + K_p^{pro}\phi + K_d^{pro}\dot{\phi}\,. \tag{4.17}$$

Where K_p^{ext}, K_d^{ext} are exproprioceptive feedback gains, K_p^{pro}, K_d^{pro} are proprioceptive feedback gains, and α_r is the reference position. During flight, the leg is reset using exproprioceptive feedback.

The stable periodic solutions of Trunk-SLIP with combined feedback were found using the same parameters as used for case (c) and (d) (excluding the hip torque control parameters). The hip torque control parameters ($K_p^{ext}, K_d^{ext}, K_p^{pro}, K_d^{pro}$ and α_r) were varied systematically nearby the previously used values, in order to find a local best case of locomotion stability.

First, a local best fixed point is found. Its corresponding hip torque control parameters are: $K_p^{pro} = 60, K_d^{pro} = -3.007, K_p^{ext} = 180.7, K_d^{ext} = 18.7$ and $\alpha_r = 9.29°$. The corresponding fixed point values are: $4.83m/s$, $13.64°$, $12.32°$, $-3.51°/s$.

Pitching stability was found to be improved by this simple combination of feedback pathways. As shown in Figure 4.9, the entire basin of attraction is much larger when compared with cases (c) and (d) in Figure 4.8. Thus, Trunk-SLIP with combined sensory feedback can resist a significantly larger perturbation in the trunk pitching states when compared to Trunk-SLIP with a single feedback pathway used. The translational dynamical stability of the center of mass does not change nearly as much. The overall size of the basin of attraction is mostly unchanged for those directions of the system state space.

Combining feedback pathways during the flight phase yields a simple result, due to the negligible mass of the leg. Effectively, the leg will quickly swing to an equilibrium position somewhere between the proprioceptive and exproprioceptive reference angles. This equilibrium position depends on the relative strengths of the feedback gains. We showed that for cases (a) and (b), no stability was found. Therefore, we used only exproprioceptive feedback in flight when studying the effects of combined feedback, and instead allowed combination during the stance phase.

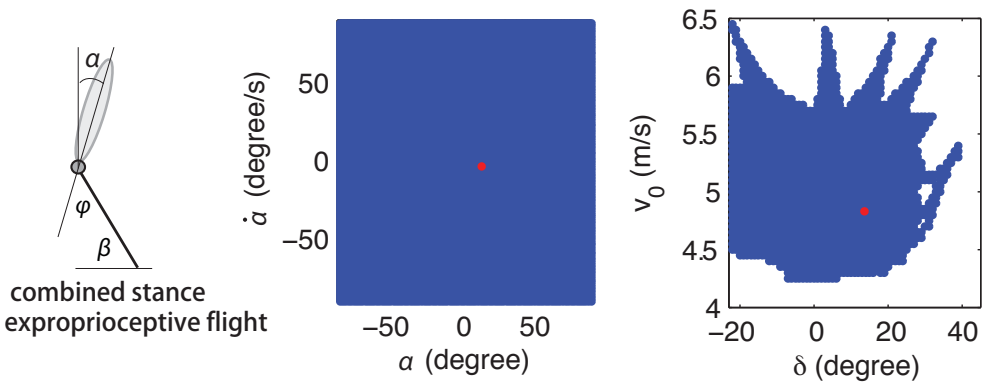

Figure 4.9. The basin of attraction of Trunk-SLIP with combined proprioceptive and exproprioceptive feedback. The red dot in each panel stands for the periodic running solution fixed point. The basin of attraction shown is the region of initial conditions from which Trunk-SLIP returns to within a small neighborhood of the fixed point within 300 steps.

4.5 Discussion and Conclusion

Hip-based locomotion, like above-knee amputee running and recent attempts at bipedal legged robot running, is an extreme under-actuated case of locomotion for which it is difficult to simultaneously stabilize translation and pitching dynamics in the sagittal plane. Currently, there is no complete explanation for how above-knee amputees accomplish such amazing athletic running despite lost limb function, and current attempts at bipedal hip-actuated robots are not based upon basic knowledge of how hip-based locomotion works, as such a body of knowledge does not yet exist, and so such robot development depends on the creative intuition and hypotheses of roboticists. Here, we aimed to provide some basic knowledge of hip-based locomotion, and expect it may yield insights for legged locomotion in general.

To provide foundational knowledge for how the dynamics and control of hip-based legged locomotion work, we compared four basic neural feedback architectures involving different combinations of proprioceptive and exproprioceptive during flight and stance phases of motion. Given that there is only one leg actuator at the hip,

the feedback is used to apply a hip torque during stance and to reset the leg to a desired position during the flight phase. In all of these cases, during each phase of the stride, a proportional and derivative control was applied with respect to the measured state (a leg or trunk angle) in order to produce a torque at the hip. We used a mathematical modeling and analysis approach to study alternative feedback architectures as it allows manipulation of sensory feedback and accurate analysis that is currently not feasible in animal experiments.

Quantification of locomotion stability: In this study we report the small perturbation stability (eigenvalues) and large perturbation stability (basins of attraction) for each case of feedback considered, and also determine how stability depends on the control and physical parameters of the system for each case. This goes much further than reporting the quality of stability. We have systematically quantified the eigenvalues and basins of attraction as well as determined where in the system parameter space the most stable solutions are found. Such quantitative results are useful for the generation of specific testable hypotheses and for applications of this knowledge to motion-related training/therapies/treatments, prostheses, and legged robots.

Well-tuned parameter ranges for achieving stability: We discovered that while stability is possible for some of the feedback cases tested, it is necessary to have well-tuned system parameters. The results reported here provide a good guide and starting point for testable hypotheses and designs regarding the system control and physical parameters. We found, for example, that intermediate ranges of many of the system parameters were needed to achieve stable locomotion solutions. If the system parameters were too low or too high, then stability was not achieved.

Large perturbation measures like basins of attraction are particularly useful: For the cases of stable locomotion reported in this chapter, the most stable small perturbation response found was when the maximum eigenvalue has a value close to 0.9. While this is not a good eigenvalue for quick reduction of errors or perturbations, it is also not a useful measure for the overall stability of the system which undergoes much larger perturbations and responds in a nonlinear manner (such

that eigenvalues are not good predictors of large perturbation response). Whether the eigenvalues are stable (max eigenvalue magnitude less than one) or not, does tell us whether there will be a stable periodic solution at all. However, given the nonlinear behavior of locomotion systems, it is not a good predictor of behavior for large perturbations, and does not provide a measure of how large perturbations can get before the system fails. To quantify large perturbation stability, we calculated the basin of attraction (the region of perturbed states that will return to a given periodic locomotion solution). Understanding first how large the systems basin of attraction is likely of higher priority to a moving animal than how fast it responds to a small perturbation, in part because a small basin of attraction almost certainly means falling down, whereas a fast response to a small perturbation may not matter much in practice when small perturbations are regularly occurring. Therefore, our primary focus is on the basin of attraction as a tool for quantifying stability, and we use eigenvalues as a quick numerical tool to inform when stability exists or does not exist in the parameter space of the system. As was reported in previous sections, the cases of stable locomotion reported were found to be relatively robust with significant-sized basins of attraction.

Unexpected results: As expected, the two extremes of the feedback cases (a) proprioception throughout the whole stride, and (d) exproprioception throughout the whole stride, were found to be, respectively, unstable and stable. However, the investigation of the intermediate cases of feedback (b)-(c) yielded multiple surprising results.

exproprioception is critical during the flight phase of motion: Cases (b) and (c) were expected to yield similar overall unstable locomotion since both have a portion of the stride where only proprioceptive feedback is present. The rationale for our original hypothesis was that since only a portion of the stride utilized inertial frame feedback to achieve stability when (b) exproprioception was used in stance and proprioception in flight, than this portion of exproprioception could just as well occur during flight rather than stance and lead to similar overall locomotion

dynamics. However, these two cases actually differed significantly. Surprisingly, case (b) is unstable while case (c) can achieve a stable basin of attraction. What is the difference between these two cases and does it make sense why case (c) turned out stable, rather than case (b)? The differences found between these cases implies that exproprioception is critical during flight to achieve stability, whereas it is not critical during the stance phase. Why might this be the case? One possibility is that since legs are not in contact with the ground during the flight phase, there are no passive dynamic means of "mechanical feedback" that can help stabilize the system, and so exproprioception is more critical during flight than it is during stance. The differences discovered for case (b) and (c) has further implications in terms of where we expect to see more exproprioceptive feedback in above-knee amputee runners, and perhaps the general human population as well.

Proprioception in stance is a close second to exproprioception: Our original expectation was that stable locomotion might not be achieved unless exproprioception was used throughout the entire stride. If stable locomotion was achieved at all when proprioception was used instead of exproprioception, we expected it to be of a significantly lower quality. Surprisingly, this did not turn out to be the case in our study. We discovered that the case (c) with proprioception during stance, could achieve a nearly identical range of eigenvalues with a basin of attraction only fractionally smaller when compared to case (d) with exproprioception used during stance. This result implies that exproprioceptive feedback is not critical in stance and does not yield a strong quantitative benefit over proprioceptive feedback. We expect that proprioception can perform the same critical functions as exproprioception during te stance phase of animal or robot locomotion. We hypothesize that proprioception will be used during the stance phase of above-knee amputee runners as well as other legged animals, especially since it can be less sensitive to time delays and errors in the neural feedback loop as exproprioception (in part because proprioceptive feedback could potentially be achieved using neural (electrical) feedforward mechanisms due to passive mechanical feedback of muscles or elastic actuators).

Combining proprioceptive and exproprioceptive feedback improves stability: In reality, it is likely that both exproprioceptive and proprioceptive feedback pathways are simultaneously available for above-knee amputees or even hip-based robots to utilize at the same time. We therefore also tested the case where both exproprioception and proprioception are combined for the feedback control of hip torque during the stance phase of motion, using a simple linear superimposition. We found that, overall, the pitching stability is significantly improved from this combined approach, as the size of the basin of attraction increased substantially. We therefore expect that humans and other bipedal animals use a similar combined feedback approach to control pitching dynamics.

Direct Applicability to Hip-Based Locomotion: The knowledge generated by this work has direct and immediate application for the design and analysis of hip-based legged robots, and for the development of new hypotheses of how above-knee amputees run and walk, as well as new insights for the development of training methods to help above-knee amputees learn to walk and run again. Despite limitations of the model, it is able to capture the basic dynamics underlying hip-based locomotion such as hip-driven springy-leg robots and above-knee amputees running on prostheses.

The objective of this study was to provide basic knowledge regarding how different feedback pathways in stance and flight can affect the stability of hip-based locomotion in the sagittal plane. Overall, the results reported here have provided some new insights into legged locomotion, as well as categorical knowledge about the types of stability achieved by different combinations of feedback in stance and flight, along with quantitative predictions for the desired ranges of parameters that would yield basic stability. The work presented here is expected to enable future studies of hip-based locomotion, new hypotheses for amputee locomotion, as well as design guidelines for hip-based robots.

5. A MODEL BASED HIERARCHICAL CONTROL STRATEGY

5.1 Background

Above knee amputee athletes in Paralympic Games demonstrated that stable running motion with regulated trunk is possible with largely hip torque actuation. However, there exists a gap between the stability of current bipedal robots and the kind of stability observed in above knee amputee running. One reason could be that the controller design and tuning process remains to be complicated due to a large number of system degrees of freedom.

Here, we seek to develop a hierarchical controller design and tuning strategy for hip torque actuated robots to achieve above knee amputee like stable running motion. It is known that mammal neocortex are physically constructed layer by layer [107, 108]. In addition, the patterns recognized by neocortex are arranged in hierarchy [109]. Inspired by these findings, we propose a hierarchical control approach to stabilize hip torque based bipedal running. To allow quick testing of the controller, we rely on numerical simulation of a locomotion model where different layers of control elements can be applied.

In Figure 5.1, we propose a new control architecture with four layers: (1) real time layer (marked as dark gray) where real time hip torque controllers are placed at, (2) discrete event to event layer (marked as medium gray) where a transition regulator updates real time control parameters every time a leg touchdown or liftoff happens. It is in place to ensure smooth transition back to the steady state once perturbed. (3) The hierarchical control also includes a discrete stride to stride layer (marked as light gray) where speed regulator updates transition regulator parameters to ensure accurate speed control, and (4) adaptation layer (marked as the dashed line) where the commanded speed is adapted to achieve a higher level target such as a smooth

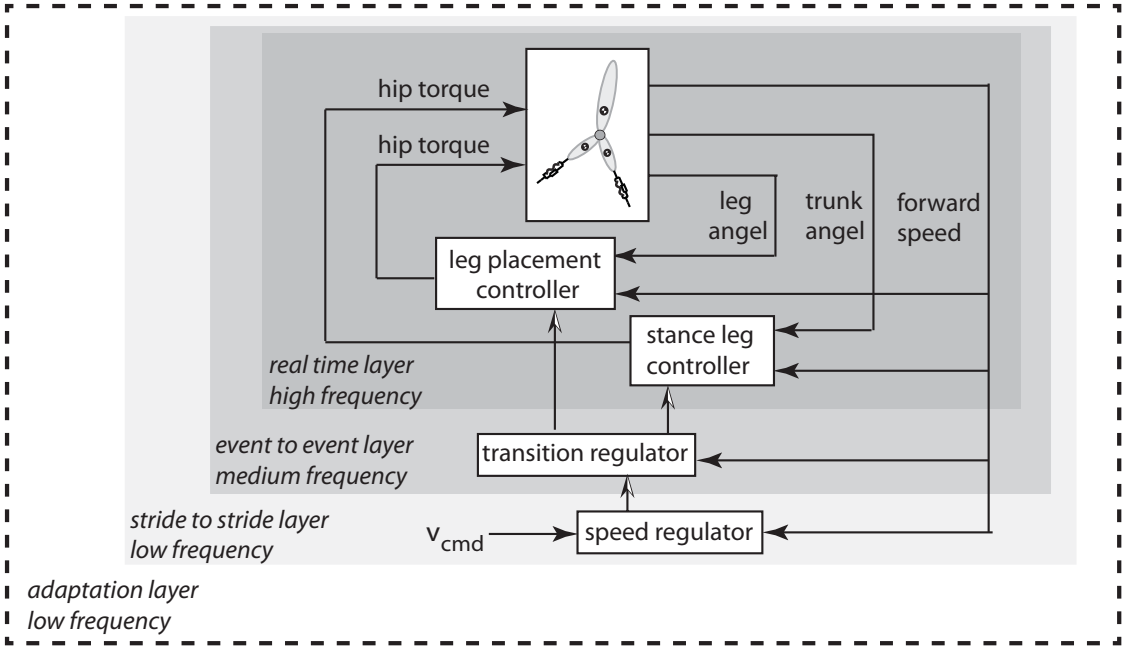

Figure 5.1. The overall control structure. The white boxes and arrows stands for control element and the direction of information flow. v_{cmd} stands for the commanded speed set point. Three types of sensory information sampled are: leg angle, trunk angle and forward speed. Torques from left and right leg are effective control actions.

walk/run transition. Here we focus on the first three layers to produce robust periodic running motion. The design of the fourth layer is future work and not covered in this thesis.

This layer by layer approach has the advantage of faster controller prototyping and tuning, as shown in Figure 5.2. It first starts with simple control where parameters can be easily tuned to obtain stable motion. An additional layer is then added upon the previously well tuned layers. Therefore, despite growing control complexity as layers are added, the number of parameters to be tuned remains small at each step. In contrast, when all the control parameters are tuned at the same time, the process is more complicated. In principle, for simultaneous tuning, a global optimal solution could be obtained. However, even if such a global optimal exists, it is in reality

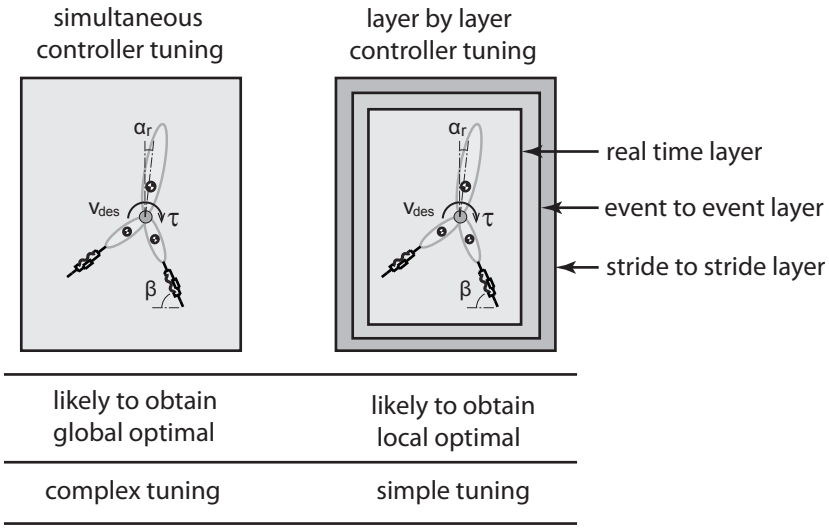

Figure 5.2. The advantage and disadvantage of two tuning methods.

challenging to find due to the control complexity. For the layer by layer controller tunning, despite the fact that a local optimal solution is usually obtained, the overall motion stability could still be substantially improved as different layers are gradually added.

5.2 Approach

One common strategy of exploring legged locomotion is modeling and analysis with simplified dynamical models [1]. This modeling approach allows accurate control of various studies which are challenging for animal or human experiments. Here we intend to develop a locomotion model representative of above knee amputees.

5.2.1 Modeling Background

During the past few years, there has been development of trunk pitching control strategies on locomotion models with trunk pitching [35, 47, 62, 63]. These models typically consist of a rigid body trunk and massless springy legs. A traditional

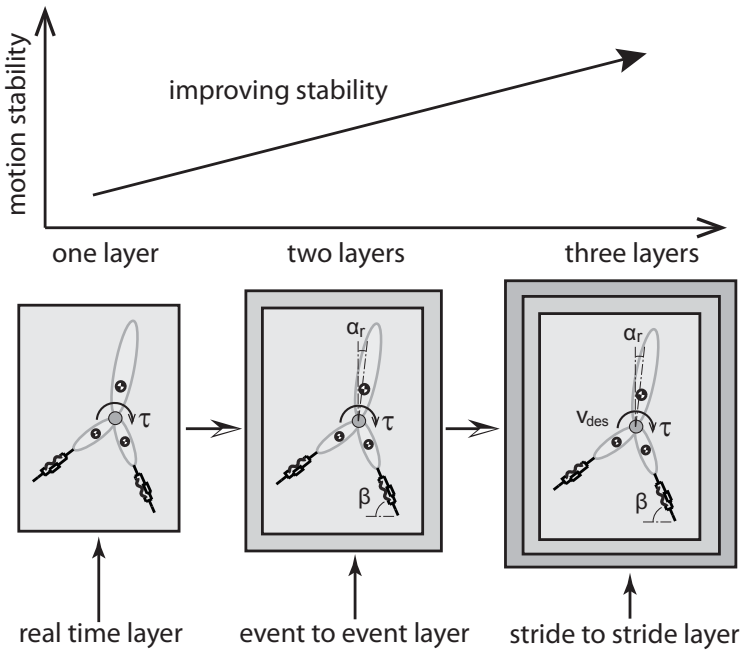

Figure 5.3. Stability improves when different layers are gradually added.

method, known as the Raibert's approach [63] was to effectively utilizing three separate controllers to regulate robot hopping motion with a trunk body. To regulate peak center-of-mass height, active thrust along the leg is required as a control action which is challenging to produce for above knee amputees without active knee and ankle joints. Another strategy called virtual pivot point (VPP) [47,64] is developed based on a bipedal Spring-Loaded Inverted Pendulum (SLIP) model by replacing the point mass with a realistic trunk as the body. It uses a controlled hip torque to redirect ground reaction forces so that overall pendulum like pitching behaviors can be realized and stabilized. Another approach uses the concept of hybrid zero dynamics and SLIP embedding [35,49] to systematically design a feedback type controller for overall locomotion stabilization including trunk pitching. However, both the VPP and SLIP embedding approaches require real time sensory feedback of leg length which is not feasible for above knee amputees.

Recently, it is demonstrated that above knee amputee like stable locomotion with only hip actuation and passive legs is possible for bipedal robots [62]. Based on the quadrupedal robot RHex [36, 60] which has damped springy legs, a bipedal version of RHex [62] is developed. It is capable of stable bipedal running, including body pitching. Its overall control strategy consists of a body pitching Proportional-Derivative (PD) controller, a forward speed proportional controller and a leg trajectory PD controller. For bipedal RHex, the hip motor actively tracks the time based desired leg trajectory without knowing the actual torque applied. In addition, the robot is unaware if it is in stance or flight as the leg touchdown and liftoff are not detected. Unlike bipedal RHex whose hip torque is implicitly controlled and locomotion phase unperceived, we propose a control approach where hip torque is explicitly controlled and locomotion phase actively detected. What is more, the proposed approach differs from the bipedal RHex by having a hierarchical structure to promote a fast controller prototyping.

5.2.2 Extended Trunk-SLIP

In order to systematically understand how different control elements could affect the overall locomotion stability, a base model where different control elements can be gradually applied upon is developed. Unlike the existing models with massless legs where flight dynamics are usually omitted, a model with realistic trunk and thigh mass is developed as shown in Figure 5.4.

Due to thigh masses, hip torque needs to be applied to swing the leg forward during flight phase. However, the shank is assumed to be massless and springy. For above knee amputee runners, the artificial shank is usually made of light materials such as carbon fiber. Therefore, we assume the shank mass is negligible compared to thigh and trunk masses. Here a human related parameter set is used for this model as shown in Table 5.1.

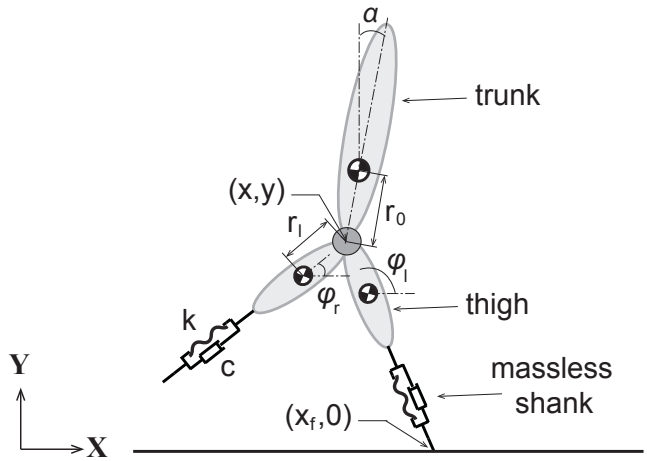

Figure 5.4. The extended Trunk-SLIP model with rigid body thigh and massless shank. The hip position can be described by coordinates x and y, while the position of the contacting foot can be described by x_f. The angular orientation of three rigid bodies are defined as α, ϕ_l and ϕ_r. r_0 and r_l are distances from hip to trunk center-of-mass and thigh center-of-mass respectively. The massless shank is assumed to be springy and damped with stiffness k and linear damping coefficient c.

Table 5.1 Physical parameters for extended Trunk-SLIP.

Constant	Description	Value	Units (SI)
g	gravitational constant	9.81	ms^{-2}
m_b	body mass	55	kg
m_l	leg mass	10	kg
I_b	body moment of inertia	5	kgm^2
I_l	leg moment of inertia	1	kgm^2
l_0	leg resting length	0.9	m
r_0	distance from hip to body mass center	0.2	m
r_l	distance from hip to thigh mass center	0.25	m
k	shank spring stiffness	10	kN/m
c	shank damping	100	Ns/m

Similar to Hip-actuated SLIP, the motion and dynamics of extended Trunk-SLIP consists of two stages: stance and flight. The stance phase starts with one leg touch-

ing the ground. Then the stance leg swings forward about the ground contacting point until the vertical component of the ground reaction force becomes zero. In the meantime, another leg swings forward and prepares for the next landing. Upon liftoff, the model enters the flight mode. Both torques from left and right hip are then used to redirect the leg towards a desired leg landing angle. When one of the feet hits the ground, the model enters the stance phase. A complete stride consists of four phases: left leg stance, flight, right leg stance, flight.

5.2.3 Flight Dynamics

Here we derive the equations of motion for extended Trunk-SLIP using the canonical TMT method. The TMT method generates factorized equations of motion in matrix form and is friendly to numerical simulation.

During the flight phase, the posture of extended Trunk-SLIP can be described by a set of general coordinates $\mathbf{q} = [x, y, \alpha, \phi_l, \phi_r]^T$ as shown in Figure 5.4. The equations of motion for the general coordinates are then generated using TMT method.

$$\mathbf{T}^T\mathbf{M}\mathbf{T}\ddot{\mathbf{q}} + \mathbf{T}^T\mathbf{M}\mathbf{D} = \mathbf{T}^T\mathbf{F} \tag{5.1}$$

The matrices in the above equation can be formulated as:

$$\mathbf{T} = \begin{bmatrix} 1 & 0 & 0 & 0 & -r_0\cos(\alpha) \\ 0 & 1 & 0 & 0 & r_0\sin(\alpha) \\ 0 & 0 & 0 & 0 & 1 \\ 1 & 0 & r_l\sin\phi_l & 0 & 0 \\ 0 & 1 & -r_l\cos\phi_l & 0 & 0 \\ 0 & 0 & 1 & 0 & 0 \\ 0 & 0 & 0 & r_l\sin\phi_r & 0 \\ 0 & 0 & 0 & -r_l\cos\phi_r & 0 \\ 0 & 0 & 0 & 1 & 0 \end{bmatrix} \tag{5.2}$$

$$\mathbf{M} = diag([\ m_b \quad m_b \quad I_b \quad m_l \quad m_l \quad I_l \quad m_l \quad m_l \quad I_l\ ]) \tag{5.3}$$

$$\mathbf{D} = [\ -r_0\dot{\alpha}^2 \sin\alpha \quad -r_0\dot{\alpha}^2 \cos\alpha \quad 0 \quad r_l\dot{\phi_l}^2 \cos\phi_l \quad r_l\dot{\phi_l}^2 \sin\phi_l \quad 0 \quad r_l\dot{\phi_r}^2 \cos\phi_r \quad r_l\dot{\phi_r}^2 \sin\phi_r \quad 0\ ]^T \tag{5.4}$$

During the flight phase, only gravity and hip torques affect the overall motion. Therefore the force vector $\mathbf{F}$ is described as follows:

$$\mathbf{F} = [\ 0 \quad -m_b g \quad \tau_l + \tau_r \quad 0 \quad -m_l g \quad -\tau_l \quad 0 \quad -m_l g \quad -\tau_r\ ]^T \tag{5.5}$$

5.2.4 Stance Dynamics

Stance dynamics differ from flight dynamics mostly in two aspects. First, the stance leg spring force is non zero and affects the overall motion. In addition, a kinematic constraint is imposed during stance. For instance, when the left leg is on ground:

$$y\cos\phi_l + (x_f - x)\sin\phi_l = 0 \tag{5.6}$$

To accommodate this kinematic constraint, we employ the concept of Lagrangian Multiplier, in this case f_l where the subscript means left leg. Also, an additional force vector is included to represent the effect of spring force. Then new equations of motion during stance are:

$$\mathbf{T}^T\mathbf{M}\mathbf{T}\ddot{\mathbf{q}} + \mathbf{T}^T\mathbf{M}\mathbf{D} = \mathbf{T}^T(\mathbf{F} + \mathbf{F_{al}}) + \mathbf{J_l}^T f_l \qquad \mathbf{J_l}\ddot{\mathbf{q}} + C_l = 0 \tag{5.7}$$

Where $\mathbf{F_{al}}$ stands for the additional spring force vector when the left leg is on ground.

$$\begin{aligned}
\mathbf{F_{al}} &= [\,0 \quad 0 \quad 0 \quad f_s\cos\phi_l \quad f_s\sin\phi_l \quad 0 \quad 0 \quad 0 \quad 0\,]^T && (5.8)\\
\mathbf{J_l} &= [\,\sin\phi_l \quad -\cos\phi_l \quad y\sin\phi_l + (x-x_f)\cos\phi_l \quad 0 \quad 0] && (5.9)\\
C_l &= 2\dot{\phi}_l\dot{x}\cos\phi_l + 2\dot{\phi}_l\dot{y}\sin\phi_l + \dot{\phi}_l^2 y\cos\phi_l + \dot{\phi}_l^2 x_f\sin\phi_l - \dot{\phi}_l^2 x\sin\phi_l && (5.10)
\end{aligned}$$

Where f_s stands for leg force along the leg due to spring.

$$f_s = k(l_0 - l) - c\dot{l} \tag{5.11}$$

Where leg length l and speed $\dot{l}$ can be calculated using the following equations using general coordinates and foot positions.

$$l = \sqrt{(x-x_f)^2 + y^2} \qquad \dot{l} = [(x-x_f)\dot{x} + y\dot{y}]/l \tag{5.12}$$

Similarly, when the right leg is on ground. The equations of motion are

$$\mathbf{T}^T\mathbf{M}\mathbf{T}\ddot{\mathbf{q}} + \mathbf{T}^T\mathbf{M}\mathbf{D} = \mathbf{T}^T(\mathbf{F} + \mathbf{F_{ar}}) + \mathbf{J_r}^T f_r \qquad \mathbf{J_r}\ddot{\mathbf{q}} + C_r = 0 \tag{5.13}$$

$$\begin{aligned}
\mathbf{F_{ar}} &= [\,0 \quad 0 \quad 0 \quad 0 \quad 0 \quad 0 \quad f_s\cos\phi_r \quad f_s\sin\phi_r \quad 0\,]^T && (5.14)\\
\mathbf{J_r} &= [\,\sin\phi_r \quad -\cos\phi_r \quad 0 \quad y\sin\phi_r + (x-x_f)\cos\phi_r \quad 0] && (5.15)\\
C_r &= 2\dot{\phi}_r\dot{x}\cos\phi_r + 2\dot{\phi}_r\dot{y}\sin\phi_r + \dot{\phi}_r^2 y\cos\phi_r + \dot{\phi}_r^2 x_f\sin\phi_r - \dot{\phi}_r^2 x\sin\phi_r && (5.16)
\end{aligned}$$

While spring force along the leg f_s can be calculated using Equation 5.11.

5.2.5 Switching Conditions

Each stride consists of alternating stance and flight phases. Here we define the switching conditions between stance and flight phases. We define touchdown as the event when the foot hits the ground:

$$y = l_0 \sin\phi_l \text{ for left leg} \qquad y = l_0 \sin\phi_r \text{ for right leg} \tag{5.17}$$

At touchdown, we assume an impulse is applied to leg to bring the foot speed to zero instantaneously. Any impulse along the leg is ineffective to thigh and trunk rigid bodies due to the buffering of shank spring. For above knee amputees, the springy leg absorbs most of impact along the leg. However, the impulse perpendicular to the leg changes system states instantaneously. The system states after foot collision can be solved using theorems of angular, linear momentum conservation and the imposing kinematic constraint equation.

First, the angular momentums of trunk and flight leg are conserved about hip joint. Without loss of generality, we derive the equations while assuming left leg touches the ground:

$$m_l r_0 \dot{x} \sin\phi_r - m_l r_l \dot{y} \cos\phi_r + (m_l {r_l}^2 + I_l)\dot{\phi}_r = constant1 \tag{5.18}$$

$$-m_b r_0 \dot{x} \cos\alpha + m_b r_0 \dot{y} \sin\alpha - (m_b {r_0}^2 + I_b)\dot{\alpha} = constant2 \tag{5.19}$$

Similarly, whole body angular momentum is conserved about the ground contacting point. In addition, whole body linear momentum along the stance leg is conserved. Therefore, two addition equations can be obtained as follows:

$$\begin{aligned}
[m_l({r_l}^2 - xr_l\cos\phi_l - yr_l\sin\phi_l) + I_l]\dot{\phi}_l + m_b x\dot{y} - m_b y\dot{x} + \\
+ m_l\dot{x}(r_l\sin\phi_l - 2y) - m_b\dot{\alpha}(xr_0\sin\alpha + yr_0\cos\alpha) + \\
+ m_l\dot{y}(2x - r_l\cos\phi_l) + m_l\dot{\phi}_r(-xr_l\cos\phi_r - yr_l\sin\phi_r) &= constant3 \quad (5.20) \\
(m_l r_l\sin\phi_r\cos\phi_l - m_l r_l\cos\phi_r\sin\phi_l)\dot{\phi}_r + \\
+ (m_b r_0\cos\alpha\cos\phi_l - m_b r_0\sin\alpha\sin\phi_l)\dot{\alpha} + \\
+ (2m_l\cos\phi_l + m_b\sin\alpha)\dot{x} + (2m_l\sin\phi_l + m_b\cos\alpha)\dot{y} &= constant4 \quad (5.21)
\end{aligned}$$

In addition, due to the imposing kinematic constraint for the stance leg:

$$\dot{x}\sin\phi_l - \dot{y}\cos\phi_l + l_0\dot{\phi}_l = 0 \tag{5.22}$$

Equations 5.18 5.19 5.20 5.21 & 5.22 together can be used to calculate $\dot{x}, \dot{y}, \dot{\alpha}, \dot{\phi}_l$ and $\dot{\phi}_r$ at each touchdown.

During stance, the leg lifts off when the vertical ground reaction force between the foot and ground becomes zero. In this case, the Lagrangian Multiplier f_l and f_r are effectively ground reaction force components acting perpendicular to the leg. Therefore, the leg lifts off when:

$$f_s\sin\phi_l - f_l\cos\phi_l = 0 \text{ for left leg} \qquad f_s\sin\phi_r - f_l\cos\phi_r = 0 \text{ for right leg} \tag{5.23}$$

5.2.6 Fixed Points and Local Stability

The model dynamics can be simulated using the derived equations of motion and switching conditions in the above subsections with necessary initial conditions. Assuming the simulation starts when the left leg touches the ground, then the necessary initial system states required are v, δ, ϕ_l, ϕ_r, $\dot{\phi}_r$, ϕ_b and $\dot{\phi}_b$ respectively. Where

$v = (\dot{x}^2 + \dot{y}^2)^{1/2}$ and $\delta = \arccos(\dot{x}/v)$ are hip point velocity magnitude and direction respectively. Then a multi-dimensional poincaré return map can be constructed: from the start of n_{th} stride $\mathbf{P}(n) = [v(n),\ \delta(n),\ \phi_l(n),\ \phi_r(n),\ \dot{\phi}_r(n),\ \alpha(n),\ \dot{\alpha}(n)]$ to the start of $(n+1)_{th}$ stride $\mathbf{P}(n+1) = [v(n+1),\ \delta(n+1),\ \phi_l(n+1),\ \phi_r(n+1),\ \dot{\phi}_r(n+1),\ \alpha(n+1),\ \dot{\alpha}(n+1)]$. When the model reaches a fixed point (a certain periodic motion), we will have $\mathbf{P}(n+1) = \mathbf{P}(n) = \mathbf{P}^* = [v^*,\ \delta^*,\ \phi_l^*,\ \phi_r^*,\ \dot{\phi}_r^*,\ \alpha^*,\ \dot{\alpha}^*]$.

The local stability of a fixed point can be quantified with the corresponding eigenvalues associated with this multi dimensional mapping. To evaluate the eigenvalues of this mapping, the Jacobian matrix $\mathbf{J}$ of the return map needs to be numerically approximated. A similar numerical approximation process as those in [48] is used. Here it is omitted to make the paper concise and focused. For small perturbation, the error dynamics can be described by:

$$\Delta\mathbf{P}(n+1) = \mathbf{J}\,\Delta\mathbf{P}(n) \tag{5.24}$$

Where $\Delta\mathbf{P}(n+1)$ and $\Delta\mathbf{P}(n)$ are the mapping error $\mathbf{P}(n+1) - \mathbf{P}^*$ and $\mathbf{P}(n) - \mathbf{P}^*$ respectively. Based on the approximated Jacobian matrix, eigenvalues of a fixed point can be calculated. When all the eigenvalues have a magnitude less than one, the fixed point is stable as $\Delta\mathbf{P}(n)$ eventually approaches zero. Among all the eigenvalues, the maximum eigenvalue magnitude can be used to measure the local stability of a fixed point as it in general represents the worst case performance.

5.3 Real Time Layer

In this section, we show that stable periodic motions can be found with just the real time control layer as shown in Figure 5.1.

It has been previously studied that locomotion with trunk pitching can be stabilized by a simple PD controlled hip torque based on trunk angle sensory feedback [**?**]. However, its ability to regulate center-of-mass translation speed is limited. This could be due to the fact that only trunk angle α sensory feedback is used. We hypothesize

that including forward speed feedback as shown in Figure 5.1 could improve its overall locomotion stability, especially its capability to resist center-of-mass speed perturbations. Here we compare locomotion models with and without forward speed feedback in terms of their perturbation response and basins of attraction.

5.3.1 Control Strategy and Periodic Motion

For the traditional trunk angle based hip torque control strategy, the stance leg (left or right) hip torque can be expressed as:

$$Stance: \ \tau_l \ or \ \tau_r = k_p^{\alpha}(\alpha - \alpha_r) + k_d^{\alpha}\dot{\alpha} \tag{5.25}$$

Where k_p^{α}, k_d^{α} and α_r are proportional, derivative control gains and trunk reference angle respectively. When a leg is off the ground, its hip torque swings the leg towards a desired leg landing angle ϕ_{des}. When the left leg is off the ground:

$$Flight: \ \tau_l = k_p^{\phi}(\phi_l - \phi_{des}) + k_d^{\phi}\dot{\phi}_l \tag{5.26}$$

Where k_p^{ϕ} and k_d^{ϕ} are leg placement proportional and derivative control gains. Similarly, when the right leg is off the ground:

$$Flight: \ \tau_r = k_p^{\phi}(\phi_r - \phi_{des}) + k_d^{\phi}\dot{\phi}_r \tag{5.27}$$

A simple extension of this traditional control strategy (Equations 5.25, 5.26 & 5.27) with additional speed feedback could be:

$$Stance: \ \tau_l \ or \ \tau_r = k_p^{\alpha}(\alpha - \alpha_r) + k_d^{\alpha}\dot{\alpha} + k_p^{vs}(\dot{x} - v_{des}) \tag{5.28}$$

Where k_p^{vs} and v_{des} are speed control gain and the desired speed. Thus, stance hip torque is directly influenced by locomotion speed. When the model runs at a lower speed than the desired speed, the additional speed feedback term in Equation 5.28

generates an additional amount of hip torque to accelerate the body forward. For the hip torque during the flight phase, they can be extended as:

$$Flight: \qquad \tau_l = k_p^{\phi}(\phi_l - \phi_{des}) + k_d\dot{\phi}_l + k_p^{vf}(\dot{x} - v_{des}) \tag{5.29}$$

$$\tau_r = k_p^{\phi}(\phi_r - \phi_{des}) + k_d\dot{\phi}_r + k_p^{vf}(\dot{x} - v_{des}) \tag{5.30}$$

When actual forward speed is higher than the desired speed, a faster leg swing is required to match the center-of-mass translation speed so that it does not crash. This can be achieved with the additional velocity feedback terms in Equations 5.29 & 5.30. When perturbed, these terms adjust hip torque such that leg swing speed and forward speed are matched.

Table 5.2 Controller parameters and fixed points for cases without and with speed feedback.

Parameter	Description	Without (a)	With (b)	Units
k_p^{α}	trunk proportional gain	-400	-400	Nm/rad
k_d^{α}	trunk derivative gain	-100	-100	Nms/rad
α_r	trunk reference angle	-17.1	-15	deg
k_p^{ϕ}	leg proportional gain	280	280	Nm/rad
k_d^{ϕ}	leg derivative gain	30	30	Nms/rad
ϕ_{des}	desired leg landing angle	110.8	111	deg
k_p^{vf}	speed proportional gain	–	100	Nm/rad
v_{des}	desired speed	–	3.45	m/s
v^*	solution speed	3.74	3.72	m/s
δ^*	solution velocity angle	18.34	21.57	deg
ϕ_l^*	solution left leg angle	112.69	112.49	deg
ϕ_r^*	solution right leg angle	107.65	110.82	deg
$\dot{\phi}_r^*$	solution right leg speed	100.21	59.35	deg/s
α^*	solution trunk angle	13.52	14.46	deg
$\dot{\alpha}^*$	solution trunk speed	-15.73	-1.59	deg/s

As shown in Figure 5.5, stable solutions are found for both models with the same physical parameters and controller gains. Both solutions are tuned to run around of $3.4m/s$ with a trunk angle regulated around $10°$, a representative value seen in human

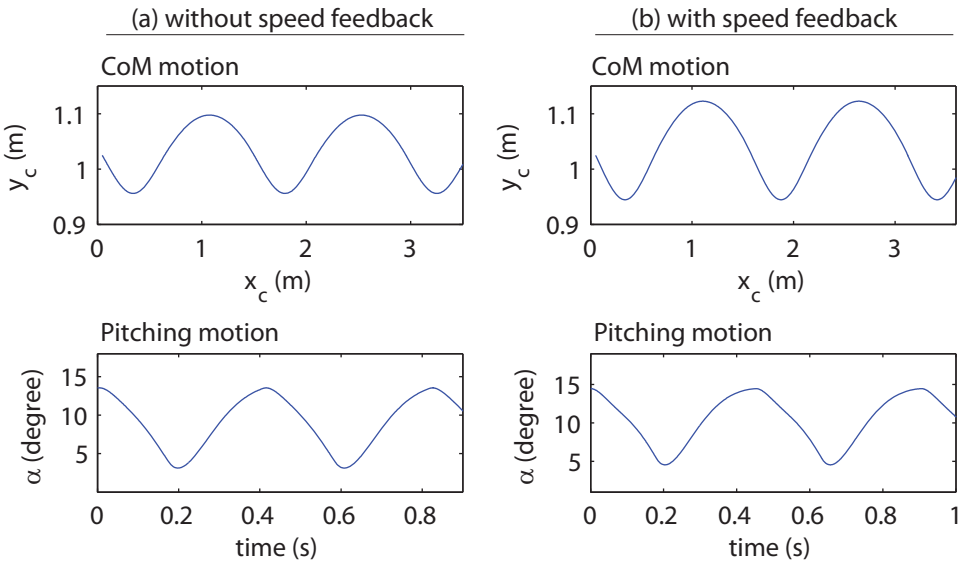

Figure 5.5. (a) & (b) Periodic motion of extended Trunk-SLIP without and with forward speed feedback. The model physical parameters are listed in Table 5.1. The controller parameter and fixed point values can be found in Table 5.2.

trunk movement during running [110]. Thus the only major difference between these two periodic running solutions is the absence (case (a)) and presence (case (b)) of forward speed feedback.

5.3.2 Perturbation Response and Basin of Attraction

We then compare these two stable solutions in terms of their perturbation response and basins of attractions.

As shown in Figure 5.6 column (a), without the additional speed feedback, it crashes a few strides after the perturbation is applied. This indicates its relatively poor stability with respect to forward speed perturbations. In contrary, the model returned back to steady state motion when the forward speed feedback is present.

To highlight their difference, we compare their basins of attraction. To make a better visual presentation, we focus on two groups of fixed point variables: (1) v and

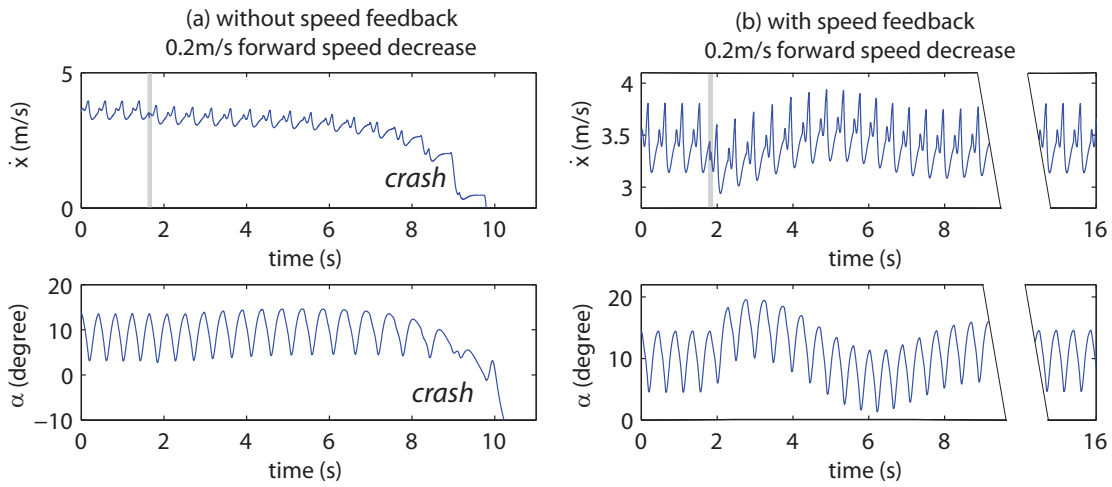

Figure 5.6. (a) & (b) Perturbation response of extended Trunk-SLIP without and with speed feedback. The model parameters and fixed point values are the same as those in Figure 5.5. The forward speed is reduced from the fixed point value by $0.2m/s$ at the end of the second stride, marked as shaded slots in the figure.

δ for whole body translation; (2) α and $\dot{\alpha}$ for trunk pitching. For each group, a two dimensional basin of attraction can be constructed, as shown in Figure 5.7.

To obtain the center-of-mass translation basin of attraction, the hip touchdown velocity magnitude v and angle δ are perturbed from fixed point values (labeled as black dots Figure 5.7) while the rest fixed point values are kept unchanged. All the velocity magnitude and angle pairs from which the model can eventually recover are recorded and formed the gray region in Figure 5.7 first row. Similarly, to obtain the pitching basin of attraction, the trunk angle α and angular velocity $\dot{\alpha}$ are perturbed while the rest fixed point values are unchanged. All the recoverable trunk angle and angular velocity pairs are recorded and presented as the gray region in Figure 5.7 bottom row.

Both basins of attractions expands significantly as additional speed feedback is used, indicating an overall improved stability. As shown in the first column of Figure 5.7, without speed feedback, The fixed point (black dot) is close to the border of

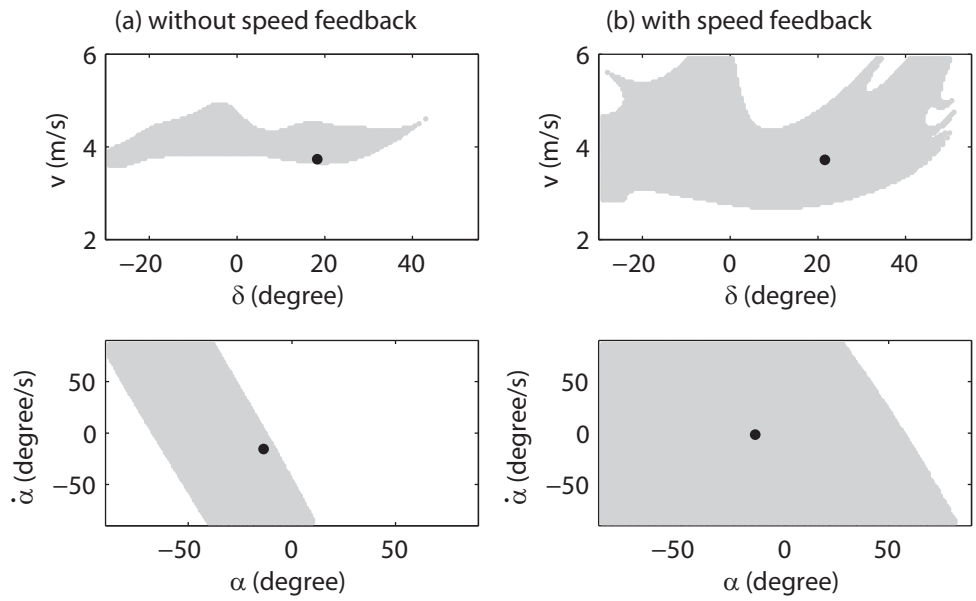

Figure 5.7. (a) Basins of attraction of extended Trunk-SLIP without speed feedback. (b) Basins of attraction of extended Trunk-SLIP with speed feedback. The model parameters and fixed point values are the same as those in Figure 5.5. The black dot in each panel stands for the fixed point.

stability basins. Therefore, despite a stable fixed point, its overall stability is poor. In comparison, the second column of Figure 5.7, speed feedback greatly expands both translation and pitching basins of attraction. More importantly, the fixed point is now well "centered" within each basin. This is a dramatic improvement in global stability.

In summary, the additional speed feedback greatly strengthens the overall locomotion stability, especially its capability to resist speed perturbations.

5.4 Event to Event Layer

Speed feedback improves model stability especially its global stability. However, as observed in Figures 5.6, the transient response to perturbations tends to be oscillatory. In addition, it takes a long time to fully recover from a specific perturbation. Here

we show that by adding the event to event discrete control layer, these problems can be effectively remedied.

5.4.1 Control Strategy and Periodic Motion

One reason that perturbation response tends to be oscillatory and slow could be the lack of hip torque controller adjustment. It is commonly observed in human running that trunk leans forward when accelerating and backward when decelerating. Inspired by this phenomena, we hypothesize that by introducing a speed based trunk reference angle regulator could improve the model response to perturbations. Therefore we propose the trunk reference angle to be updated at each touchdown based on the following equation:

$$\alpha_r = \alpha_b - k_\alpha(\dot{x} - v_{des}) \tag{5.31}$$

Where α_b and k_α are trunk reference angle base value and regulator gain respectively. When forward speed $\dot{x}$ is increased from the steady state value, the resulting trunk angle reference α_r will decrease. Therefore, the trunk motion will be regulated around a backward position to help decelerate center-of-mass translation. Otherwise when forward decreases, the trunk reference angle will increase and in turn helps to accelerate.

In addition, it is known that leg landing angle could have a significant impact on locomotion stability [26, 31, 32]. A canonical control approach developed by Raibert was to use leg landing angle to control locomotion speed [63]. Also, it is known that human leg landing angle and running speed exhibits a certain linear relationship [19]. We therefore hypothesize that additional mechanism that adapts leg landing angle could also help reduce oscillation in perturbation response. We then introduce leg landing angle ϕ_{des} regulation at each liftoff as:

$$\phi_{des} = \phi_b - k_\phi \dot{x} \tag{5.32}$$

Where ϕ_b and k_ϕ are base leg landing angle and leg landing angle adjustment gain.

Note that, unlike hip torque controllers which runs in real time, both reference angles are updated only once at each touchdown or liftoff. Therefore, transition regulator (governed by Equations 5.31 & 5.32) runs at a lower frequency with a small control cost. To test the effect of the proposed transition regulator. We seek to compare fixed point solutions with and without transition regulator .

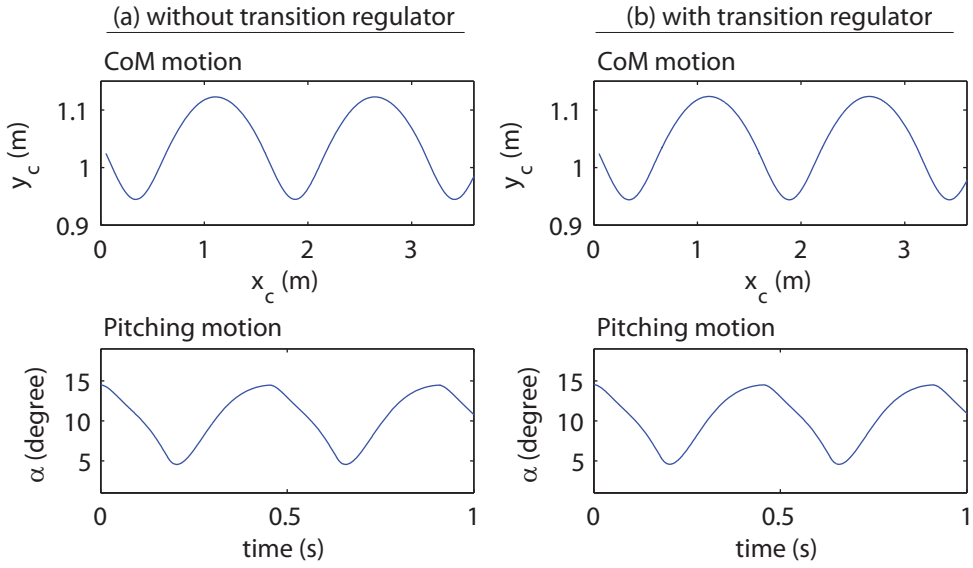

Figure 5.8. (a) & (b) Periodic motion of extended Trunk-SLIP without and with the transition regulator. The model physical parameters for both models are listed in Table 5.1. For the case without transition regulator, its control parameter and fixed point values are the same as those of Table 5.2. While for the case with the transition regulator, stance and hip torque control gains remains the same as those without transition regulator. The additional transition regulator parameter k_α, α_b, k_ϕ, ϕ_b values are $1.1459°s/m$, $-15°$, $2.5°s/m$ and $101.5°$ respectively. The corresponding fixed point values $[v^*, \delta^*, \phi_l^*, \phi_r^*, \dot{\phi}_r^*, \alpha^*, \dot{\alpha}^*]$ are: $[3.73m/s,\ 21.62°,\ 112.53°,\ 110.96°,\ 58.11°/s,\ 14.50°,\ -1.20°/s]$. In addition, the initial ϕ_{des} are $111.03°$.

We then extend the previously found fixed point solution as shown in Figure 5.5 (the case with speed feedback) by incorporating the transition regulator. The new transition regulator parameters are tuned to find fixed points while the other parame-

ters are fixed. As shown in Figure 5.8, a fixed point similar to that of the case without transition regulator was found. The center-of-mass motion and trunk pitching angle are nearly identical. The only major difference between these two models are the absence and presence of transition regulator.

5.4.2 Perturbation Response and Basin of Attraction

In this subsection, we demonstrate the effect of transition regulator by comparing two periodic solutions in Figure 5.5. Here we focus on the model's ability to resist perturbations in locomotion speed and trunk pitching.

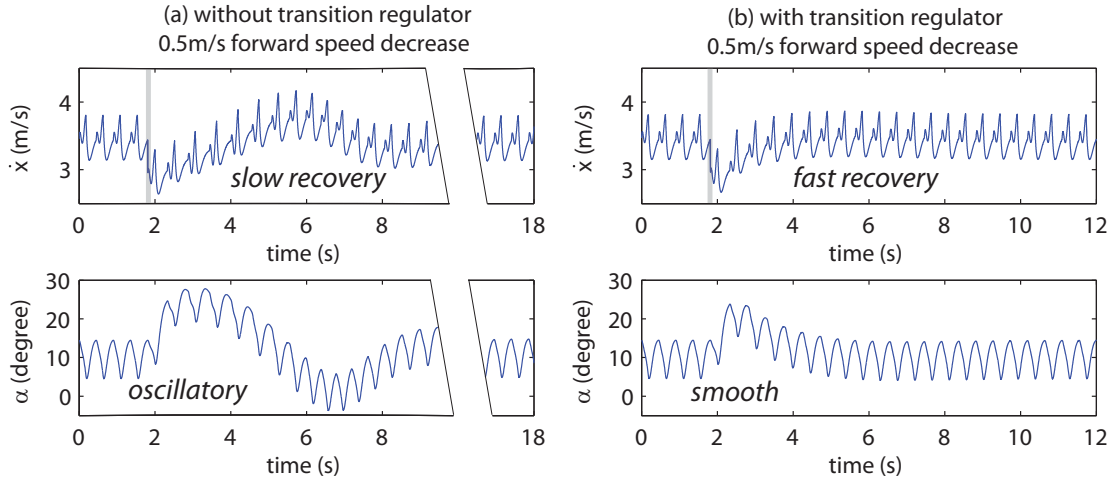

Figure 5.9. (a) & (b) Perturbation response of extended Trunk-SLIP without and with transition regulator . The model parameters and fixed point values are shown in Figure 5.8. The forward speed is decreased from the fixed point value by $0.5m/s$ at the end of second stride,marked as shaded slots in the figure.

In Figure 5.9, we show their response to a sudden forward speed decrease. As observed in the first column of Figure 5.9, without transition regulator , the trunk leans forward quickly after the perturbation is applied. However, the speed quickly gets over compensated and becomes higher than the steady state value. This in turn causes the trunk body to lean backward to decelerate. As a result of this behavior,

the overall perturbation response becomes oscillatory. In addition, a slow recovery is observed as it dose not fully recover until about 16s after perturbation. In comparison, when the transition regulator is present, the response is significantly smoother. As shown in the right column of Figure 5.9, the body leans forward to accelerate. Thanks to the trunk reference and leg landing angle adjustment, a well damped smooth response is found. Besides, the recovery time gets reduced. With transition regulator, a full recovery happens at about 4s after perturbation.

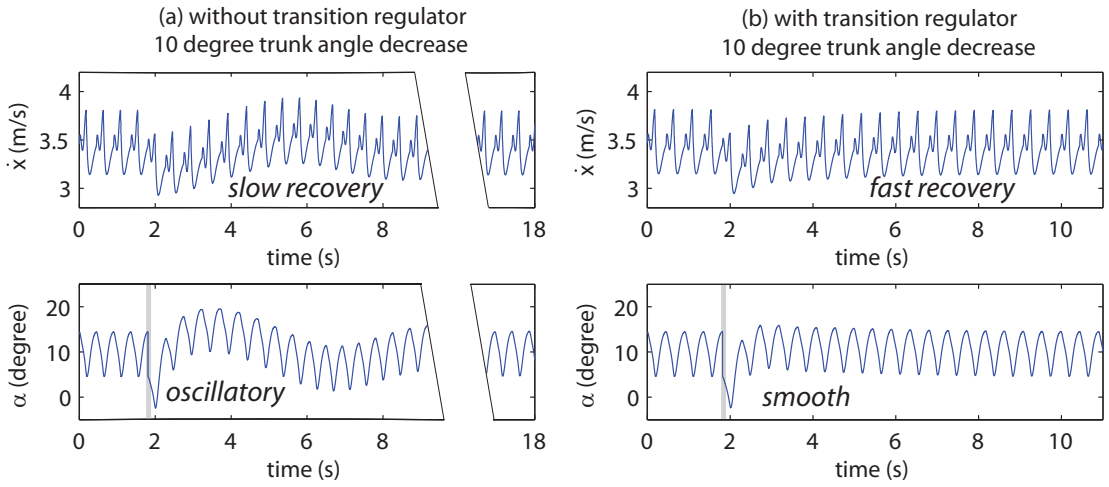

Figure 5.10. (a) & (b) Perturbation response of extended Trunk-SLIP without and with transition regulator . The model parameters and fixed point values are the same as those in Figure 5.8. The trunk pitching angle is decreased from the fixed point value by 10° at the end of second stride,marked as shaded slots in the figure.

Similarly, as shown in Figure 5.10, when a large perturbation in the trunk angle is applied, smoother recovery motion and shorter recovery time is observed when transition regulator is present.

The stabilizing effect of the transition regulator is further highlighted by comparing their basins of attraction, as shown in Figure 5.11. Both translation and pitching basins of attraction expand dramatically when transition regulator is in-

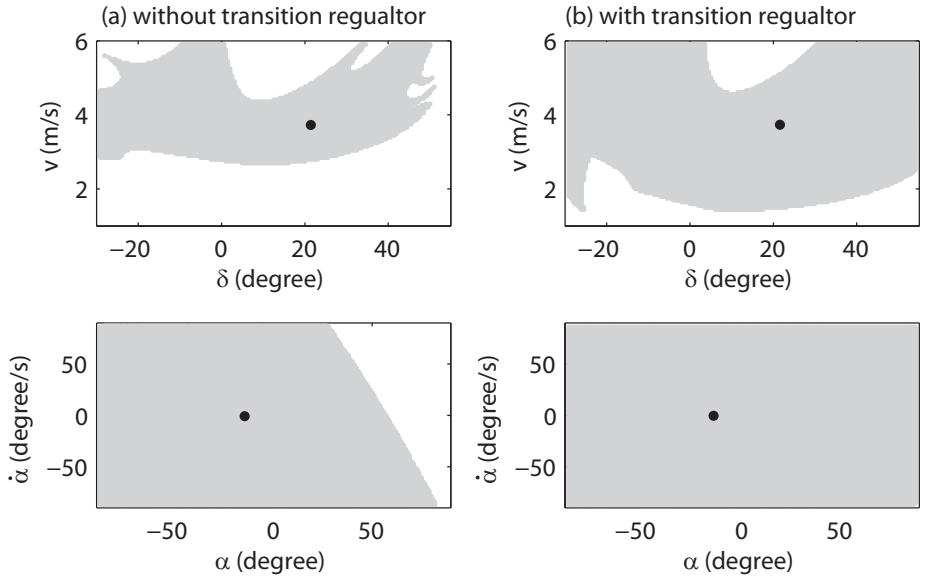

Figure 5.11. (a) & (b) Basins of attraction of extended Trunk-SLIP without and with transition regulator . The model parameters and fixed point values are the same as those in Figure 5.8. The black dot in each panel stands for the fixed point.

cluded. Specifically, for the translational basin of attraction, the model can recover from a significantly greater speed reduction with transition regulator .

In summary, the transition regulator improves the perturbation rejection response by making it smoother and faster. Also, it dramatically improves model global stability in terms of the size of maximum allowable perturbation.

5.5 Stride to Stride Layer

Despite the additional speed feedback and transition regulator , there still exist difference between the speed reference v_{des} and the actual average speed v_{avg} within a stride. Where the actual average speed v_{avg} can be measured as the distance traveled within a single stride divided by stride time. To realize accurate speed control, we propose an additional speed regulator which adjusts the speed reference v_{des} such that the actual average speed equals to the commanded speed v_{cmd}. We therefore propose

an integrator which accumulates the error between the commanded speed and actual speed after every stride:

$$v_{des}(n) = v_{cmd} + k_i \sum_{i=1}^{n-1} (v_{cmd} - v_{avg}(i)) \qquad \text{if } \mid v_{cmd} - v_{avg}(i) \mid < 0.5m/s \quad (5.33)$$

$$v_{des}(n) = v_{cmd} \qquad \text{if } \mid v_{cmd} - v_{avg}(i) \mid > 0.5m/s \quad (5.34)$$

Where k_i is the integrator gain for speed reference. To reduce oscillation when perturbed, the integrator action is reset to zero when the error between command speed and current speed is larger than $0.5m/s$. This speed regulator comes with minimal control cost as it operates at the stride frequency which is even lower than the transition regulator control frequency. We then seek to determine if this additional layer could achieve tight speed control. If so, is the overall robust stability maintained?

5.5.1 Perturbation Response and Basin of Attraction

The speed regulator is added upon the previously tuned fixed point solution (as shown in Figure 5.8 (b)). Only the integrator gain k_i is tuned to find similar solution while the rest parameters are unchanged. As expected, a similar fixed point is found.

It is found that zero steady state error of locomotion speed is obtained with the speed regulator . As shown in Figure 5.12, we compare the model response when forward speed is perturbed. Without speed regulator, the locomotion speed eventually settles to a value lower than the desired speed v_{des}. In comparison, the offset disappeared when speed regulator is present. The steady state speed settles exactly to the command speed v_{cmd} of 3.45m/s.

Also, the robust global stability is not affected by the inclusion of this speed regulator. In Figure 5.13, we shown the basins of attraction for the solutions with and without speed regulator. In general, the size and shape of both basins are almost

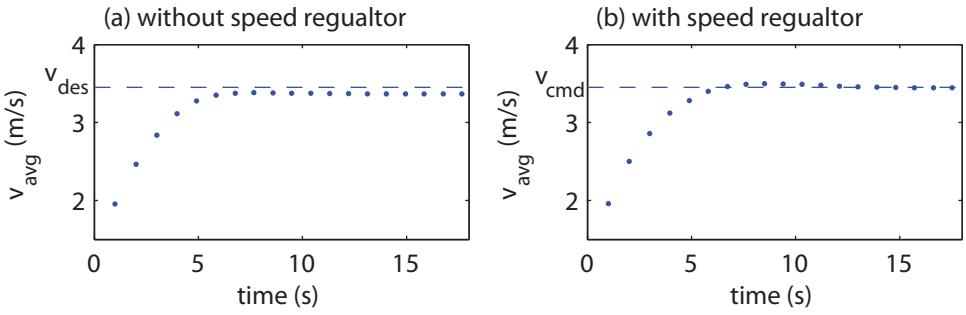

Figure 5.12. (a) & (b) Perturbation response of extended Trunk-SLIP without and with speed regulator. The model parameter and fixed point values for the case without speed regulator are the same as those in Figure 5.8 (b). For the model with speed regulator , additional parameters v_{cmd} and k_i are $3.45m/s$ and 0.15 respectively. The corresponding fixed point values $[v^*,\ \delta^*,\ \phi_l^*,\ \phi_r^*,\ \dot{\phi}_r^*,\ \alpha^*,\ \dot{\alpha}^*]$ are: $[3.80m/s,\ 21.04°,\ 112.81°,\ 111.07°,\ 60.87°/s,\ 75.55°,\ -1.72°/s]$. In addition, the initial ϕ_{des} are 111.26°.

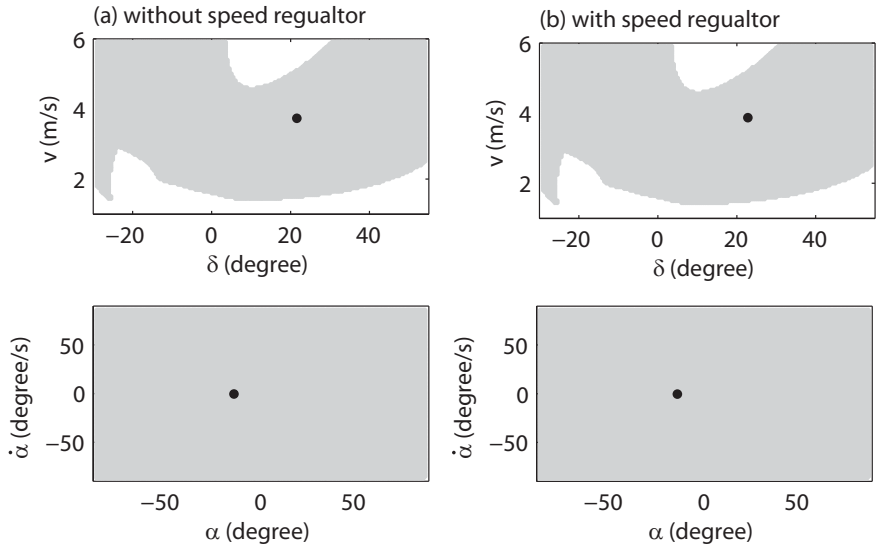

Figure 5.13. (a) & (b) Basins of attraction of extended Trunk-SLIP without and with speed regulator. The model parameters and fixed point values are the same as those in Figure 5.12. The black dot in each panel stands for the fixed point.

identical for these two cases. Therefore, the overall robust global stability is still maintained.

5.5.2 Local Stability Dependence on Physical Parameter Variation

To further validate the effect of the overall control scheme. We investigate the change of model local stability (represented as the maximum eigenvalue) with respect to model physical parameters. Model physical parameters such as trunk inertia sometimes cannot be accurately measured. Therefore, this is also in order to determine if this strategy could be applied to legged robots whose physical parameters are uncertain.

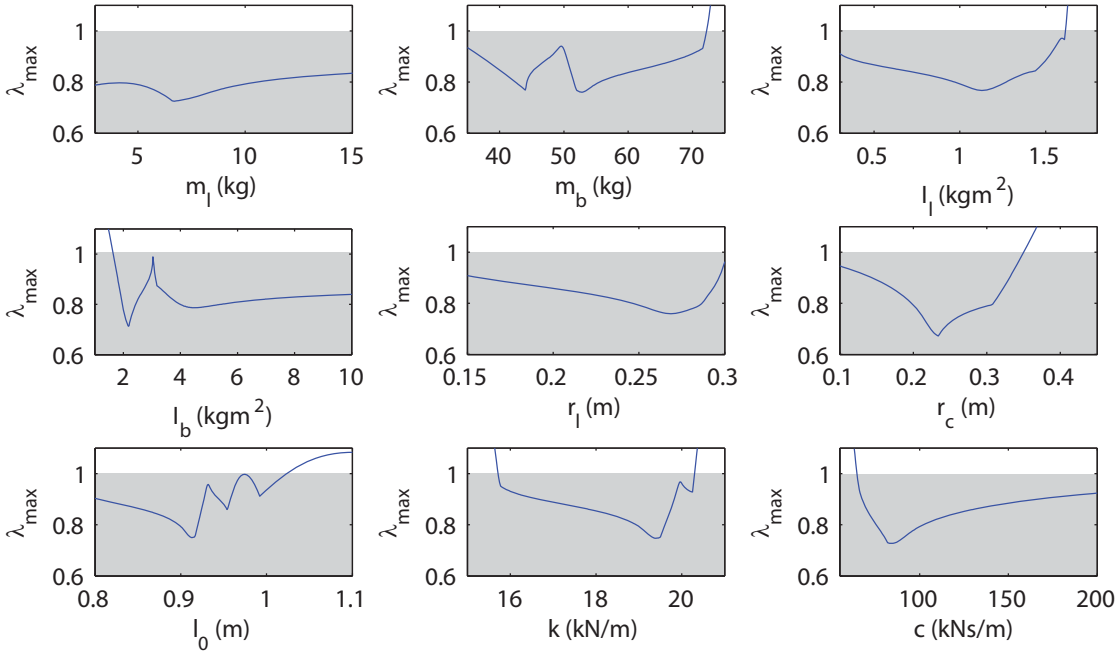

Figure 5.14. Maximum eigenvalue magnitude (solid blue curve) against model physical parameters. The shaded region stands for the stable region where the maximum eigenvalue magnitude is less than one.

In Figure 5.14, we show the maximum eigenvalue versus physical parameters. For each panel, only one parameter is varied while the rest is fixed as those of the complete controlled case in Figure 5.12. Note that in Figure 5.14, in order to make the analysis simple, control parameters are fixed and not tuned when each model physical parameters is changed. Therefore the obtained fixed points and local stability are not local optimal. For an actual robot, the control parameter can be tuned to obtain more stable solutions. However, as can be seen in Figure 5.14, stable solutions with maximum eigenvalue magnitude less than one can still be found over a wide range of parameter values. What is more, with proper tuning, even very stable solutions with maximum eigenvalue magnitude less than 0.8 can be found.

In summary, the speed regulator minimizes the error between actual and commanded speed. The overall stability is maintained with the inclusion of speed regulator. Besides, this strategy remains effective with respect to model parameter changes.

5.6 Conclusion

It is amazing that above knee athletes in Paralympic Games can demonstrate robust running motion with regulated trunk motion. Inspired by the hierarchical structure of mammal neocortex, we develop a simple layer by layer control and tuning strategy for bipedal robots with hip torque actuation. To validate the developed control strategy, a locomotion model called "extended Trunk-SLIP" is developed based on existing SLIP based models. Unlike traditional models with massless legs, its trunk and thigh are modeled as rigid bodies while each shank is assumed to be massless and springy.

In total, four layers are proposed while we focus on the first three layers to demonstrate this strategy. At first, the base layer control is applied on to extended Trunk-SLIP to form basic motion stability. Afterwards, each layer is added and tuned upon the previously tuned periodic solutions to demonstrate the particular effect of each

layer. This approach could enable a fast controller parameter tuning as only a small number of control parameters need to be tuned at each step.

At first, the stance and flight hip torque controllers are applied in the real time layer. By comparing perturbation response and basins of attraction, it is found that forward speed feedback greatly helps improve locomotion stability with respect to speed perturbations. Further, we introduce a simple transition regulator to adjust leg landing and trunk angle reference at each touchdown or liftoff. Unlike the hip torque controllers which run in real time, the transition regulator operates at a lower frequency. It greatly smooths the system response and shortens settling time with respect to large perturbations. In addition, it improves global stability for both translation and pitching basins. Then the speed regulator is introduced and runs only once a stride. With the speed regulator, locomotion speed is accurately tracked with its overall robust stability unchanged. Also, stable solutions can still be found despite large physical parameter uncertainty.

The proposed control strategy is simple in nature and could be applied in bipedal legged robot design with springy legs. It could also help towards better understanding of how stable running motion is formed in above knee amputee running. This knowledge in turn could be applied to the field of legged locomotion in general. Further, the proposed layer by layer controller design approach could be applied to other complex systems with under actuated dynamics.

6. SUMMARY

Despite the development of robotics in the past few decades, the performance of existing legged robots is still behind what is observed in biology. Especially, currently, there does not exist a bipedal robot capable of high speed running. On the contrary, above knee amputee athletes in Paralympics, with largely only hip torque actuation and compliant legs, are capable of sprinting. Overall, there still exists a gap between the state-of-art and what is possible for animals and humans. One reason is that locomotion dynamics are not completely understood as they are nonlinear and hybrid. Current theories about linear systems cannot be easily applied. To further improve legged robot and assistive device design, more principles and knowledge about locomotion dynamics and control need to be gained.

Here we investigate general locomotion dynamics and control using the mathematical modeling and analysis approach. More specifically, we show how locomotion models can be gradually developed as shown in Figure 6.1.

At first, we utilize the simulation of actuated-SLIP to explain a general behavior among legged animals: a universal preference of relative leg stiffness. We then incorporate trunk pitching dynamics into actuated-SLIP to form Trunk-SLIP. By doing so, we are able to investigate how different combinations of sensory feedback could affect overall locomotion stability. The knowledge obtained are then used to create the more complicated extended Trunk-SLIP model. We show that by applying a simple layer by layer control strategy, extended Trunk-SLIP can exhibit robust center-of-mass motion with tightly regulated trunk pitching.

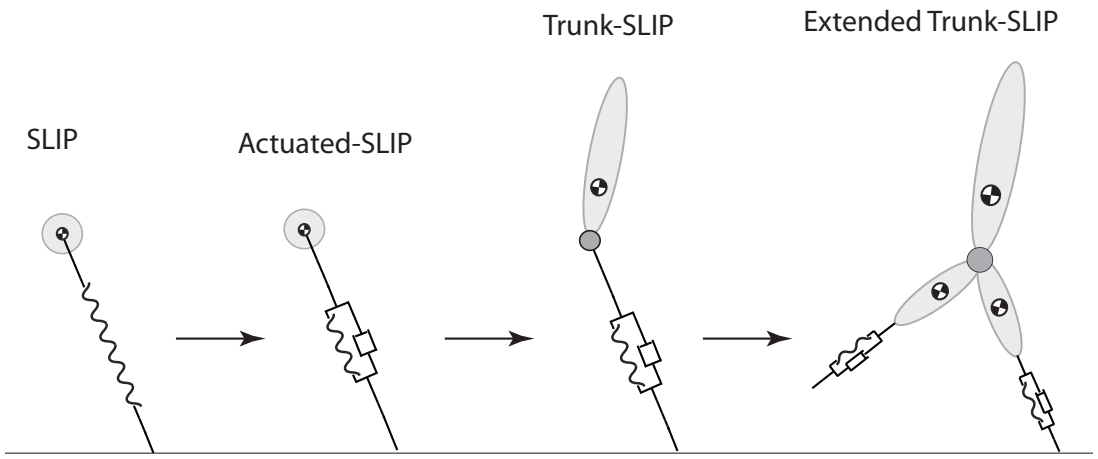

Figure 6.1. The development of locomotion models from simple SLIP to more complex extended Trunk-SLIP. The arrows stands for the direction of evolvement.

6.1 Simple Models and General Principles

It has been shown that legged animals, across species, exhibits the same kind of spring mass running pattern. Also, animal leg stiffness when normalized by leg length and body weight tightly distribute within a narrow range between 7 and 27. This is surprising as there exists a wide variation of animal size, weight, specie and morphology. Very few universal behaviors like this exists in biology. We show that the animal preference of this particular relative stiffness range tightly relates to the optimization of locomotion energetic cost as well as center-of-mass translation stability.

Through simulation of the simple actuated-SLIP model using a human related parameter set. It is discovered that the mechanical cost of transport for actuated-SLIP is at its minimum when the relative leg stiffness is at the human value. In addition, the predicted minimal mechanical cost of transport agrees with human experimental value. Then actuated-SLIP is explored within the biological relevant parameter space. It is found that the relative stiffness region where mechanical cost of transport is minimal for the model coincides with the biological preferred values between

7 and 27. This strongly implies that animals and human might adapt leg stiffness to reduce energetic cost. Similarly, it was found that this relative stiffness region also corresponds to the region where the stability of actuated-SLIP is optimal. This implies that animals could select leg stiffness to optimize locomotion energy efficiency and stability at the same time. Overall, this is the first time such an explanation is offered. In addition, these results also help explain how high level control targets such as energy efficiency might influence overall physiological parameters and the underlying neuromechanics that produce it.

6.2 Complex Models and Locomotion Control

We then developed a general control strategy for legged robots by gradually increasing model and control complexity. As the first step, we extended actuated-SLIP with a rigid body trunk to form Trunk-SLIP. Four different combinations of sensory feedback were applied onto Trunk-SLIP. Their respective stability is studied and compared. exproprioceptive feedback during flight were found to be critical to overall motion stability with trunk pitching. Exproprioceptive and proprioceptive feedback during stance generate similar stable solutions. When both feedback pathways are combined using a simple linear superimposition, the overall stability is improved.

Inspired the physical structure of the human neocortex and the layer by layer approach adopted by the human brain for complex pattern recognition, we developed a hierarchical control strategy with multiple layers. Different layers of control were applied on a more complex Trunk-SLIP model with trunk and leg masses. Three layers of control achieves basic stable motion, smooth perturbation response and accurate speed tracking respectively. Overall stability is gradually improved when different layers are added in sequence. This layer by layer approach reduces controller design and tuning complexity. Each time only a few number of controller parameters need to be added and tuned. Further, we propose a fourth layer where a higher level of performance targets can be realized by controlling the commanded speed.

The knowledge gained through mathematical modeling and analysis can be applied to the design of future legged robots. In addition, it could serve as the base where more sophisticated locomotion models and control strategies could be developed upon.

LIST OF REFERENCES

LIST OF REFERENCES

[1] D. Koditschek P. Holmes, R. Full and J. Guckenheimer. The dynamics of legged locomotion: Models, analyses, and challenges. *SIAM Rev.*, 48:207–304, February 2006.

[2] W. Schwind. *Spring loaded inverted pendulum running: a plant model*. PhD thesis, Ann Arbor, MI, USA, 1998.

[3] R. Alexander. *Principles of Animal Locomotion*. Princeton University Press, 2003.

[4] T. McGeer. Passive bipedal running. *Proc. Roy. Soc. Lond.*, B 240:107–134, 1990.

[5] T. McGeer. Passive dynamic walking. *Int. J. Robotics Research*, 9:62–82, 1990.

[6] T. McGeer. Dynamics and control of bipedal locomotion. *J. Theor. Biol.*, 163(3):277–314, 1993.

[7] R. Full and D. Koditschek. Templates and anchors: neuromechanical hypotheses of legged locomotion on land. *J. Theor. Biol.*, 202(23):3325–3332, 1999.

[8] R. Blickhan and R. Full. Similarity in multilegged locomotion: Bouncing like a monopode. *J. Comp. Phys. A*, 173:509–517, 1993.

[9] R. Blickhan. The spring-mass model for running and hopping. *J. Biomech.*, 22:1217–1227, 1989.

[10] H. Gunther A. Seyfarth, H. Geyer and R. Blickhan. A movement criterion for running. *J. Biomech.*, 35:649–655, 2002.

[11] P. Holmes R. Ghigliazza, R. Altendorfer and D. Koditschek. A simply stabilized running model. *SIADS*, 2(2):187–218, 2003.

[12] H. Komsuoglu M. Buehler N. Moore R. Altendorfer, D. Koditschek and D. Mcmordie. Evidence for spring loaded inverted pendulum running in a hexapod robot. *Exp. Rob. VII*, 271:291–302, 2001.

[13] J. Glasheen C. Farley and T. McMahon. Running springs: speed and animal size. *J. Theor. Biol.*, 185:71–86, dec 1993.

[14] J. Saito C. Farley, R. Blickhan and C. Taylor. Hopping frequency in humans: a test of how springs set stride frequency in bouncing gaits. *J Appl Physiol*, 71(6):2127–32, Dec 1991.

[15] R. Kram J. He and T. McMahon. Mechanics of running under simulated low gravity. *J Appl Physiol*, 71(3):863–870, 1991.

[16] D. Ferris and C. Farley. Interaction of leg stiffness and surface stiffness during human hopping. *J. Appl. Physiol.*, 82(1):15–22, 1997.

[17] M. Louie D. Ferris and C. Farley. Running in the real world: adjusting leg stiffness for different surfaces. 265(1400):989–994, jun 1998.

[18] K. Liang D. Ferris and C. Farley. Runners adjust leg stiffness for their first step on a new running surface. *J. Biomech.*, 32(8):787 – 794, 1999.

[19] C. Lee and C. Farley. Determinants of the center of mass trajectory in human walking and running. *J. Exp. Biol.*, 201(21):2935–2944, 1998.

[20] A. Seyfarth H. Geyer and R. Blickhan. Compliant leg behavior explains basic dynamics of walking and running. *Bio. Sci. Proc. R. Soc. A*, 273(1603):2861–7, 2006.

[21] J. Jun and J. Clark. Dynamic stability of variable stiffness running. In *ICRA 2009*, ICRA'09, pages 3985–3990, 2009.

[22] D. Koditschek R. Altendorfer and P. Holmes. Towards a factored analysis of legged locomotion models. *In proceeding of: ICRA 2003*, pages 37–44, sep 2003.

[23] J. Seipel and P. Holmes. Three dimensional translational dynamics and stability of multi-legged runners. *Int. J. Robot. Res.*, 25(9), 2006.

[24] M. Gunther S. Grimmer, M. Ernst and R. Blickhan. Running on uneven ground: leg adjustment to vertical steps and self-stability. *J Exp Biol*, 211:2989–3000, 2008.

[25] J. Schmitt. A simple stabilizing control for sagittal plane locomotion. *J. Comput. Nonlinear Dynam.*, 1:348–357, 2006.

[26] J. Schmitt and J. Clark. Modeling posture-dependent leg actuation in sagittal plane locomotion. *Bioinspir Biomim*, 4(4):046005, 2009.

[27] F. Jafari S. Tamaddoni and A. Medhdari. Biped hopping control on spring loaded inverted pendulum. *Int. J. Hum. Robot.*, 07(2), jun 2010.

[28] S. Oh Y. Kimura and Y. Hori. Leg space observer on biarticular actuated two-link manipulator for realizing spring loaded inverted pendulum model. *AMC 2012*, pages 1–6, mar 2012.

[29] G. Piovan and K. Byl. Enforced symmetry of the stance phase for the spring-loaded inverted pendulum. *ICRA 2012*, (May), 2012.

[30] A. Sato and M. Buehler. A planar hopping robot with one actuator: design, simulation, and experimental results. *IROS 2004*, (Sep), 2004.

[31] H. Geyer A. Seyfarth and H. Herr. Swing-leg retraction: a simple control model for stable running. *J. Exp. Biol.*, 206:2547–2555, 2003.

[32] J. Rummel Y. Blum, S. Lipfert and A. Seyfarth. Swing leg control in human running. *Bioinspir. Biomim.*, 5(2):026006, 2010.

[33] J. Yeon K. Kim, O. Kwon and J. Park. Elliptic trajectory generation for galloping quadruped robots. pages 103–108. IEEE Computer Society, 2006.

[34] J. Schmitt B. Andrews, B. Miller and J. Clark. Running over unknown rough terrain with a one-legged planar robot. *Bioinspir. Biomim.*, 026009, 2011.

[35] I. Poulakakis and J. Grizzle. The spring loaded inverted pendulum as the hybrid zero dynamics of an asymmetric hopper. *IEEE T. Automat. Contr.*, 54, 2009.

[36] M. Buehler U. Saranli and D. Koditschek. Rhex: A simple and highly mobile hexapod robot. *Int. J. Robot. Res.*, 20(1):616 – 631, July 2001.

[37] Y. Aydin H. Komsuoglu, A. Majumdar and D. Koditschek. Characterization of dynamic behaviors in a hexapod robot. In *ISER 2010*, 2010.

[38] H. Komsuoglu. Dynamic legged mobility—an overview. In *IJRC 2009*, 2009.

[39] D. Koepl and J. Hurst. Force control for planar spring-mass running. In *IROS 2011*, pages 3758 – 3763, 2011.

[40] M. Lasa I. Mordatch and A. Hertzmann. Robust Physics-Based Locomotion Using Low-Dimensional Planning. *ACM Transactions on Graphics*, 29(3), 2010.

[41] R. Davison B. Kenwright and G. Morgan. Dynamic balancing and walking for real-time 3d characters. pages 63–73, 2011.

[42] B. Kenwright. Responsive biped character stepping: When push comes to shove. *Cyberworlds 2012*, pages 151–156, sep 2012.

[43] B. Kenwright and C. Huang. Beyond keyframe animations: A controller character-based stepping approach. pages 10:1–10:4, 2013.

[44] T. Kwon and J. Hodgins. Control systems for human running using an inverted pendulum model and a reference motion capture sequence. pages 129–138, 2010.

[45] J. Seipel and P. Holmes. A simple model for clock-actuated legged locomotion. *Rrgul. Chaotic Dyn.*, 12:502–520, 2007.

[46] J. Seipel C. Mullens and R. Full A. Spence, S. Revzen. Insects running on elastic surfaces. *J Exp Biol*, 213(11):1907–1920, 2010.

[47] J. Rummel H. Maus and A. Seyfarth. Stable upright walking and running using a simple pendulum based control scheme. *CLAWAR 2008*, pages 623–629, 2008.

[48] Z. Shen and J. Seipel. A fundamental mechanism of legged locomotion with hip torque and leg damping. *Bioinspir. Biomim.*, 7(4):046010, 2012.

[49] I. Poulakakis K. Sreenath, H. Park and J. Grizzle. Embedding active force control within the compliant hybrid zero dynamics to achieve stable, fast running on MABEL. *IJRR.*, 32(3):324–345, March 2013.

[50] P. Larson and J. Seipel. Analysis of a spring-loaded inverted pendulum locomotion model with radial forcing. *ASME IDETC 2012*, (August), 2012.

[51] M. Ankaral and U. Saranli. Stride-to-stride energy regulation for robust self-stability of a torque-actuated dissipative spring-mass hopper. *Chaos*, 20(3), September 2010.

[52] M. Ankaral Ö. Arslan and Ö. Morgül. Approximate analytic solutions to non-symmetric stance trajectories of the passive spring-loaded inverted pendulum with damping. *Nonlinear Dynam.*, 61, 2010.

[53] A. Seyfarth H. Geyer and R. Blickhan. Spring-mass running: simple approximate solution and application to gait stability. *J. Theor. Biol.*, 232(3):315 – 328, 2005.

[54] W. Schwind and D. Koditschek. Approximating the stance map of a 2-dof monoped runner. *J. Nonliner Sci.*, 10:533–568, 2000.

[55] J. Robilliard and A. Wilson. Prediction of kinetics and kinematics of running animals using an analytical approximation to the planar spring-mass system. *J. Exp. Biol.*, 10:4377–4389, 2005.

[56] U. Saranli Ö. Arslan and Ö. Morgül. An approximate stance map of the spring mass hopper with gravity correction for nonsymmetric locomotions. In *In proceeding of: ICRA 2009*, pages 2388–2393, 2009.

[57] D. Koditschek R. Altendorfer and P. Holmes. Stability analysis of legged locomotion models by symmetry-factored return maps. *IJRR.*, 23:10–11, 2004.

[58] J. Seipel and J. Park. Existence and absence of stable locomotion of the slip model: towards robustly stable models of legged locomotion. In *USNCTAM 2010*, 2010.

[59] J. Rummel and A. Seyfarth. Stable Running with Segmented Legs. *Int. J. Robot. Res.*, 27(8):919–934, August 2008.

[60] U. Saranli. *Dynamic locomotion with a hexapod robot*. PhD thesis, Ann Arbor, MI, USA, 2002.

[61] P. Larson Z. Shen and J. Seipel. Rotary and radial forcing effects on center-of-mass locomotion dynamics. *Bioinspir. Biomim.*, 9(3):036020, 2014.

[62] M. Buehler N. Neville and I. Sharf. A bipedal running robot with one actuator per leg. *ICRA 2006.*, (May):848–853, 2006.

[63] M. Raibert. *Legged robots that balance*. Massachusetts Institute of Technology, Cambridge, MA, USA, 1986.

[64] H. Maus A. Seyfarth M. Ahmadabadi M. Sharbafi, C. Maufroy and M. Yazdanpanah. Controllers for robust hopping with upright trunk based on the virtual pendulum concept. In *IROS 2012*, pages 2222 –2227, Oct. 2012.

[65] M. Dickinson *et al.* How animals move: an integrative view. *Science*, 288:100–106, 2000.

[66] B. Conrad D. Brunt M. Bishop, P. Fiolkowski and M. Horodyski. Athletic footwear, leg stiffness, and running kinematics. *J. Athl. Train.*, 41(4):387–92, 2006.

[67] A. Bejan. Unifying constructal theory for scale effects in running, swimming and flying. *J. Exp. Biol.*, 209:238–248, 2006.

[68] R. Nudds G. Taylor and A. Thomas. Flying and swimming animals cruise at a strouhal number tuned for high power efficiency. *Nature*, 425:707–711, oct 2003.

[69] D. Hoyt and R. Taylor. Gait and the energetics of locomotion in horses. *Nature*, 292:239–240, jul 1981.

[70] E. Cogger S. Wickler, D. Hoyt and M. Hirschbein. Preferred speed and cost of transport: the effect of incline. *J. Expe. Biol.*, 203:2195–2200, 2000.

[71] R. Alexander. Energetics and optimization of human walking and running. *Am. J. Hum. Biol.*, 14:641–648, 2002.

[72] H. Ralston. Energy-speed relation and optimal speed during level walking. *Int. Z. angew. Physiol. einschl. Arbeitsphysiol.*, 17(4):277–83, 1958.

[73] J. Bertram and A. Ruina. Multiple walking speed-frequency relations are predicted by constrained optimization. *J. Theor. Biol.*, 209(4):445–453, 2001.

[74] R. Kram J. Donelan and A. Kuo. Mechanical and metabolic determinants of the preferred step width in human walking. *Proc. Biol. Sci.*, 268:1985–1992, October 2001.

[75] A. Kuo. A simple model of bipedal walking predicts the preferred speed-step length relationship. *J. Biomech. Eng.*, pages 264–269, 2001.

[76] J. Donelan A. Kuo and A. Ruina. Energetic consequences of walking like an inverted pendulum: step-to-step transitions. *Exer. Spor. Sci. Rev.*, 33(2):88–97, April 2005.

[77] R. Alexander. Optimization and gaits in the locomotion of vertebrates. *Phys. Rev.*, 69(4):1199–1227, October 1989.

[78] M. Srinivasan and A. Ruina. Computer optimization of a minimal biped model discovers walking and running. *Nature*, sep 2005.

[79] K. Nielsen. Locomotion: Energy cost of swimming, flying, and running. *Science*, 177:222–228, 1972.

[80] R. Alexander. Models and the scaling of energy costs for locomotion. *J. Theor. Biol.*, 208:1645–52, may 2005.

[81] D. Winter. A new definition of mechanical work done in human movement. 46:79–83, 1979.

[82] J. Nilsson and A. Thorstensson. Ground reaction forces at different speeds of human walking and running. *Acta Physiol. Scand.*, 136(2):217–227, 1989.

[83] P. Cavanagh and M. Lafortune. Ground reaction forces in distance running. *J. Biomech.*, 13(5):397–406, 1980.

[84] G. Luder E. Stussi A. Stacoff, C. Diezi and I. Kramers-De. Ground reaction forces on stairs: effects of stair inclination and age. *Gait Posture*, 21(1):24–38, jan 2005.

[85] R. Neptune L. Turns and S. Kautz. Relationships between muscle activity and anteroposterior ground reaction forces in hemiparetic walking. *Arch Phys Med Rehabil.*, 88(9):1127–1135, sep 2007.

[86] R. Blickhan L. Ting and R. Full. Dynamic and static stability in hexapedal runners. *J Exp Biol*, 197(1):251–269, dec 1994.

[87] P. Holmes J. Seipel and R. Full. Dynamics and stability of insect locomotion: A hexapedal model for horizontal plane motions. *Biol. Cybern.*, 91:76–90, 2004.

[88] J. Schmitt P. Holmes R. Full, T. Kubow and D. Koditschek. Quantifying dynamic stability and maneuverability in legged locomotion. *Integr Comp Biol.*, 42(1):149–157, 2002.

[89] R. Razo P. Holmes J. Schmitt, M. Garcia and R. Full. Dynamics and stability of legged locomotion in the horizontal plane: a test case using insects. *Biol. Cybern.*, 86(5):343–353, 2002.

[90] F. Zajac. Muscle coordination of movement: A perspective. *J. Biomech.*, 26(0):109–124, 1993.

[91] D. Noll R. Seidler and G. Thiers. Feedforward and feedback processes in motor control. *NeuroImage*, 22(4):1775–1783, 2004.

[92] J. Duysens and H. Crommert. Neural control of locomotion; the central pattern generator from cats to humans. *Gait Posture*, 7(2):131–141, 1998.

[93] T. Mulder H. Crommert and J. Duysens. Neural control of locomotion; the central pattern generator from cats to humans. *Gait Posture*, 7(3):251–263, 1998.

[94] R. Full D. Koditschek and M. Buehler. Mechanical aspects of legged locomotion control. *Arthropod Struct Dev.*, 33(3):251–272, 2004.

[95] N. Bernstein. *The Co-ordination and Regulation of Movements*. Oxford, UK: Pergamo, 1967.

[96] K. Hagbarth. Exteroceptive, proprioceptive, and sympathetic activity recorded with microelectrodes from human peripheral nerves. *Mayo Clin Proc*, 54(6):353–65, 1979.

[97] D. Legrand and S. Ravn. Perceiving subjectivity in bodily movement: The case of dancers. *Phenomenol. Cogn. Sci.*, 8:389–408, 2009.

[98] D. Lee and E. Aronson. Visual proprioceptive control of standing in human infants. *Percept. Psychophys.*, 15:529–532, 1974.

[99] J. Paillard and M. Brouchon. A proprioceptive contribution to the spatial encoding of position cues for ballistic movements. *Brain Res.*, 71(2-3):273–84, may 1978.

[100] D. Burke R. Fitzpatrick, R. Gorman and S. Gandevia. Postural proprioceptive reflexes in standing human subjects: bandwidth of response and transmission characteristics. *J. Physiol.*, 458:69–83, dec 1992.

[101] A. Tessier G. Gauchard, C. Jeandel and P. Perrin. Beneficial effect of proprioceptive physical activities on balance control in elderly human subjects. *Neurosci Lett.*, 273:81–84, 1999.

[102] O. Gur and U. Saranli. Model-based proprioceptive state estimation for spring-mass running. In *RSS 2011*, Los Angeles, CA, USA, June 2011.

[103] A. Patla. Understanding the roles of vision in the control of human locomotion. *Gait Posture*, 5:54–69, 1997.

[104] M. Troch C. Lafosse, E. Kerckhofs and E. Vandenbussche. Upper limb exteroceptive somatosensory and proprioceptive sensory afferent modulation of hemispatial neglect. *J. Clin. Eep. Neuropsyc.*, 25:308–323, 2003.

[105] R. Rodriguez. Shaquille vance and richard whitehead, December 2012.

[106] T. Sullivan. Design of a running robot and the effects of foot placement in the transverse plane. *Masters Thesis, Purdue University*, 2013.

[107] S. Bayer and J. Altman. *Neocortical Development*. New York, Raven Press, 1991.

[108] L. Tsai A. Gupta and A. Wynshaw-Boris. Life is a journey: a genetic look at neocortical development. *Nat. Rev. Genet.*, 3:342–355, May 2002.

[109] D. Felleman and D. Essen. Distributed hierarchical processing in the primate cerebral cortex. *Ciba. F. Symp.*, 1(1):1–47, 1991.

[110] H. Carlson A. Thorstensson, J. Nilsson and M. Zomlefer. Trunk movements in human locomotion. *Acta Physiol Scand.*, 121(1):9–22, May 1984.

VITA

VITA

Zhuahua Shen

School of Mechanical Engineering,Purdue University

585 Purdue Mall, West Lafayette, IN, U.S.A 47906

Email: shen38@purdue.edu

EDUCATION

Purdue University, West Lafayette, Indiana:

Ph.D. in Mechanical Engineering, December 2014 (expected)

Purdue University, West Lafayette, Indiana:

M.S. in Mechanical Engineering, December 2011

Shanghai Jiao Tong University, Shanghai, China:

B.S. in Mechanical Engineering, July 2009

AREA OF SPECIALIZATION

Nonlinear dynamics, Modeling and Simulation, Robotics

EMPLOYMENT EXPERIENCE

Purdue University, Spira Laboratories:

Graduate Research/Teaching Assistant, September 2009 - December 2014.

Purdue University, Mechanical Engineering:

Lambert Teaching Fellow, January 2014 - December 2014.

JOURNAL PUBLICATION

Z. Shen, and J. Seipel. "A fundamental mechanism of legged locomotion with hip torque and leg damping." Bioinspiration & biomimetics 7.4 (2012): 046010.

Z. Shen, P. Larson, and J. Seipel. "Rotary and radial forcing effects on center-of-

mass locomotion dynamics." Bioinspiration & biomimetics 9.3 (2014): 036020.

(accepted) **Z. Shen**, and J. Seipel. "Why animals have a preferred leg stiffness." Journal of Theoretical Biology.

(accepted) I. Abraham, **Z. Shen**, and J. Seipel. "A Nonlinear Damping Model for the Prediction of Legged Locomotion Forces and Stability." ASME Journal of Computational Nonlinear Dynamics.

(submitted) Z. Shen, and J. Seipel. "Animals Prefer Leg Stiffness Values that Optimize the Stability of Motion." Journal of Theoretical Biology.

(submitted) Z. Shen, and J. Seipel. "A Piecewise-Linear Approximation of the Canonical Spring-Loaded-Inverted-Pendulum Model of Legged Locomotion." ASME Journal of Computational Nonlinear Dynamics.

(in preparation) Z. Shen, and J. Seipel. "Rapid Prototyping and Tuning of Hip Based Bipedal Running: A Hierarchical Approach."

CONFERENCE PUBLICATION AND TALKS

Z. Shen, and J. Seipel. "A spring-mass model of locomotion with full asymptotic stability." ASME 2011 International Mechanical Engineering Congress and Exposition. American Society of Mechanical Engineers, 2011.

Z. Shen, and J. Seipel. "Actuated-SLIP: A Spring Mass Model with a Full Asymptotic Stability." Dynamic Walking 2012.

Z. Shen, and J. Seipel. "A Simple Analytical Tool for Legged Robot Design." ASME 2012 International Design Engineering Technical Conferences and Computers and Information in Engineering Conference. American Society of Mechanical Engineers, 2012.

Z. Shen, and J. Seipel. "Towards the Understanding of Hip Torque and Leg Damping Effects on Model Stability." ASME 2012 International Design Engineering Technical Conferences and Computers and Information in Engineering Conference. American Society of Mechanical Engineers, 2012.

Y. Che, **Z. Shen**, and J. Seipel. "A Simple Model for Body Pitching Stabilization."

ASME 2013 International Design Engineering Technical Conferences and Computers and Information in Engineering Conference. American Society of Mechanical Engineers, 2013.

Z. Shen, P. Larson, and J. Seipel. "Comparison of Hip Torque and Radial Forcing Effects on Locomotion Stability and Energetics." ASME 2013 International Design Engineering Technical Conferences and Computers and Information in Engineering Conference. American Society of Mechanical Engineers, 2013.

Z. Shen, and J. Seipel. "Effects of Open-Loop Leg Forcing in Rotary and Radial Directions." Dynamic Walking 2013.

Z. Shen, and J. Seipel. "A Theoretical Explanation for the Relative Leg Stiffness of Animals." Dynamic Walking 2013.

Z. Shen, J. Zhang, M. Anand, J. Schwartzentruber, and J. Seipel. "Design of Elastic Element and Controller Algorithm." ASME 2014 International Mechanical Engineering Congress and Exposition. American Society of Mechanical Engineers, 2014.

TEACHING EXPERIENCE

Purdue University, ME352 Machine Design I

Teaching Assistant, August 2010 - May 2012.

Purdue University, ME270 Basic Mechanics I

Instructor, Lambert Fellow, August 2014 - December 2014.

HONORS

2014 Purdue Teaching Academy Graduate Teaching Award, Purdue University

2014 Lambert Fellowship, Purdue University

2012 Magoon Award for Excellence in Teaching, Purdue University

2008 Shanghai Municipal Scholarship, Shanghai Jiao Tong University

2007 National Scholarship for Academic Excellence, Shanghai Jiao Tong University